

Several Families of Entanglement-Assisted Quantum Quasi-Cyclic LDPC Codes

Pavan Kumar, Abhi Kumar Sharma, and Shayan Srinivasa Garani

Department of Electronic Systems Engineering, Indian Institute of Science, Bengaluru 560012, India

We introduce several families of entanglement-assisted (EA) Calderbank-Shor-Steane (CSS) codes derived from two distinct classes of low-density parity-check (LDPC) codes. We derive two families of EA quantum QC-LDPC codes, namely, the spatially coupled (SC) and the non-spatially coupled cases. These two families are constructed by tiling permutation matrices of prime and composite orders. We establish several code properties along with conditions for guaranteed girth for the proposed code families. The Tanner graphs of the proposed EA quantum QC-LDPC and EA quantum QC-SC-LDPC codes have girths greater than four, which is required for good error correction performance. Some of the proposed families of codes require only *minimal* Bell pairs to be shared across the quantum transceiver. Furthermore, we construct two families of EA quantum QC-LDPC codes based on a single classical code, with Tanner graphs having girths greater than six, further improving the error correction performance. We evaluate the performance of these codes using both depolarizing and Markovian noise models to assess the random and burst error performance. Using a modified version of the sum-product algorithm over a quaternary alphabet, we show how correlated Pauli errors can be handled within the decoding setup. Simulation results show that nearly an order of improvement in the error correction performance can be achieved with quaternary decoder compared to binary decoder over the depolarizing and Markovian error channels, thereby generalizing the approach of EA quantum QC-LDPC code designs to work with both random and burst quantum error models, useful in practice.

1 Introduction

Low-density parity-check (LDPC) codes, introduced by Gallager [1] in the 1960s, are a class of linear error-correcting codes known for their near-optimal performance and efficient decoding algorithms. These codes are characterized by sparse bipartite graphs, which enable effective error correction. Although initially proposed by Gallager, LDPC codes gained renewed interest in the 1990s due to their capacity-approaching performance, particularly with iterative decoding algorithms. LDPC codes have become widely adopted in modern communication systems, including wireless networks (e.g., Wi-Fi), digital television broadcasting, deep-space communications [2], etc. Carefully designed LDPC codes can approach

Pavan Kumar: pavankumar1@iisc.ac.in

Abhi Kumar Sharma: abhisharma@iisc.ac.in

Shayan Srinivasa Garani: shayang@iisc.ac.in

Shannon capacity along with amenable hardware implementation, making them essential in high-performance communication systems [3, 1]. There are various subfamilies of low-density parity-check (LDPC) codes, and in this work, we will focus on quasi-cyclic (QC) LDPC codes and quasi-cyclic spatially-coupled (QC-SC) LDPC codes. QC-LDPC codes are a subclass of LDPC codes where the parity-check matrix exhibits a cyclic structure. This structure makes QC-LDPC codes highly efficient in terms of encoding [4] and decoding [5], allowing for efficient hardware implementation [6, 7], while still maintaining excellent error-correction performance typical of LDPC codes. QC-LDPC codes have become popular in modern communication systems due to their scalability and amenability toward hardware implementation and have found their way in standards related to digital video broadcasting (DVB-S2) [8], Wi-Fi [9] and wireless systems [10]. In addition, QC LDPC codes based on tiled permutation matrices [11] are part of data storage devices [12, 13] as they are capacity-approaching [14], showing resilience to both random and burst errors.

Spatially-coupled LDPC (SC-LDPC) codes are constructed by coupling together a series of L disjoint, or uncoupled, LDPC code Tanner graphs into a single coupled chain. They can be viewed as a type of LDPC convolutional code (LDPC-CC), since spatial coupling is equivalent to introducing memory into the encoding process. If the coupled chain is unterminated ($L \rightarrow \infty$), a SC-LDPC convolutional code (SC-LDPC-CC) is formed, and if the chain is terminated (finite L), we get a SC-LDPC block code (SC-LDPC-BC).

Recently, it has been proven by Kudekar et al. that SC-LDPC-BC ensembles are capacity achieving on memoryless binary-input symmetric-output (MBS) channels under belief propagation (BP) decoding [15, 16]. Consequently, the principle of spatial graph coupling has attracted significant attention and has been successfully applied in communications and signal processing applications; for example, in broadcast channels [17], multiuser detection [18], random access [19], and source coding [20], etc., to name a few.

With the phenomenal success of quasi-cyclic LDPC and quasi-cyclic spatially-coupled LDPC codes in practice, it is natural to explore their quantum counterparts.

1.1 Quantum Error-Correcting Codes

The potential of quantum technologies to alter the computing landscape has already been successfully demonstrated by the early pioneering works of Shor and Grover, with efficient solutions to the problem of prime factorization [21] and an optimal quantum search algorithm for unstructured databases [22], respectively. With the practical deployment of quantum key distribution protocols in communication networks, quantum guarantees of information security have been demonstrated [23]. Quantum computing is inevitable for the simulation of the dynamics of complex macromolecules with applications in computational chemistry toward drug design and development [24], etc. Further, simulations of complex processes in biological systems are efficiently possible only using quantum computers. Quantum technologies along with artificial intelligence [25] have the potential to bring about significant changes in the way computing and information processing can be done, applicable to all areas of science and engineering.

Quantum information is susceptible to errors due to decoherence (noise) and faulty gates. As a result, preserving quantum information through quantum error correcting codes (QECCs) becomes inevitable towards realizing functional quantum computing and communication systems. Thus, designing efficient QECCs is of fundamental importance.

The first quantum error correction code (QECC) was introduced by Shor [26], who demonstrated that it is possible to protect quantum information from errors. This seminal work laid the foundation for quantum error correction and sparked the search for optimal quantum error-correcting codes. Subsequently, a significant milestone in the development

of QECCs occurred with Gottesman’s introduction of the stabilizer code [27], defined as the fixed subspace of a commutative subgroup of the Pauli group. Following this, QECCs have been extensively studied and further developed [28, 29, 30]. In particular, the Calderbank-Shor-Steane (CSS) codes form a subclass of stabilizer codes to handle Pauli X and Z errors independently [28, 29]. The stabilizer formalism, along with the CSS subclass, provides a powerful framework for constructing new families of quantum codes from well-known classical codes. For a more comprehensive background on general quantum codes, we refer the reader to Terhal’s review [31] and to Preskill’s lecture notes [32].

Shortly after Shor’s and Gottesman’s contributions, Kitaev introduced the toric code [33, 34], a family of topological codes. Subsequently, the planar surface code was proposed by Freedman et al. [35] and Bravyi [36]. Surface codes have been well-studied for fault-tolerant quantum computation, largely due to their high error-correction threshold and planar layout. These codes are scalable, with the number of physical qubits n varying, and encoding a single logical qubit ($k = 1$), i.e., with diminishing code rate. The minimum distance d of the code scales as \sqrt{n} . It is likely that small-scale instances of surface codes will soon be realized experimentally (see Ref. [37] for recent results and a historical overview of experimental progress). However, despite their advantages, surface codes do not perform as well as the best-known classical error-correcting codes, where both the logical dimension k and the distance d scale linearly with n . While quantum codes having similar scaling properties as classical codes exist [38, 39], they face a significant technical challenge: the parity checks required to detect and correct errors involve an increasingly large number of physical qubits for each logical qubit. This poses a problem, as arbitrarily large and high-weight parity checks cannot be reliably performed without additional fault tolerance mechanisms. Furthermore, these checks cannot be parallelized, leading to the accumulation of errors due to idling qubits during measurement. Many decoding algorithms also assume that parity checks are sparse, which may not hold in these quantum codes. These issues are reminiscent of the challenges encountered in classical coding theory, which were addressed by LDPC codes. Given their success in classical communications, it is natural to explore the potential of quantum LDPC codes within a quantum setup.

1.2 Quantum LDPC Codes

Quantum low-density parity-check (QLDPC) codes form a subfamily of stabilizer codes and are constructed using sparse bipartite graphs, similar to their classical counterparts, but with the added complexity of handling quantum errors. Drawing inspiration from the remarkable success of classical LDPC codes in practical deployments, quantum LDPC codes are now being explored for applications in quantum computing and communication systems. Recent research has concentrated on developing practical decoding algorithms, including iterative methods, to make quantum LDPC codes viable for future quantum technologies. For further insights into various types of quantum LDPC codes, such as geometrically constructed QLDPC codes like hyperbolic surface codes, higher-dimensional hyperbolic codes, Freedman-Meyer-Luo codes, and tensor product-based quantum codes, readers can refer to the review by Breuckmann and Eberhard [40].

Although classical LDPC codes have been extensively studied in coding theory over the last few decades, their quantum analogs have only recently garnered significant attention. Much of this interest was spurred by Gottesman’s landmark result in 2013 [41], which showed that quantum LDPC codes with a constant encoding rate could reduce the overhead of fault-tolerant quantum computation to a constant. This is in stark contrast to other quantum fault-tolerance schemes, where longer computations require suppressing errors to an increasingly smaller threshold, necessitating larger codes and a growing number

of physical qubits [33, 42, 43]. Moreover, there is hope that quantum LDPC codes can approach channel capacity, similar to their classical counterparts. Although the challenging field of quantum channel capacities is beyond the scope of this discussion, interested readers can refer to [44, 45, 46] for further details.

Random LDPC codes can achieve a constant encoding rate $\frac{k}{n}$ and a linear distance $d \propto n$ with high probability [47, 48]. In comparison, constructing quantum LDPC codes is significantly more difficult, and it remains an open problem whether quantum LDPC codes exist that rival the parameters of their classical counterparts [49, 50]. Despite these challenges, recent progress has been made toward improving quantum LDPC codes, with several families of codes constructed that significantly outperform surface codes and color codes in terms of their asymptotic parameters. This progress indicates the potential of quantum LDPC codes, although they have not yet received the same level of attention as surface codes.

Constructing good quantum LDPC codes requires classical codes to satisfy the dual-containment property [29, 30], leading to cycles of length 4 in the overall Tanner graph of the code. This problem can be circumvented using the entanglement-assisted construction [51], requiring preshared maximally entangled bits (ebits) between the sender and the receiver. Preshared entangled bits with the receiver are assumed to be error-free and involved in measuring the stabilizer generators to obtain the syndromes for the entanglement-assisted codes since the support of the stabilizer generators¹ of the EA-quantum code involves all the qubits, i.e., the qubits received from the transmitter as well as preshared ebits with the receiver. Since preshared entangled bits with the receiver are not involved in the decoding process, the nodes corresponding to these entangled qubits are removed, circumventing cycles of length 4 that can lead to high error floors during decoding otherwise. After obtaining the syndromes, the syndrome-based decoders are applied to obtain the erroneous Pauli operator to nullify the error operator due to the noisy quantum channel.

After the seminal work of Brun et al. on EA quantum codes over the binary field, there has been a significant progress toward generalization of EA QECCs over arbitrary finite fields (see, for instance, [52, 53, 54, 55, 56, 57, 58, 59, 60]) along with efficient encoding and decoding circuits.

Quantum QC-LDPC codes constructed by Hagiwara et al. [61], Pantaleev and Kalachev [50] and Miao et al. [62] have short cycles in the overall Tanner graph since the code constructions are based on the CSS framework. In [63], the authors constructed spatially-coupled quasi-cyclic quantum LDPC codes based on CSS construction, which again results in the presence of short cycles in the Tanner graph. The reader must note that when the X and Z errors are statistically independent, the decoding of these errors can be carried out independently based on their individual Tanner graph representations. The design strategy for such codes requires well-known approaches towards the optimization of classical LDPC codes, such as choosing large girth, avoiding harmful trapping sets, etc., to correct independent X and Z errors [64].

Hsieh et al. [65] provided an example of an EA quantum QC-LDPC code using a single classical QC-LDPC code. It is desirable to work with a family of quantum QC-LDPC codes devoid of short cycles with known properties, such as the precise rank of the parity check matrix, etc., along with flexible code rate and block length.

In [66], the authors constructed QC-LDPC codes with a Tanner graph of girth greater than six by utilizing Sidon sequences. Specifically, they designed the code using a parity-

¹The support of any operator on a quantum code is a set of indices of qubits where the operator does not apply trivial operator (Pauli I).

check matrix with column weight three. This construction suggests that one could first design QC-LDPC codes with girth greater than six by exploring alternative sequences and higher column weights, and subsequently use these designs to construct quantum LDPC codes. Motivated by the works in [61, 50, 65, 62, 63], we construct a few families of EA quantum QC-LDPC codes based on classical designs.

1.3 Our Contribution

Our contributions in this paper are the following: (a) We first construct a family of parity-check matrices by tiling permutation matrices of prime order and derive the exact rank of the parity-check matrix *analytically* to compute the code rate. Next, we propose another family of parity-check matrices based on tiling permutation matrices of composite order and obtain an upper bound on the rank of the parity-check matrix *analytically*, which allows us to compute a lower bound on the code rate. (b) Based on the proposed classical designs, we extend our construction to EA quantum codes and propose two families of EA quantum QC-LDPC codes. The first family is constructed using two distinct classical QC-LDPC codes and requires the sharing of only a *single Bell pair* between the transmitter and receiver. The second family is proposed by employing a single classical QC-LDPC code. Additionally, the overall Tanner graph of the family constructed using two different classical codes has a girth greater than 4, while the Tanner graph of the classical QC-LDPC code used to construct the second family also has a girth greater than 4. (c) We propose two classes of entanglement-assisted quantum QC-SC-LDPC codes, derived from classical QC-SC-LDPC codes. One family is constructed using two distinct classical QC-SC-LDPC codes, while the other family is constructed by employing a single classical QC-SC-LDPC code. Further, the overall Tanner graph of the family constructed using two distinct QC-SC-LDPC codes has a girth greater than 4, while the Tanner graph of the classical QC-SC-LDPC code used to construct the second family also has a girth greater than 4. (d) We present two classes of entanglement-assisted quantum QC-LDPC codes derived from classical QC-LDPC codes, where the Tanner graphs of the underlying classical codes have a girth greater than 6. (e) Finally, we provide simulation results for different classes of EA quantum QC-LDPC codes against both random depolarizing channel and the random depolarizing channel with Markovian burst errors. The EA quantum QC-LDPCs are compared against the binary and quaternary decoders on separate and combined Tanner graphs to show improvements using the quaternary decoders. The EA quantum QC-LDPC codes are shown to correct a constant number of burst errors. Further, an EA quantum QC-LDPC code $[[390, 132; 128]]_2$ with girth greater than 6 and an EA quantum QC-LDPC code $[[529, 44; 1]]_2$ of girth greater than 4 are compared to show improvements due to the large girth, even though the length of $[[390, 132; 128]]_2$ code is less than that of $[[529, 44; 1]]_2$ code. Last, the EA quantum QC-LDPC codes are simulated by increasing the order of the permutation matrices.

The paper is organized as follows: Section 2 contains some basic definitions and preliminary results useful for establishing our main results. In Section 3, we revisit classical QC-LDPC codes and provide new code designs based on tiling permutation matrices with prime and composite orders. Several code properties are derived analytically. In Section 4, we construct two families of EA quantum QC-LDPC codes along with two other classes of EA quantum QC-SC-LDPC codes. Some of the families require a minimal number of preshared EPR pairs. In Section 5, two families of entanglement-assisted quantum QC-LDPC codes are proposed by employing single classical QC-LDPC code. For each family, the Tanner graph of the employed classical QC-LDPC code has girth greater than 6. In Section 6, we assess the performance of the proposed codes over the random depolarizing

and random depolarizing with Markovian burst quantum channels, followed by conclusions in Section 7.

2 Preliminaries

For a better presentation of the paper, we have divided this section into a few subsections and provided some required definitions and preliminary results, to be useful later.

2.1 Classical Quasi-Cyclic Linear Codes

In this subsection, we revisit classical quasi-cyclic linear codes with a detailed example [67].

Let t and b be two positive integers. Consider the following tb -tuple over the binary field \mathbb{F}_2 :

$$\begin{aligned} \mathbf{V} &= (\underbrace{v_0, v_1, \dots, v_{b-1}}_{\mathbf{V}_0}, \underbrace{v_b, v_{b+1}, \dots, v_{2b-1}}_{\mathbf{V}_1}, \dots, \underbrace{v_{(t-1)b}, v_{(t-1)b+1}, \dots, v_{tb-1}}_{\mathbf{V}_{t-1}}) \\ &= (\mathbf{V}_0, \mathbf{V}_1, \dots, \mathbf{V}_{t-1}), \end{aligned}$$

comprising t sections, $\mathbf{V}_0, \mathbf{V}_1, \dots, \mathbf{V}_{t-1}$ with each section consisting of b bits, i.e., a b -tuple. For $0 \leq j < t$, denote the b bits in the j^{th} section \mathbf{V}_j of \mathbf{V} as follows:

$$\mathbf{V}_j = (v_{j,0}, v_{j,1}, \dots, v_{j,b-1}).$$

Let $\mathbf{V}_j^{(1)} = (v_{j,b-1}, v_{j,0}, v_{j,1}, \dots, v_{j,b-2})$ be the b -tuple over \mathbb{F}_2 obtained by cyclically shifting each component of \mathbf{V}_j one place to the right. We call $\mathbf{V}_j^{(1)}$ the (right) cyclic-shift of \mathbf{V}_j . Consider the cyclic-shifts of all the t sections, $\mathbf{V}_0^{(1)}, \mathbf{V}_1^{(1)}, \dots, \mathbf{V}_{t-1}^{(1)}$, of \mathbf{V} and form the following tb -tuple:

$$\mathbf{V}^{(1)} = (\mathbf{V}_0^{(1)}, \mathbf{V}_1^{(1)}, \dots, \mathbf{V}_{t-1}^{(1)}).$$

The tb -tuple $\mathbf{V}^{(1)}$ comprises t sections, each consisting of b bits. We call $\mathbf{V}^{(1)}$ the section-wise cyclic-shift of \mathbf{V} , and the parameter b is called the section size.

Definition 1. [67, Definition 4.4] *Let t , b , and k be positive integers such that $k < tb$. A $[tb, k, d]$ linear code C_{qc} over \mathbb{F}_2 is called a QC code if it satisfies the following two conditions:*

1. *Each codeword in C_{qc} comprises t sections, each consisting of b bits; and*
2. *Section-wise cyclic-shifting a codeword in C_{qc} l places to the right for $0 \leq l < b$ yields another codeword in C_{qc} .*

Under the above definition, if $t = 1$ the QC code C_{qc} is a cyclic code. Therefore, cyclic codes form a subclass of QC codes.

Example 1. *Consider the following generator matrix \mathbf{G}_{qc} of a $[8, 4]$ linear code C_{qc} :*

$$\mathbf{G}_{qc} = \left[\begin{array}{cccc|cccc} 1 & 0 & 0 & 0 & 1 & 0 & 1 & 1 \\ 0 & 1 & 0 & 0 & 1 & 1 & 0 & 1 \\ 0 & 0 & 1 & 0 & 1 & 1 & 1 & 0 \\ 0 & 0 & 0 & 1 & 0 & 1 & 1 & 1 \end{array} \right].$$

The sixteen codewords of C_{qc} are listed in Table 1, from which, we see that the code C_{qc} is a QC code with $t = 2$ and $b = 4$, i.e., each codeword in C_{qc} consists of two sections of four bits each and section-wise cyclically shifting any codeword in C_{qc} results in another codeword.

Note that the generator matrix \mathbf{G}_{qc} for this QC code is a 1×2 array of right circulants of size 4×4 .

Table 1: The sixteen codewords of the $[8, 4]$ QC code C_{qc} given in Example 1.

Messages (u_0, u_1, u_2, u_3)	Codewords $(v_0, v_1, v_2, v_3, v_4, v_5, v_6, v_7)$
(0, 0, 0, 0)	(0, 0, 0, 0, 0, 0, 0, 0)
(1, 0, 0, 0)	(1, 0, 0, 0, 1, 0, 1, 1)
(0, 0, 0, 1)	(0, 0, 0, 1, 0, 1, 1, 1)
(1, 0, 0, 1)	(1, 0, 0, 1, 1, 1, 0, 0)
(0, 0, 1, 0)	(0, 0, 1, 0, 1, 1, 1, 0)
(1, 0, 1, 0)	(1, 0, 1, 0, 0, 1, 0, 1)
(0, 0, 1, 1)	(0, 0, 1, 1, 1, 0, 0, 1)
(1, 0, 1, 1)	(1, 0, 1, 1, 0, 0, 1, 0)
(0, 1, 0, 0)	(0, 1, 0, 0, 1, 1, 0, 1)
(1, 1, 0, 0)	(1, 1, 0, 0, 0, 1, 1, 0)
(0, 1, 0, 1)	(0, 1, 0, 1, 1, 0, 1, 0)
(1, 1, 0, 1)	(1, 1, 0, 1, 0, 0, 0, 1)
(0, 1, 1, 0)	(0, 1, 1, 0, 0, 0, 1, 1)
(1, 1, 1, 0)	(1, 1, 1, 0, 1, 0, 0, 0)
(0, 1, 1, 1)	(0, 1, 1, 1, 0, 1, 0, 0)
(1, 1, 1, 1)	(1, 1, 1, 1, 1, 1, 1, 1)

2.2 Low-Density Parity-Check (LDPC) Codes and Their Tanner Graph

We begin this subsection by discussing LDPC codes and their associated Tanner graph. We discuss the conditions for the existence of a $2n$ -length cycle in the Tanner graph when the parity-check matrix is generated by tiling permutation matrices.

Definition 2. *Low-density parity-check (LDPC) codes are a class of linear error-correcting codes characterized by a sparse bipartite graph representation. They are defined by a parity-check matrix H having low density of ones, leading to a small number of non-zero elements per row and column.*

Example 2. *Consider the following parity-check matrix*

$$H = \begin{bmatrix} 1 & 1 & 1 & 1 & 0 & 0 & 0 \\ 0 & 1 & 0 & 0 & 0 & 1 & 0 \\ 0 & 0 & 1 & 0 & 1 & 0 & 1 \\ 1 & 0 & 0 & 1 & 0 & 1 & 0 \end{bmatrix}.$$

The Tanner graph of the LDPC code with the parity-check matrix H is represented by Figure 1.

Low-density parity-check (LDPC) codes can be categorized into two types: **regular** and **irregular** LDPC codes. An LDPC code is called a (d_v, d_c) -**regular LDPC code** if it has a parity-check matrix in which each row (corresponding to a parity-check equation) has a fixed weight d_c and each column (corresponding to a bit) has a fixed weight d_v .

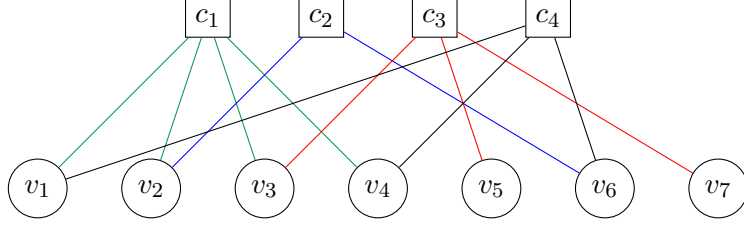


Figure 1: Tanner graph of the LDPC code given in Example 2.

Example 3. A regular LDPC code associated with the parity check matrix

$$H = \begin{bmatrix} 1 & 1 & 0 & 0 & 0 & 1 \\ 0 & 1 & 1 & 0 & 1 & 0 \\ 0 & 0 & 1 & 1 & 0 & 1 \\ 1 & 0 & 0 & 1 & 1 & 0 \end{bmatrix}$$

is a (2,3)-regular LDPC code.

An **irregular LDPC code** has a parity-check matrix where the row and column weights can vary. This means that different rows can have different numbers of 1's, and similarly, different columns can also have varying numbers of 1's as given in Example 2. Irregular LDPC codes can be tailored for specific applications, potentially leading to better performance than regular LDPC codes [68, 69].

Regular LDPC codes are simpler to analyze and implement due to their uniform structure. Further, regular codes are amenable to hardware implementation since irregular codes require additional logic in the implementation, leading to higher latencies[70, 71]. Last, irregular codes without a constraint on the minimum degree for each variable node can lead to poor minimum distance of the code, leading to higher error floors, etc. Throughout the paper our focus will be on regular LDPC codes.

For a positive integer n , let $\mathbb{Z}_n = \{0, 1, 2, \dots, (n-1)\}$ be the ring of integers and P be a right circulant permutation matrix of order n . We define the parity-check matrix H and the corresponding model matrix M using the following equations:

$$H = \begin{bmatrix} P^{a_{0,0}} & P^{a_{0,1}} & \dots & P^{a_{0,t-1}} & P^{a_{0,t}} \\ P^{a_{1,0}} & P^{a_{1,1}} & \dots & P^{a_{1,t-1}} & P^{a_{1,t}} \\ \vdots & \vdots & \ddots & \vdots & \vdots \\ P^{a_{m-1,0}} & P^{a_{m-1,1}} & \dots & P^{a_{m-1,t-1}} & P^{a_{m-1,t}} \\ P^{a_{m,0}} & P^{a_{m,1}} & \dots & P^{a_{m,t-1}} & P^{a_{m,t}} \end{bmatrix}, \quad (1)$$

$$M = \begin{bmatrix} a_{0,0} & a_{0,1} & \dots & a_{0,t-1} & a_{0,t} \\ a_{1,0} & a_{1,1} & \dots & a_{1,t-1} & a_{1,t} \\ \vdots & \vdots & \ddots & \vdots & \vdots \\ a_{m-1,0} & a_{m-1,1} & \dots & a_{m-1,t-1} & a_{m-1,t} \\ a_{m,0} & a_{m,1} & \dots & a_{m,t-1} & a_{m,t} \end{bmatrix}, \quad (2)$$

where $a_{i,j} \in \mathbb{Z}_n$ for all i, j . In the parity-check matrix, defined by (1), $[P^{a_{i,0}}, P^{a_{i,1}}, \dots, P^{a_{i,t}}]$ is known as i^{th} block-row, whereas $[(P^{a_{0,j}})^T, (P^{a_{1,j}})^T, (P^{a_{2,j}})^T, \dots, (P^{a_{m,j}})^T]^T$ stands for the j^{th} block-column.

A closed path of length $2k$ in any parity-check matrix of the form in (1) is a sequence of block-row and block-column index pairs $(i_0, j_0), (i_0, j_1), (i_1, j_1), (i_1, j_2), \dots, (i_{k-1}, j_{k-1}), (i_{k-1}, j_0)$, with $i_\ell \neq i_{\ell+1}, j_\ell \neq j_{\ell+1}$, for $\ell = 0, 1, \dots, k-2$, and $i_{k-1} \neq i_0, j_{k-1} \neq j_0$.

The significance of closed paths arises from the following simple but important result.

Theorem 1. [72, Theorem 1] *A cycle of length $2k$ exists in the Tanner graph of a quasi-cyclic LDPC code with parity-check matrix H , defined by (1), if and only if there exists a closed path $(i_0, j_0), (i_0, j_1), (i_1, j_1), (i_1, j_2), \dots, (i_{k-1}, j_{k-1}), (i_{k-1}, j_0)$ in H such that*

$$P^{a_{i_0, j_0}} (P^{a_{i_0, j_1}})^{-1} P^{a_{i_1, j_1}} (P^{a_{i_1, j_2}})^{-1} \dots P^{a_{i_{k-1}, j_{k-1}}} (P^{a_{i_{k-1}, j_0}})^{-1} = I \text{ (identity matrix)}. \quad (3)$$

Proof. In [72], the proof of the theorem is omitted. Consequently, it is imperative to present the complete proof. Therefore, we shall provide a detailed proof, utilizing certain hints provided in [73].

Let $m, t \geq 1$ be positive integers, and let $P^{a_{i,j}}$ be the permutation matrix defined by a permutation $R^{a_{i,j}} : \mathbb{Z}_n \rightarrow \mathbb{Z}_n$ as follows; $P^{a_{i,j}}(u, v) = 1$ if and only if $u = R^{a_{i,j}}(v)$, where (u, v) stands for (u, v) -th entry in the permutation matrix. Then we define the parity check-matrix in terms of permutation matrix and permutations, respectively as follows:

$$H = \begin{bmatrix} P^{a_{0,0}} & P^{a_{0,1}} & P^{a_{0,2}} & \dots & P^{a_{0,t}} \\ P^{a_{1,0}} & P^{a_{1,1}} & P^{a_{1,2}} & \dots & P^{a_{1,t}} \\ P^{a_{2,0}} & P^{a_{2,1}} & P^{a_{2,2}} & \dots & P^{a_{2,t}} \\ \vdots & \vdots & \vdots & \ddots & \vdots \\ P^{a_{m,0}} & P^{a_{m,1}} & P^{a_{m,2}} & \dots & P^{a_{m,t}} \end{bmatrix}, \text{ or } H = \begin{bmatrix} R^{a_{0,0}} & R^{a_{0,1}} & R^{a_{0,2}} & \dots & R^{a_{0,t}} \\ R^{a_{1,0}} & R^{a_{1,1}} & R^{a_{1,2}} & \dots & R^{a_{1,t}} \\ R^{a_{2,0}} & R^{a_{2,1}} & R^{a_{2,2}} & \dots & R^{a_{2,t}} \\ \vdots & \vdots & \vdots & \ddots & \vdots \\ R^{a_{m,0}} & R^{a_{m,1}} & R^{a_{m,2}} & \dots & R^{a_{m,t}} \end{bmatrix}.$$

For each pair (i, j) , where $0 \leq i \leq m$ and $0 \leq j \leq t$, we can write the entries of $P^{a_{i,j}}$ as $h_{in+i', jn+j'}$, $0 \leq i', j' \leq n-1$. Then $h_{in+i', jn+j'} = 1 \iff i' = R^{a_{i,j}}(j')$. Consider the closed path of indices as follows:

$$(i_0, j_0), (i_0, j_1); (i_1, j_1), (i_1, j_2); \dots, (i_{k-2}, j_{k-2}), (i_{k-2}, j_{k-1}); (i_{k-1}, j_{k-1}), (i_{k-1}, j_0).$$

For some pairs (r_i, c_i) , where $0 \leq r_i, c_i \leq (n-1)$, the simple path between (i_0, j_0) and (i_{k-1}, j_0) passing through all the indices must satisfy the following set of equations:

$$\begin{aligned} P^{a_{i_0, j_0}}(r_0, c_0) = P^{a_{i_0, j_1}}(r_0, c_1) = 1 &\iff R^{a_{i_0, j_0}}(c_0) = R^{a_{i_0, j_1}}(c_1) \\ &\iff c_1 = (R^{a_{i_0, j_1}})^{-1}(R^{a_{i_0, j_0}}(c_0)); \\ P^{a_{i_1, j_1}}(r_1, c_1) = P^{a_{i_1, j_2}}(r_1, c_2) = 1 &\iff R^{a_{i_1, j_1}}(c_1) = R^{a_{i_1, j_2}}(c_2) \\ &\iff c_2 = (R^{a_{i_1, j_2}})^{-1}(R^{a_{i_1, j_1}}(c_1)); \\ P^{a_{i_2, j_2}}(r_2, c_2) = P^{a_{i_2, j_3}}(r_2, c_3) = 1 &\iff R^{a_{i_2, j_2}}(c_2) = R^{a_{i_2, j_3}}(c_3) \\ &\iff c_3 = (R^{a_{i_2, j_3}})^{-1}(R^{a_{i_2, j_2}}(c_2)); \\ &\vdots \\ &\vdots \\ P^{a_{i_{k-1}, j_{k-1}}}(r_{k-1}, c_{k-1}) = P^{a_{i_{k-1}, j_0}}(r_{k-1}, c_k) = 1 &\iff R^{a_{i_{k-1}, j_{k-1}}}(c_{k-1}) = R^{a_{i_{k-1}, j_0}}(c_k) \\ &\iff c_k = (R^{a_{i_{k-1}, j_0}})^{-1}(R^{a_{i_{k-1}, j_{k-1}}}(c_{k-1})). \end{aligned}$$

From the above equations, one can easily conclude that

$$c_k = (R^{a_{i_{k-1}, j_0}})^{-1} R^{a_{i_{k-1}, j_{k-1}}} (R^{a_{i_1, j_2}})^{-1} R^{a_{i_1, j_1}} \dots (R^{a_{i_0, j_1}})^{-1} R^{a_{i_0, j_0}}(c_0). \quad (4)$$

Since, each $R^{a_{i,j}}$, where $0 \leq i \leq m$ and $0 \leq j \leq t$, corresponds to some exponent of right circulant permutation matrix P , their composition

$$(R^{a_{i_{k-1}, j_0}})^{-1} R^{a_{i_{k-1}, j_{k-1}}} (R^{a_{i_1, j_2}})^{-1} R^{a_{i_1, j_1}} \dots (R^{a_{i_0, j_1}})^{-1} R^{a_{i_0, j_0}}$$

as mappings corresponds to some power of right circulant permutation matrix P . Consequently, from equation (4), a cycle of length $2k$ will exist in the Tanner graph of the parity-check matrix H if and only if $c_k = c_0$, which is only possible under the following condition:

$$(R^{a_{i_{k-1},j_0}})^{-1} R^{a_{i_{k-1},j_{k-1}}} (R^{a_{i_1,j_2}})^{-1} R^{a_{i_1,j_1}} \dots (R^{a_{i_0,j_1}})^{-1} R^{a_{i_0,j_0}} = id_{\mathbb{Z}_n}, \quad (5)$$

where $id_{\mathbb{Z}_n}$ is the identity map on \mathbb{Z}_n . The Equation (5) holds if and only if

$$\begin{aligned} & (P^{a_{i_{k-1},j_0}})^{-1} P^{a_{i_{k-1},j_{k-1}}} (P^{a_{i_1,j_2}})^{-1} P^{a_{i_1,j_1}} \dots (P^{a_{i_0,j_1}})^{-1} P^{a_{i_0,j_0}} = I \text{ (identity matrix)} \\ \iff & P^{a_{i_0,j_0}} (P^{a_{i_0,j_1}})^{-1} P^{a_{i_1,j_1}} (P^{a_{i_1,j_2}})^{-1} \dots P^{a_{i_{k-1},j_{k-1}}} (P^{a_{i_{k-1},j_0}})^{-1} = I \text{ (identity matrix),} \end{aligned}$$

since for any $n \times n$ matrix A , it holds that $A^{k_1+k_2} = A^{k_2+k_1}$ (for all integers k_1, k_2). Hence the result established. \square

Alternatively, the condition given by (3) for the existence of a cycle of length $2k$ in the Tanner graph of a quasi-cyclic LDPC code with parity-check matrix H can be expressed as:

$$(a_{i_0,j_0} - a_{i_0,j_1}) + (a_{i_1,j_1} - a_{i_1,j_2}) + \dots + (a_{i_{k-1},j_{k-1}} - a_{i_{k-1},j_0}) = 0 \pmod{n}, \quad (6)$$

where n is the size of the right circulant permutation matrix P .

Corollary 1. *There does not exist a cycle of length 4 in the Tanner graph of a quasi-cyclic LDPC code with parity-check matrix H , defined by (1), if and only if*

$$(a_{i_0,j_0} - a_{i_0,j_1}) + (a_{i_1,j_1} - a_{i_1,j_0}) \neq 0 \pmod{n} \text{ for all } 0 \leq i_0 < i_1 \leq m, 0 \leq j_0 < j_1 \leq n.$$

Corollary 2. *There does not exist a cycle of length 6 in the Tanner graph of a quasi-cyclic LDPC code with parity-check matrix H , defined by (1), if and only if*

$$(a_{i_0,j_0} - a_{i_0,j_1}) + (a_{i_1,j_1} - a_{i_1,j_2}) + (a_{i_2,j_2} - a_{i_2,j_0}) \neq 0 \pmod{n},$$

where $i_\ell \neq i_{\ell+1}, j_\ell \neq j_{\ell+1}$, for $\ell = 0, 1$, and $i_2 \neq i_0, j_2 \neq j_0$.

Consider the parity-check matrix H and the associated model matrix M defined by equations (1) and (2), respectively. Let i, j, k be any three row indices and p, q, r be any three column indices from the matrix M . Then, by Corollary 2, Figure 2 shows all possible 6-cycles along with their conditions:

Definition 3. *A vector $(v_1, v_2, v_3, \dots, v_m)$ over \mathbb{Z}_n is said to be **multiplicity free** if all entries in the vector are different.*

Example 4. *The vector $(0, 1, 2, 3, 4, 5)$ is multiplicity free over \mathbb{Z}_7 whereas $(0, 0, 1, 1, 2, 3, 4)$ is not.*

Let $R_i = (a_{i,0}, a_{i,1}, a_{i,2}, \dots, a_{i,t})$ and $R_j = (a_{j,0}, a_{j,1}, a_{j,2}, \dots, a_{j,t})$ be any two rows from the model matrix, defined by (2), of H . Based on the Corollary 1 and above definition, we have the following simple but important result.

Proposition 1. *The Tanner graph of a QC-LDPC code with parity check matrix H defined by (1) is free from cycles of length 4 if and only if $R_i - R_j$ is multiplicity free for any $0 \leq i < j \leq m$.*

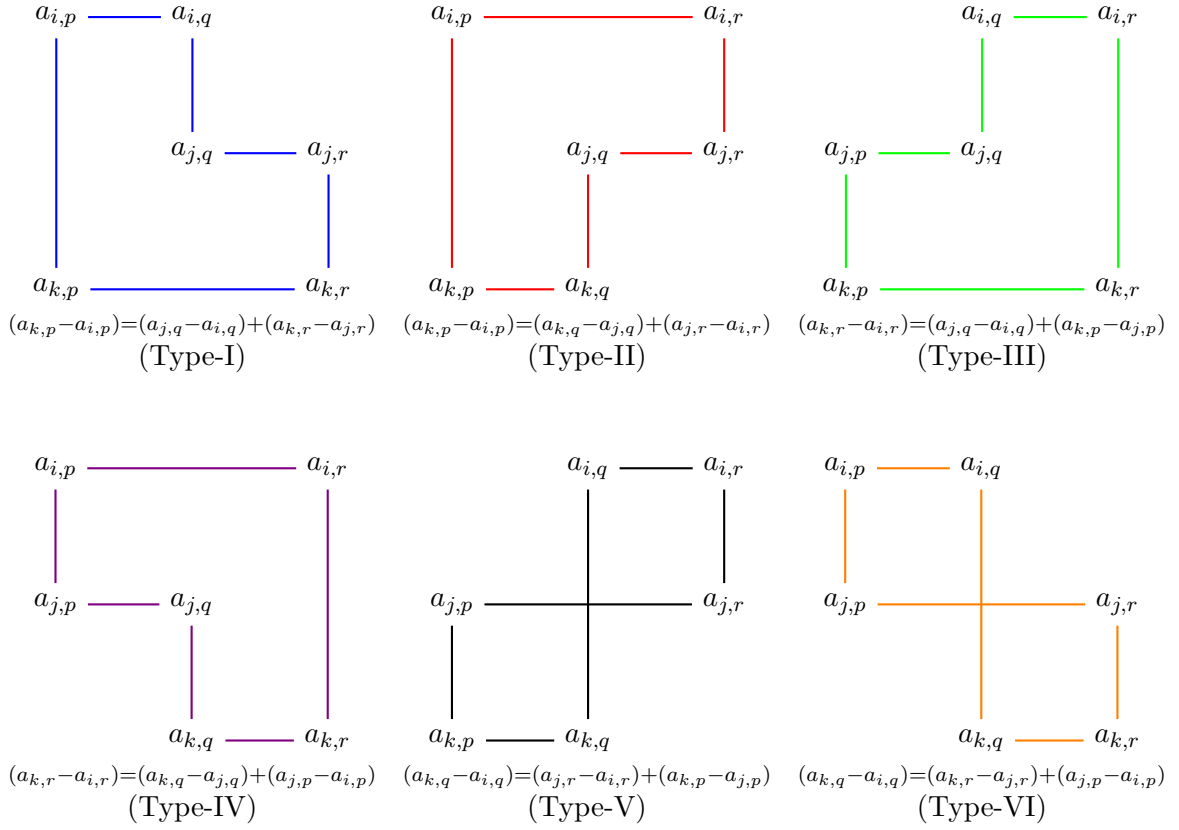


Figure 2: All possible cycles of length 6 with their corresponding conditions.

2.3 Quasi-Cyclic (QC) Spatially-Coupled (SC) Classical Low-Density Parity-Check Codes

In this subsection, we revisit quasi-cyclic spatially-coupled low-density parity-check (QC-SC-LDPC) codes with a detailed example.

Given a binary matrix $\mathbf{H}^{(P)}$, the parity check matrix of a **quasi-cyclic** LDPC code is constructed by replacing each non-zero element $(\mathbf{H}^{(P)})_{i,j}$ in $\mathbf{H}^{(P)}$ with a some power of the right circulant² permutation matrix, whereas the zero element is replaced by the $n \times n$ zero matrix. The Tanner graph associated with $\mathbf{H}^{(P)}$ is referred to as the **protograph** of the QC-LDPC code, and the QC-LDPC code is said to be **lifted** from the protograph.

Three $\gamma \times \kappa$ matrices \mathbf{B} , \mathbf{P} and \mathbf{L} determine a QC-SC-LDPC code. The **partitioning matrix** \mathbf{P} defines how the **base matrix** \mathbf{B} is divided into $m+1$ component matrices $\mathbf{H}_i^{(P)}$ of the protograph. The **lifting matrix** \mathbf{L} specifies how $\mathbf{H}_i^{(P)}$ are lifted into component matrices \mathbf{H}_i in the QC-SC LDPC code, where $i = 0, \dots, m$. The entries of \mathbf{P} range from 0 through m and the entries of \mathbf{L} range from 0 through $(n-1)$. For $1 \leq s \leq \gamma$, $1 \leq t \leq \kappa$, the (s, t) -th element of $\mathbf{H}_i^{(P)}$ and the (s, t) -th block of \mathbf{H}_i are specified as follows:

$$(\mathbf{H}_i^{(P)})_{s,t} = \begin{cases} (\mathbf{B})_{s,t}, & \text{if } (\mathbf{P})_{s,t} = i; \\ 0, & \text{otherwise.} \end{cases} \quad \text{and } \mathbf{H}_{i;s,t} = \begin{cases} P_z^{(\mathbf{L})_{s,t}}, & \text{if } (\mathbf{H}_i^{(P)})_{s,t} = 1; \\ \mathbf{0}_{z \times z}, & \text{otherwise.} \end{cases} \quad (7)$$

The component matrices are vertically concatenated into a **replica**, and these replicas are coupled horizontally. QC-SC-LDPC codes are categorized as **tail-biting** (TB) or **non-tail-**

²The reader must note that one can either populate right or left circulant permutation matrices but the orientation must be consistent throughout the construction of the parity-check matrix.

biting (NTB) depending on the form taken by the parity-check matrix, as shown in (8). The **memory** of the QC-SC-LDPC code is m and the number of replicas is referred to as the **coupling length** and is denoted by L .

$$\mathbf{H}_{\text{TB}} = \begin{bmatrix} \mathbf{H}_0 & \mathbf{0} & \cdots & \mathbf{0} & \mathbf{H}_m & \cdots & \mathbf{H}_1 \\ \mathbf{H}_1 & \mathbf{H}_0 & \mathbf{0} & \cdots & \mathbf{0} & \ddots & \vdots \\ \vdots & \mathbf{H}_1 & \mathbf{H}_0 & \ddots & \ddots & \ddots & \mathbf{H}_m \\ \mathbf{H}_m & \vdots & \ddots & \ddots & \mathbf{0} & \ddots & \mathbf{0} \\ \mathbf{0} & \mathbf{H}_m & \cdots & \mathbf{H}_1 & \mathbf{H}_0 & \ddots & \vdots \\ \vdots & \ddots & \ddots & \vdots & \ddots & \ddots & \mathbf{0} \\ \mathbf{0} & \cdots & \mathbf{0} & \mathbf{H}_m & \cdots & \mathbf{H}_1 & \mathbf{H}_0 \end{bmatrix}, \quad \mathbf{H}_{\text{NTB}} = \begin{bmatrix} \mathbf{H}_0 & \mathbf{0} & \cdots & \mathbf{0} \\ \mathbf{H}_1 & \mathbf{H}_0 & \ddots & \vdots \\ \vdots & \mathbf{H}_1 & \ddots & \mathbf{0} \\ \mathbf{H}_m & \vdots & \ddots & \mathbf{H}_0 \\ \mathbf{0} & \mathbf{H}_m & \ddots & \mathbf{H}_1 \\ \vdots & \ddots & \ddots & \vdots \\ \mathbf{0} & \cdots & \mathbf{0} & \mathbf{H}_m \end{bmatrix}. \quad (8)$$

Example 5. Let $n = 5$, $\gamma = 2$, $\kappa = 4$, $m = 1$, and $L = 4$. The 2×3 base matrix \mathbf{B} , partitioning matrix \mathbf{P} , and lifting matrix \mathbf{L} are as follows:

$$\mathbf{B} = \begin{bmatrix} 1 & 1 & 1 & 1 \\ 1 & 1 & 1 & 1 \end{bmatrix}, \quad \mathbf{P} = \begin{bmatrix} 0 & 1 & 0 & 1 \\ 1 & 0 & 1 & 0 \end{bmatrix} \quad \text{and} \quad \mathbf{L} = \begin{bmatrix} 1 & 2 & 3 & 4 \\ 2 & 4 & 1 & 3 \end{bmatrix}.$$

The protograph $\mathbf{H}^{(\text{P})}$ specified by \mathbf{B} and \mathbf{P} is given by:

$$\mathbf{H}^{(\text{P})} = \begin{bmatrix} \mathbf{H}_0^{(\text{P})} & \mathbf{0} & \mathbf{0} & \mathbf{H}_1^{(\text{P})} \\ \mathbf{H}_1^{(\text{P})} & \mathbf{H}_0^{(\text{P})} & \mathbf{0} & \mathbf{0} \\ \mathbf{0} & \mathbf{H}_1^{(\text{P})} & \mathbf{H}_0^{(\text{P})} & \mathbf{0} \\ \mathbf{0} & \mathbf{0} & \mathbf{H}_1^{(\text{P})} & \mathbf{H}_0^{(\text{P})} \end{bmatrix},$$

where $\mathbf{H}_0^{(\text{P})} = \begin{bmatrix} 1 & 0 & 1 & 0 \\ 0 & 1 & 0 & 1 \end{bmatrix}$ and $\mathbf{H}_1^{(\text{P})} = \begin{bmatrix} 0 & 1 & 0 & 1 \\ 1 & 0 & 1 & 0 \end{bmatrix}$. The parity-check matrix \mathbf{H} lifted from $\mathbf{H}^{(\text{P})}$ with respect to \mathbf{L} is

$$\mathbf{H} = \begin{bmatrix} \mathbf{H}_0 & \mathbf{0} & \mathbf{0} & \mathbf{H}_1 \\ \mathbf{H}_1 & \mathbf{H}_0 & \mathbf{0} & \mathbf{0} \\ \mathbf{0} & \mathbf{H}_1 & \mathbf{H}_0 & \mathbf{0} \\ \mathbf{0} & \mathbf{0} & \mathbf{H}_1 & \mathbf{H}_0 \end{bmatrix}, \quad \text{where}$$

$$H_0 = \left[\begin{array}{cccc|cccc|cccc|cccc} 0 & 1 & 0 & 0 & 0 & 0 & 0 & 0 & 0 & 0 & 0 & 0 & 0 & 0 & 0 & 0 & 0 \\ 0 & 0 & 1 & 0 & 0 & 0 & 0 & 0 & 0 & 0 & 0 & 0 & 0 & 0 & 0 & 0 & 0 \\ 0 & 0 & 0 & 1 & 0 & 0 & 0 & 0 & 1 & 0 & 0 & 0 & 0 & 0 & 0 & 0 & 0 \\ 0 & 0 & 0 & 0 & 1 & 0 & 0 & 0 & 0 & 0 & 1 & 0 & 0 & 0 & 0 & 0 & 0 \\ 1 & 0 & 0 & 0 & 0 & 0 & 0 & 0 & 0 & 0 & 0 & 1 & 0 & 0 & 0 & 0 & 0 \\ \hline 0 & 0 & 0 & 0 & 0 & 0 & 0 & 0 & 0 & 0 & 0 & 0 & 0 & 0 & 1 & 0 & 0 \\ 0 & 0 & 0 & 0 & 0 & 1 & 0 & 0 & 0 & 0 & 0 & 0 & 0 & 0 & 0 & 0 & 1 \\ 0 & 0 & 0 & 0 & 0 & 0 & 1 & 0 & 0 & 0 & 0 & 0 & 0 & 0 & 1 & 0 & 0 \\ 0 & 0 & 0 & 0 & 0 & 0 & 0 & 1 & 0 & 0 & 0 & 0 & 0 & 0 & 0 & 1 & 0 \\ 0 & 0 & 0 & 0 & 0 & 0 & 0 & 0 & 1 & 0 & 0 & 0 & 0 & 0 & 0 & 0 & 0 \end{array} \right],$$

$$H_1 = \left[\begin{array}{cc|cc|cc|cc|cc} 0 & 0 & 0 & 0 & 0 & 0 & 0 & 1 & 0 & 0 & 0 & 0 & 0 & 0 & 0 & 1 \\ 0 & 0 & 0 & 0 & 0 & 0 & 0 & 1 & 0 & 0 & 0 & 0 & 0 & 0 & 0 & 0 \\ 0 & 0 & 0 & 0 & 0 & 0 & 0 & 0 & 1 & 0 & 0 & 0 & 0 & 0 & 0 & 0 \\ 0 & 0 & 0 & 0 & 0 & 1 & 0 & 0 & 0 & 0 & 0 & 0 & 0 & 0 & 0 & 0 \\ 0 & 0 & 0 & 0 & 0 & 0 & 1 & 0 & 0 & 0 & 0 & 0 & 0 & 0 & 0 & 0 \\ \hline 0 & 0 & 1 & 0 & 0 & 0 & 0 & 0 & 0 & 0 & 0 & 0 & 0 & 0 & 0 & 0 \\ 0 & 0 & 0 & 1 & 0 & 0 & 0 & 0 & 0 & 0 & 0 & 0 & 0 & 0 & 0 & 0 \\ 0 & 0 & 0 & 0 & 0 & 1 & 0 & 0 & 0 & 0 & 0 & 0 & 0 & 0 & 0 & 0 \\ 1 & 0 & 0 & 0 & 0 & 0 & 0 & 0 & 0 & 0 & 0 & 0 & 0 & 0 & 0 & 0 \\ 0 & 1 & 0 & 0 & 0 & 0 & 0 & 0 & 0 & 0 & 0 & 0 & 0 & 0 & 0 & 0 \end{array} \right].$$

Remark 1. *In the classical world, non-tail-biting (NTB) codes are associated with better thresholds than tail-biting (TB) codes, due to the existence of low degree check nodes at the two ends of the coupling chain (see the discussion of low threshold saturation in SC codes [74, 75, 76]). However, due to the commutativity conditions required by stabilizer codes, in the quantum world, NTB code suffer from low minimum distance. This is because component matrices must pairwise commute, and the block length of the stabilizer code C' generated by the component matrices is small ($n = N/L$). Any product of stabilizers in C' gives rise to a non-correctable error pattern in the NTB code.*

2.4 Entanglement-Assisted Quantum Codes (EAQCs)

Entanglement-assisted quantum codes (EAQCs) forms a subclass of quantum error correcting codes that use preshared maximally entangled bits (ebits) between the sender and receiver to enhance coding efficiency. This entanglement enables a more effective utilization of quantum resources, facilitating the transmission of quantum information through noisy channels. The code rates for entanglement-assisted quantum codes are defined as follows:

1. **Entanglement-assisted rate:** This rate assumes that the maximally entangled bits (ebits) shared between sender and receiver are error-free. Bennett et al. adopted this assumption to derive the entanglement-assisted capacity of a quantum channel for transmitting quantum information [77, 78]. For the parameters $[[n, k, d; c]]_2$, the entanglement-assisted rate is given by $\frac{k}{n}$.
2. **Trade-off rate:** This rate takes into account that entanglement is not free and describes a rate pair that determines performance. The first number in the pair indicates the number of noiseless qubits generated per channel use, while the second represents the number of consumed entangled bits (ebits). For the parameters $[[n, k, d; c]]_2$, the rate pair is $(\frac{k}{n}, \frac{c}{n})$. Researchers in quantum information theory have derived asymptotic trade-off curves that outline the achievable rate regions [79]. Brun et al. proposed a construction for an entanglement-assisted quantum block code that minimizes the number of ebits for fixed values of k and n [51, 80].
3. **Catalytic rate:** This rate assumes that entangled bits are generated at the expense of transmitted qubits [51, 80]. Two methods for accumulating entanglement between sender and receiver include using a noiseless quantum channel or the encoded use of a noisy quantum channel. The catalytic rate of an $[[n, k; c]]_2$ quantum code is $\frac{k-c}{n}$.

EA-QECCs provide several benefits; below are some of the main advantages:

1. **Increased Capacity:** They can achieve higher coding rates compared to traditional quantum codes that do not utilize entanglement.
2. **Flexibility:** The use of entanglement enables more robust error correction, allowing for protection against a broader range of errors.
3. **Removal of Short Cycles in the Tanner Graph:** In the EA-QECCs based on CSS construction, we can eliminate short cycles presented in the overall Tanner graph.
4. **Utilization of Arbitrary Classical Codes:** Any one or two classical codes can be utilized to construct entanglement-assisted quantum codes using the CSS construction method, as outlined, for qubit case, in the following theorem.

Theorem 2. [81, Corollary 1] *Let $[n, k_1, d_1]$ and $[n, k_2, d_2]$ be two binary linear codes with their parity-check matrices H_1 and H_2 , respectively. There exists an $[[n, k_1 + k_2 - n + c, \min(d_1, d_2); c]]_2$ entanglement-assisted quantum code, and requires c ebits where*

$$c = \text{gfrank} \left(H_1 H_2^T \right). \quad (9)$$

3 Classical QC-LDPC Codes: Tiling Permutation Matrices of Prime and Composite orders

This section is divided into two subsections. In the first subsection, we construct a family of parity-check matrices by tiling permutation matrices of prime order, and we derive the exact rank of the parity-check matrix to compute the code rate. In the second subsection, we introduce a different family of parity-check matrices formed by tiling permutation matrices of composite order, and we obtain an upper bound on the rank of the parity-check matrix, which enables us to compute a lower bound on the code rate.

3.1 Classical QC-LDPC Codes by Tiling Permutation Matrices of Prime Order

Let $\mathbb{F}_p = \{0, 1, 2, \dots, p-1\}$ be the finite field of odd prime order p . We define a matrix M as follows:

$$M = \begin{bmatrix} b_{0,0} & b_{0,1} & \cdots & b_{0,p-1} \\ b_{1,0} & b_{1,1} & \cdots & b_{1,p-1} \\ \vdots & \vdots & \ddots & \vdots \\ b_{p-1,0} & b_{p-1,1} & \cdots & b_{p-1,p-1} \end{bmatrix}, \quad (10)$$

where $b_{i,j} \in \mathbb{F}_p$ for all $0 \leq i, j \leq (p-1)$ and the entries in M are populated based on the Algorithm 1. Let C_M be the collection of all possible distinct $p \times p$ matrices constructed by using Algorithm 1. For each $M \in C_M$, we define a block matrix \mathbf{A}_M as follows:

$$\mathbf{A}_M = \begin{bmatrix} P^{b_{0,0}} & P^{b_{0,1}} & \cdots & P^{b_{0,p-1}} \\ P^{b_{1,0}} & P^{b_{1,1}} & \cdots & P^{b_{1,p-1}} \\ \vdots & \vdots & \ddots & \vdots \\ P^{b_{p-1,0}} & P^{b_{p-1,1}} & \cdots & P^{b_{p-1,p-1}} \end{bmatrix}, \quad (11)$$

where P is the right circulant permutation matrix of order p and M is known as the model matrix of \mathbf{A}_M . Define a class \mathcal{C}_A of block matrices that is associated with the class C_M as follows:

$$\mathcal{C}_A = \{\mathbf{A}_M : \text{for all } M \in C_M\}. \quad (12)$$

Algorithm 1 Constructing the Matrix M in the Class C_M

```

1: procedure CONSTRUCT MATRIX M
2:   Input: Odd prime  $p$  and  $\mathbb{F}_p = \{0, 1, \dots, p-1\}$ .
3:   Output: Matrix  $M \in C_M$ .
4:   Initialize matrix  $M = [b_{i,j}]$  of size  $p \times p$  with all entries set to zero.
5:   for each  $j \in \{1, 2, \dots, p-1\}$  do
6:     Randomly choose  $b_{1,j} \in \mathbb{F}_p \setminus \{0\}$  without repetition.
7:   end for
8:   Choose  $k_1 \in \mathbb{F}_p \setminus \{0, 1\}$ 
9:   for each  $j \in \{0, 1, \dots, p-1\}$  do
10:    Set  $b_{2,j} = (k_1 b_{1,j}) \bmod (p)$ .
11:  end for
12:  for each  $i \in \{3, 4, \dots, p-1\}$  do
13:    Choose  $k_{i-1} \in \mathbb{F}_p \setminus \{0, 1, k_1, \dots, k_{i-2}\}$ .
14:    for each  $j \in \{0, 1, \dots, p-1\}$  do
15:      Set  $b_{i,j} = (k_{i-1} b_{1,j}) \bmod (p)$ .
16:    end for
17:  end for
18:  return  $M$ 
19: end procedure

```

Let r_i and r_j be two distinct arbitrary rows from the matrix M . Then there exist distinct $k_i, k_j \in \mathbb{F}_p$ such that $r_i = (k_i x_0, k_i x_1, \dots, k_i x_{(p-1)})$ and $r_j = (k_j x_0, k_j x_1, \dots, k_j x_{(p-1)})$, where $x_q \in \mathbb{F}_p$, for all $0 \leq q \leq (p-1)$ and $x_\lambda \neq x_\mu$, for $\lambda \neq \mu$. It is easy to check that the vector $r_i - r_j$ has non-repeated elements under modulo p . Therefore, by Proposition 1, the Tanner graph of the classical QC-LDPC code having \mathbf{A}_M as a parity check matrix is devoid of cycles of length 4.

To determine the code rate of the classical QC-LDPC code corresponding to a parity check matrix \mathbf{A}_M in the class C_A , first we compute the gfrank of the following particular block matrix \mathbf{H} from the class C_A

$$\mathbf{H} = \begin{bmatrix} h_{0,0} & h_{0,1} & \cdots & h_{0,p-1} \\ h_{1,0} & h_{1,1} & \cdots & h_{1,p-1} \\ \vdots & \vdots & \ddots & \vdots \\ h_{p-1,0} & h_{p-1,1} & \cdots & h_{p-1,p-1} \end{bmatrix}, \quad (13)$$

where $h_{ij} = P^{\text{mod}(ij,p)}$ and then we comment on $\text{gfrank}(\mathbf{A}_M)$. We require the following lemma to compute the $\text{gfrank}(\mathbf{H})$.

Lemma 1. For $0 \leq i, k \leq (p-1)$, let $R_i^{(k)}$ represents i^{th} row in the k^{th} block row³ of \mathbf{H} , and let $\langle (v_1, \dots, v_{p^2}), (u_1, \dots, u_{p^2}) \rangle = v_1 u_1 + \dots + v_{p^2} u_{p^2}$, where v_i and u_j are the binary scalars for all i and j . Then, we have

$$\langle R_i^{(k)}, R_j^{(l)} \rangle = \begin{cases} p, & \text{if } i = j \text{ and } k = l, \\ 0, & \text{if } i \neq j \text{ and } k = l, \\ 1, & \text{otherwise.} \end{cases}$$

³ $R^{(k)} = [h_{k,0}, h_{k,1}, \dots, h_{k,(p-1)}]$ stands for k^{th} block row of \mathbf{H}

Proof. First, with $k = l$, it is easy to check that

$$\langle R_i^{(k)}, R_j^{(l)} \rangle = \begin{cases} p, & \text{if } i = j, \\ 0, & \text{otherwise.} \end{cases}$$

Next, we consider the case $k \neq l$. One can easily see that the position of entry 1 in the j^{th} block column ⁴ of $R_r^{(s)}$ is $jp + \text{mod}(r + \text{mod}(js, p), p)$. Let $R_x^{(k)}$ and $R_y^{(l)}$ be arbitrary given rows from two arbitrary block rows k and l , respectively. If we choose $j = \frac{(y-x)}{(k-l)} \in \mathbb{F}_p$, then it is easy to check that

$$jp + \text{mod}(x + \text{mod}(kj, p), p) = jp + \text{mod}(y + \text{mod}(lj, p), p),$$

which concludes that $R_x^{(k)}$ and $R_y^{(l)}$ have the same position of entry 1 in j^{th} block column. We cannot find more than one such j since by construction the Tanner graph of \mathbf{H} is devoid of cycles of length 4. So, for each pair $(R_x^{(k)}, R_y^{(l)})$ there exists a unique j in \mathbb{F}_p such that $\langle R_x^{(k)}, R_y^{(l)} \rangle = 1$, proving the result. \square

Remark 2. *The above lemma also holds for any block matrix from the class \mathcal{C}_A .*

Theorem 3. *Let H be a submatrix of \mathbf{H} consisting distinct k ($1 \leq k \leq p$) block rows. Then, $\text{gfrank}(H) = p + (k - 1)(p - 1)$.*

Proof. Assume that $k = 1$. Then, $\text{gfrank}(H) = p$ since the matrix is already in row echelon form. Next, consider the case when $k = 2$. The vector sum of all rows in the first block row is equal to the vector sum of all rows in the second block row, i.e.,

$$\sum_{i=0}^{p-1} R_i^{(0)} = \sum_{j=0}^{p-1} R_j^{(1)} \implies \sum_{i=0}^{p-1} R_i^{(0)} + \sum_{j=0}^{p-1} R_j^{(1)} = 0,$$

concluding that the rows are linearly dependent. Hence, one can delete at least one row from the first block row or the other. Now, consider the k block rows of H , and delete one row from every block row except the first one. Without loss of generality, let us delete the last row from all block rows except the first one, and let

$$\sum_{i_1=0}^{p-1} \alpha_{i_1}^{(0)} R_{i_1}^{(0)} + \sum_{i_2=0}^{p-2} \alpha_{i_2}^{(1)} R_{i_2}^{(1)} + \dots + \sum_{i_k=0}^{p-2} \alpha_{i_k}^{(k-1)} R_{i_k}^{(k-1)} = 0, \quad (14)$$

where coefficients are the binary scalars. Define the inner product on $\mathbb{F}_2^{p^2}$, where \mathbb{F}_2 is the binary field, as follows:

$$\langle (v_1, \dots, v_{p^2}), (u_1, \dots, u_{p^2}) \rangle_{\mathbb{F}_2} = \sum_{i=1}^{p^2} v_i u_i \pmod{2}. \quad (15)$$

Taking the inner product, as defined by (15), of equation (14) with each of the remaining rows from all the block rows $R^{(0)}, R^{(1)}, \dots, R^{(k-1)}$, and applying Lemma 1, results in the following system of linear equations:

$$\alpha_{j_1}^{(0)} + \sum_{i_2=0}^{p-2} \alpha_{i_2}^{(1)} + \dots + \sum_{i_k=0}^{p-2} \alpha_{i_k}^{(k-1)} = 0, \quad \forall 0 \leq j_1 \leq (p-1);$$

⁴ $\mathcal{C}^{(j)} = [h_{0,j}^T, h_{1,j}^T, \dots, h_{p-1,j}^T]^T$ denotes j^{th} block column of \mathbf{H}

$$\begin{aligned}
\sum_{i_1=0}^{p-1} \alpha_{i_1}^{(0)} + \alpha_{j_2}^{(1)} + \cdots + \sum_{i_k=0}^{p-2} \alpha_{i_k}^{(k-1)} &= 0, \quad \forall 0 \leq j_2 \leq (p-2); \\
&\vdots \\
\sum_{i_1=0}^{p-1} \alpha_{i_1}^{(0)} + \sum_{i_2=0}^{p-2} \alpha_{i_2}^{(1)} + \cdots + \alpha_{j_k}^{(k-1)} &= 0, \quad \forall 0 \leq j_k \leq (p-2).
\end{aligned}$$

Now, consider the first system of linear equations. The number of terms in any equation of the first system is odd; so, one of the terms must be zero. If $\alpha_{j_1}^{(0)} = 0$ for some $0 \leq j_1 \leq (p-1)$, then the first system gives $\alpha_{j_1}^{(0)} = 0$ for all j_1 . If $\alpha_m^{(l)} = 0$ for some $0 \leq m \leq (p-2)$ and $1 \leq l \leq (k-1)$, then by using the l^{th} system we can get $\alpha_m^{(l)} = 0$ for all $0 \leq m \leq (p-2)$. By using similar arguments one can easily show that $\alpha_i^{(j)} = 0$ for all i and j . Hence, the result follows. \square

Corollary 3. *Let B be any submatrix of \mathbf{A}_M with distinct λ ($1 \leq \lambda \leq p$) block rows. Then, $\text{gfrank}(B) = p + (\lambda - 1)(p - 1)$.*

Proof. Let B be any submatrix of \mathbf{A}_M consisting λ number of block rows, and let

$$D = \begin{bmatrix} d_{0,0} & d_{0,1} & \cdots & d_{0,p-1} \\ d_{1,0} & d_{1,1} & \cdots & d_{1,p-1} \\ \vdots & \vdots & \ddots & \vdots \\ d_{\lambda-1,0} & d_{\lambda-1,1} & \cdots & d_{\lambda-1,p-1} \end{bmatrix} \quad (16)$$

be the corresponding model matrix of B . By employing elementary row and column operations on the model matrix D , we can get the model matrix associated with some submatrix of \mathbf{H} consisting of distinct λ block rows. This proves the result. \square

Example 6. *Let E be any submatrix of \mathbf{A}_M consisting distinct λ ($1 \leq \lambda \leq p$) block rows. Then, by Corollary 3, there exists a classical QC-LDPC code \mathcal{C} with parameters $[p^2, (p-1)(p-\lambda+1)]$ such that the Tanner graph of \mathcal{C} has girth > 4 .*

3.2 Classical QC LDPC Codes by Tiling Permutation Matrices of Composite Order

Let \mathbb{Z}_n denote a finite ring with n elements, where n is any positive integer. Given two positive integers q and r such that $q < r$, we aim to find the smallest composite number n such that the following matrix G can be defined:

$$G = \left[\begin{array}{c|ccc} a_{0,0} & a_{0,1} & \cdots & a_{0,r-1} \\ \hline a_{1,0} & a_{1,1} & \cdots & a_{1,r-1} \\ \vdots & \vdots & \ddots & \vdots \\ a_{q-1,0} & a_{q-1,1} & \cdots & a_{q-1,r-1} \end{array} \right], \quad (17)$$

where $a_{i,j} = 0$ (for $i = 0$ or $j = 0$), $a_{i,j} \in \mathbb{Z}_n \setminus \{0\}$ for all $1 \leq i \leq q-1$ and $1 \leq j \leq r-1$, and the nonzero entries are populated according to Algorithm 2. We now define \mathcal{C}_G as the collection of all possible G matrices that can be constructed using Algorithm 2 for the same n .

Let P be the right circulant permutation matrix of order n . We define a class \mathcal{C}_K of block matrices $\mathbf{K}_G = [P^{a_{i,j}}]$ associated with $G \in \mathcal{C}_G$. In the subsequent theorem, we have provided an upper bound on the gfrank of the matrix \mathbf{K}_G .

Algorithm 2 Constructing the Matrix G in the Class C_G

```

1: procedure CONSTRUCT MATRIX  $G$ 
2:   Input: Composite integer  $n$ ,  $\mathbb{Z}_n = \{0, 1, \dots, n-1\}$  and integers  $q, r$  such that
    $q < r < n$ .
3:   Output: Matrix  $G \in C_G$ .
4:   Initialize matrix  $G' = [a_{i,j}]$ , where  $1 \leq i \leq q-1, 1 \leq j \leq r-1$ , with all entries set
   to zero.
5:   for each  $i \in \{1, 2, \dots, q-1\}$  do
6:     Initialize  $\text{itr}_{\max} = \frac{(n-1)!}{(n-r)!}$ .
7:     Create a set  $S = \{1, \dots, i\}$ .  $\triangleright$  Include all the indices of the filled rows.
8:     if  $\text{itr} < \text{itr}_{\max}$  then
9:       Randomly generate a vector  $R_i$  of length  $(r-1)$  over  $\mathbb{Z}_n \setminus \{0\}$  such that the
       entries of  $R_i$  are distinct,  $R_i \neq R_j$  for all  $j \leq i$ , and  $R_i$  is not in the set of previously
       generated vectors.
10:      Replace the  $i^{\text{th}}$  row in  $G'$  by the vector  $R_i$ .
11:      for each  $j \in S \setminus \{i\}$  do
12:        if The vector  $\text{mod}((R_i - R_j), n)$  contains repeated entries from  $\mathbb{Z}_n$  then
13:          Error:  $\text{itr} = \text{itr} + 1$  return to step 8
14:        end if
15:      end for
16:    else
17:      Choose next  $n$  and go to step 2.
18:    end if
19:  end for
20:  return  $G$ 
21: end procedure

```

Theorem 4. Let \mathbf{K}_G be a matrix from the class C_K and let S be a set such that $i \in S$ if and only if $\gcd(a_{i,0}, a_{i,1}, \dots, a_{i,r-1}) \geq 2$ and $\gcd(a_{i,0}, a_{i,1}, \dots, a_{i,r-1})$ divides n , where $(a_{i,0}, a_{i,1}, \dots, a_{i,r-1})$ is the i^{th} ($0 \leq i \leq (q-1)$) row in the model matrix of \mathbf{K}_G . Then we have

$$\text{frank}(\mathbf{K}_G) \leq 1 + q(n-1) + |S| - \sum_{i \in S} \gcd(a_{i,0}, \dots, a_{i,r-1}).$$

Proof. Let $\gcd(a_{i,0}, a_{i,1}, \dots, a_{i,r-1}) = d \geq 2$ for some i^{th} row. Now, consider the j^{th} block column of i^{th} block row of the matrix \mathbf{K}_G . Since d is a divisor of n and $a_{i,j}$, we assume that $n = \ell d$, $a_{i,j} = md$ for some positive integers ℓ and m , where $m < \ell$. We partition the identity matrix and $P^{a_{i,j}}$ into ℓ parts, each part with d rows as in Figure 3. Let $1 \leq t \leq d$, then the positions of entry 1 in all the t^{th} rows from each part of the partition of the identity matrix are given by the set

$$Y_1 = \{t, t+d, t+2d, \dots, t+(\ell-1)d\}.$$

Similarly, the positions of entry 1 in all the t^{th} rows from each part of the partition of the matrix $P^{a_{i,j}}$ are given by the following set:

$$Y_2 = \{\text{mod}(a_{i,j} + t, n), \dots, \text{mod}(a_{i,j} + (\ell-1)d + t, n)\}.$$

By substituting $n = \ell d$ and $a_{i,j} = md$ in the set Y_2 , we have

$$Y_2 = \{\text{mod}(md + t, \ell d), \dots, \text{mod}((m + (\ell-1))d + t, \ell d)\}.$$

Example 7. *Let*

$$H = \begin{bmatrix} I & I & I & I & I \\ I & P & P^2 & P^3 & P^4 \\ I & P^2 & P^4 & P^6 & P^8 \end{bmatrix}$$

be a parity-check matrix, for $n = 10$. Computationally, we get $\text{gfrank}(H)=27$ that meets the upper bound given in Theorem 4 with the corresponding $(50, 23)$ classical QC-LDPC code.

4 Entanglement-assisted Quantum Codes

To improve readability, this section has been divided into two subsections.

4.1 Entanglement-Assisted Quantum QC-LDPC Codes

In this subsection, we discuss the construction of EA quantum QC-LDPC codes. Based on Theorem 2, we construct two families of EA quantum QC-LDPC codes, depending on the classical QC-LDPC codes used, i.e., one in which a single classical QC-LDPC code is employed, and another where two distinct classical QC-LDPC codes are used. Furthermore, when the EA CSS code is constructed using two different classical QC-LDPC codes, the overall Tanner graph has girth greater than 4.

Let

$$H_x = \begin{bmatrix} A_{0,0} & A_{0,1} & \cdots & A_{0,p-1} \\ A_{1,0} & A_{1,1} & \cdots & A_{1,p-1} \\ \vdots & \vdots & \ddots & \vdots \\ A_{\ell_1-1,0} & A_{\ell_1-1,1} & \cdots & A_{\ell_1-1,p-1} \end{bmatrix}, \quad (18)$$

$$H_z = \begin{bmatrix} B_{0,0} & B_{0,1} & \cdots & B_{0,p-1} \\ B_{1,0} & B_{1,1} & \cdots & B_{1,p-1} \\ \vdots & \vdots & \ddots & \vdots \\ B_{\ell_2-1,0} & B_{\ell_2-1,1} & \cdots & B_{\ell_2-1,p-1} \end{bmatrix}, \quad (19)$$

be two submatrices of the matrix \mathbf{A}_M . Assume that $2 \leq \ell_1, \ell_2 \leq p$ and $\ell_1 + \ell_2 \leq p$. In addition, consider that there is no block row common to H_x and H_z . Further, let all the block rows in each matrix be distinct.

Theorem 5. *Let C_1 and C_2 be two classical QC-LDPC codes, and let H_x and H_z be their parity-check matrices, respectively. Then there exists an entanglement-assisted quantum QC-LDPC code with the parameters $[[p^2, p^2 - 2p - (p-1)(\ell_1 + \ell_2 - 2) + 1; 1]]_2$. Further, overall Tanner graph of EA quantum QC-LDPC code has girth greater than 4.*

Proof. The result follows from Corollary 3 and Remark 2. \square

Example 8. *For $p = 3$, let $H_x = [I \ P \ P^2]$ and $H_z = [I \ P^2 \ P]$ be two parity-check matrices of the classical QC-LDPC codes C_1 and C_2 , respectively. Then, by Theorem 5, there exists an entanglement-assisted quantum QC-LDPC code with the parameters $[[9, 4, 2; 1]]_2$. Moreover, the associated Tanner graph is shown in Figure 4.*

Lemma 2. *Let $p \geq 3$ be a prime, and let*

$$H = \begin{bmatrix} I & P^i & P^{2i} & \cdots & P^{(p-1)i} \\ I & P^j & P^{2j} & \cdots & P^{(p-1)j} \end{bmatrix},$$

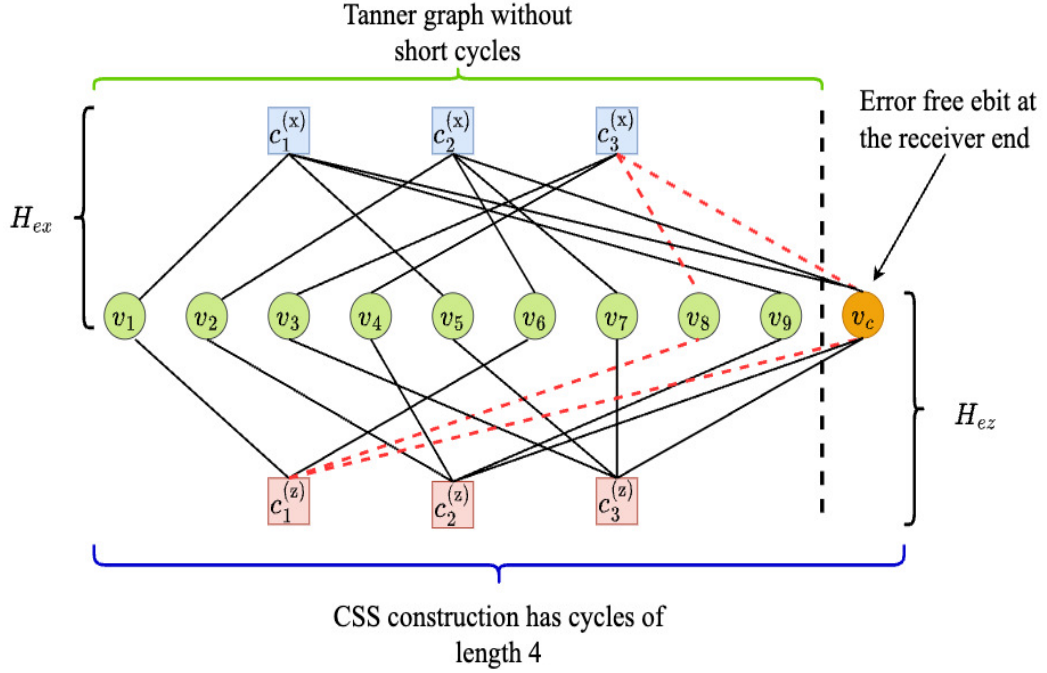


Figure 4: Tanner graph for the code $[[9, 4, 2; 1]]_2$ contains nine variable nodes v_1, \dots, v_9 at the transmitter end and variable node v_c at the receiver end corresponding to the pre-shared entangled bits. Since the node v_c is assumed to be error-free, it does not participate in the decoding. For entanglement-unassisted case, the Tanner graph has short cycles of length 4, as shown by red dotted lines. This is due to the CSS construction.

where $0 \leq i < j \leq (p-1)$, be a parity-check matrix of classical QC-LDPC code \mathcal{C} . The code \mathcal{C} has minimum distance 4.

Proof. Since every column in H is non-zero, it follows that any single column of H is linearly independent. Now consider any two columns from H . If both are from the same block column, they are obviously linearly independent. If they are from different block columns again they are linearly independent since by Lemma 1, the sum of these columns cannot be zero. Next, suppose on the contrary that there exist three distinct columns namely c_1, c_2 and c_3 such that

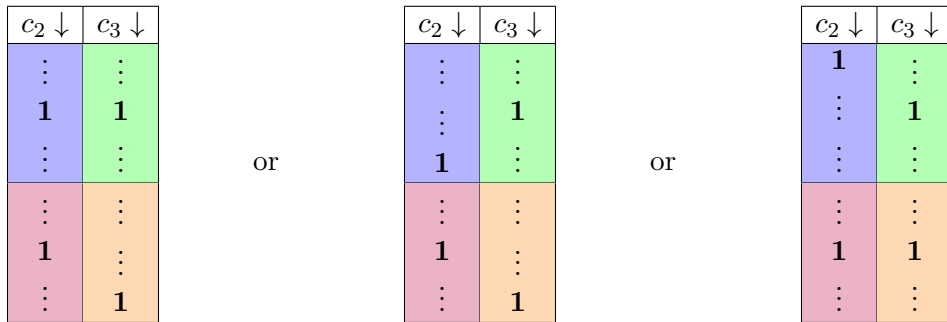


Figure 5: Different possible combinations, depending on the positions of entry 1, of the columns c_2 and c_3 from the matrix H .

$$c_1 + c_2 + c_3 = 0 \implies \text{wt}(c_1) = \text{wt}(c_2 + c_3). \quad (20)$$

By Figure 5, we have $\text{wt}(c_2 + c_3) = 4$ or $\text{wt}(c_2 + c_3) = 2$. If $\text{wt}(c_2 + c_3)$ is 4, then, by Equation (20), $\text{wt}(c_1) = 4$ which leads to a contradiction since the weight of each column vector is 2. If $\text{wt}(c_2 + c_3)$ is 2, then $\text{wt}(c_2 + c_3)$ must be zero in one of the block rows whereas $\text{wt}(c_1)$ is 1 in both block rows. Therefore, the column vectors c_1, c_2 and c_3 are linearly independent. Finally, we will prove that there exist four linearly dependent columns in H . Consider the first, second and third block columns of the parity-check matrix H . The sum of the first column from the first block column and $(i + 1)^{\text{th}}$ column from the second block column is given as follows:

$$[e_1, e_1]^T + [e_1, e_{p-j+i+1}]^T = [\mathbf{0}, e_1 + e_{p-j+i+1}]^T,$$

where $e_i = \underbrace{[0, \dots, \overset{i^{\text{th place}}}{1}, \dots, 0]}_{p\text{-tuple}}$, and $\mathbf{0} = \underbrace{[0, \dots, 0]}_{p\text{-tuple}}$. Similarly, the sum of the $(j + 1)^{\text{th}}$ column from the second block column and $(j + i + 1)$ column from the third block column is given as follows:

$$[e_{p-i+j+1}, e_1]^T + [e_{p-i+j+1}, e_{p-j+i+1}]^T = [\mathbf{0}, e_1 + e_{p-j+i+1}]^T.$$

We have shown that any three columns of the parity-check matrix are linearly independent and there exist four linearly dependent columns. Hence, by [82, Corollary 4.5.7], the proof is completed. \square

Lemma 3. *Let the symbols have the same significances as before. Let $p \geq 3$ be a prime, and let*

$$H = \begin{bmatrix} I & P^i & P^{2i} & \dots & P^{(p-1)i} \\ I & P^j & P^{2j} & \dots & P^{(p-1)j} \end{bmatrix},$$

where $0 \leq i < j \leq (p - 1)$, be a parity-check matrix of classical QC-LDPC code \mathcal{C} . Then

$$\min \left\{ \text{wt} \left(\sum_{i=1}^s R_i^{(1)} + \sum_{j=1}^t R_j^{(2)} \right) : s \in \{1, 2, \dots, p\}, t \in \{1, 2, \dots, p - 1\} \right\} = p.$$

Proof. By [82, Lemma 4.3.5] and Lemma 1, we have

$$\text{wt} \left(\sum_{i=1}^s R_i^{(1)} + \sum_{j=1}^t R_j^{(2)} \right) = \sum_{i=1}^s \text{wt}(R_i^{(1)}) + \sum_{j=1}^t \text{wt}(R_j^{(2)}) - 2st = (s + t)p - 2st.$$

Consider the function $f(s, t) = (s + t)p - 2st$, where $s \in [1, p], t \in [1, p - 1]$. Our aim to find the minimum value of the function $f(s, t)$ by employing the second order derivative test.

We begin by finding the first-order partial derivatives of $f(s, t)$ with respect to s and t . First-order partial derivatives of $f(s, t)$ with respect to s and t are

$$\frac{\partial f}{\partial s} = \frac{\partial}{\partial s} ((s + t)p - 2st) = p - 2t \text{ and } \frac{\partial f}{\partial t} = \frac{\partial}{\partial t} ((s + t)p - 2st) = p - 2s,$$

respectively. To find the critical points, we set both of the first-order partial derivatives equal to zero, i.e.,

$$\frac{\partial f}{\partial s} = p - 2t = 0 \implies t = \frac{p}{2} \text{ and } \frac{\partial f}{\partial t} = p - 2s = 0 \implies s = \frac{p}{2}.$$

So, we have only one critical point $(s, t) = (\frac{p}{2}, \frac{p}{2})$ within the interior of the domain ($s \in [1, p], t \in [1, p-1]$). It is trivial to check that second-order partial derivatives with respect to s and t are both zero. Further, the second-order mixed partial derivative is

$$\frac{\partial^2 f}{\partial s \partial t} = \frac{\partial^2 f}{\partial s \partial t} = \frac{\partial}{\partial t}(p-2t) = -2.$$

At the critical point $(s, t) = (\frac{p}{2}, \frac{p}{2})$, discriminant D is

$$\left(\frac{\partial^2 f}{\partial s^2}\right) \left(\frac{\partial^2 f}{\partial t^2}\right) - \left(\frac{\partial^2 f}{\partial s \partial t}\right)^2 = -4 < 0.$$

Therefore, the point $(s, t) = (\frac{p}{2}, \frac{p}{2})$ is a **saddle point**, meaning it is neither a maximum nor a minimum. Since the second derivative test indicates a saddle point, we must examine the boundary points of $f(s, t)$ within the given intervals $s \in [1, p]$ and $t \in [1, p-1]$. The values of the function $f(s, t)$ at different boundary points are as follows:

$$f(1, 1) = 2(p-1), \quad f(1, p-1) = p^2 - 2p + 2, \quad f(p, 1) = p^2 - p, \quad f(p, p-1) = p.$$

We find that the minimum value occurs at $(s, t) = (p, p-1)$, and the minimum value of the function is p . Since $\{1, 2, \dots, p\} \subset [1, p]$ and $\{1, 2, \dots, p-1\} \subset [1, p-1]$, this completes the proof. \square

Example 9. For a prime $p \geq 5$, let

$$H_x = \begin{bmatrix} I & P^{i_1} & P^{2i_1} & \dots & P^{(p-1)i_1} \\ I & P^{i_2} & P^{2i_2} & \dots & P^{(p-1)i_2} \end{bmatrix}, \quad (21)$$

$$H_z = \begin{bmatrix} I & P^{i_3} & P^{2i_3} & \dots & P^{(p-1)i_3} \\ I & P^{i_4} & P^{2i_4} & \dots & P^{(p-1)i_4} \end{bmatrix}, \quad (22)$$

be two parity-check matrices of the classical QC-LDPC codes \mathcal{C}_1 and \mathcal{C}_2 , respectively. Then, by Theorem 5, Lemma 2 and Lemma 3, there exists a non-degenerate entanglement-assisted quantum QC-LDPC code with the parameters $[[p^2, (p-1)(p-3), 4; 1]]_2$. The minimum stabilizer generators of the code are given as follows:

X-stabilizers: $\otimes_{w=0}^{(p-1)} (I^{\otimes(i_1 w+i)} \otimes X \otimes I^{\otimes((p-1)-i_1 w-i)} \otimes X)$ is the stabilizer generator corresponding to i^{th} ($0 \leq i \leq (p-1)$) row in the first block row of H_x . Further, $\otimes_{w=0}^{(p-1)} (I^{\otimes(i_2 w+i)} \otimes X \otimes I^{\otimes((p-1)-i_2 w-i)} \otimes X)$ is the stabilizer generator corresponding to the i^{th} ($0 \leq i \leq (p-2)$) row in the second block rows of H_x .

Z-stabilizers: $\otimes_{w=0}^{(p-1)} (I^{\otimes(i_3 w+i)} \otimes Z \otimes I^{\otimes((p-1)-i_3 w-i)} \otimes Z)$ is the stabilizer generator corresponding to i^{th} ($0 \leq i \leq (p-1)$) row in the first block row of H_z . Further, $\otimes_{w=0}^{(p-1)} (I^{\otimes(i_4 w+i)} \otimes Z \otimes I^{\otimes((p-1)-i_4 w-i)} \otimes Z)$ is the stabilizer generator corresponding to the i^{th} ($0 \leq i \leq (p-2)$) row in the second block rows of H_z .

Extended parity-check matrices of H_x and H_z are given as follows:

$$H_{ex} = \left[\begin{array}{cccc|c} I & P^{i_1} & P^{2i_1} & \dots & P^{(p-1)i_1} & \mathbf{A} \\ I & P^{i_2} & P^{2i_2} & \dots & P^{(p-1)i_2} & \mathbf{A} \end{array} \right],$$

$$H_{ez} = \left[\begin{array}{cccc|c} I & P^{i_3} & P^{2i_3} & \dots & P^{(p-1)i_3} & \mathbf{A} \\ I & P^{i_4} & P^{2i_4} & \dots & P^{(p-1)i_4} & \mathbf{A} \end{array} \right],$$

where $\mathbf{A} = \underbrace{[1, 1, \dots, 1]^T}_{p \text{ tuple}}$.

Example 10. For $p = 7$, let

$$H_x = \begin{bmatrix} I & I & I & I & I & I & I \\ I & P & P^2 & P^3 & P^4 & P^5 & P^6 \\ I & P^2 & P^4 & P^6 & P & P^3 & P^5 \end{bmatrix},$$

$$H_z = \begin{bmatrix} I & P^4 & P & P^5 & P^2 & P^6 & P^3 \\ I & P^5 & P^3 & P & P^6 & P^4 & P^2 \\ I & P^6 & P^5 & P^4 & P^3 & P^2 & P \end{bmatrix}$$

be two parity-check matrices of the classical QC-LDPC codes \mathcal{C}_1 and \mathcal{C}_2 , respectively. Then, by Theorem 5, there exists an entanglement-assisted quantum QC-LDPC code with the parameters $[[49, 12, 6; 1]]_2$. The minimum stabilizer generators of the code are given as follows:

X-stabilizers: $(I^{\otimes i} \otimes X \otimes I^{\otimes(6-i)})^{\otimes 7} \otimes X$ is the stabilizer generator corresponding to i^{th} ($0 \leq i \leq 6$) row in the first block row of H_x . Further, $\otimes_{w=0}^6 (I^{\otimes(w+i)} \otimes X \otimes I^{\otimes(6-w-i)}) \otimes X$ and $\otimes_{w=0}^6 (I^{\otimes(2w+i)} \otimes X \otimes I^{\otimes(6-2w-i)}) \otimes X$ are the stabilizer generators corresponding to the i^{th} ($0 \leq i \leq 5$) row in the second and third block rows of H_x , respectively.

Z-stabilizers: $\otimes_{w=0}^6 (I^{\otimes(4w+i)} \otimes Z \otimes I^{\otimes(6-4w-i)}) \otimes Z$ is the stabilizer generator corresponding to i^{th} ($0 \leq i \leq 6$) row in the first block row of H_z . In addition, $\otimes_{w=0}^6 (I^{\otimes(5w+i)} \otimes Z \otimes I^{\otimes(6-5w-i)}) \otimes Z$ and $\otimes_{w=0}^6 (I^{\otimes(6w+i)} \otimes Z \otimes I^{\otimes(6-6w-i)}) \otimes Z$ are the stabilizer generators corresponding to i^{th} ($0 \leq i \leq 5$) row in the second and third block rows of H_z , respectively.

Extended parity check matrices of H_x and H_z are given as follows:

$$H_{ex} = \left[\begin{array}{ccccccc|c} I & I & I & I & I & I & I & \mathbf{A} \\ I & P & P^2 & P^3 & P^4 & P^5 & P^6 & \mathbf{A} \\ I & P^2 & P^4 & P^6 & P & P^3 & P^5 & \mathbf{A} \end{array} \right],$$

$$H_{ez} = \left[\begin{array}{ccccccc|c} I & P^4 & P & P^5 & P^2 & P^6 & P^3 & \mathbf{A} \\ I & P^5 & P^3 & P & P^6 & P^4 & P^2 & \mathbf{A} \\ I & P^6 & P^5 & P^4 & P^3 & P^2 & P & \mathbf{A} \end{array} \right],$$

where $\mathbf{A} = [1, 1, 1, 1, 1, 1, 1]^T$.

Lemma 4. Let $p > 3$ be a prime, and let $M = J_p + I_p$, where J_p is the $p \times p$ all-ones matrix and I_p is the $p \times p$ identity matrix. Then, $\text{gfrank}(M) = (p - 1)$.

Proof. For all $3 \leq i \leq p$, replacing R_i by $R_i + R_2$ in the given matrix M results in the following matrix M_1 :

$$M \sim M_1 = \left[\begin{array}{cc|cccc} 0 & 1 & 1 & 1 & \cdots & 1 & 1 \\ 1 & 0 & 1 & 1 & \cdots & 1 & 1 \\ \hline 0 & 1 & 1 & 0 & \cdots & 0 & 0 \\ 0 & 1 & 0 & 1 & \cdots & 0 & 0 \\ \vdots & \vdots & \vdots & \vdots & \ddots & \vdots & \vdots \\ 0 & 1 & 0 & 0 & \cdots & 1 & 0 \\ 0 & 1 & 0 & 0 & \cdots & 0 & 1 \end{array} \right].$$

Next, replacing R_1 by $R_1 + \sum_{i=3}^p R_i$ followed by interchanging R_2 and R_1 ($R_2 \leftrightarrow R_1$) in the above matrix M_1 results in the following matrix M_2 :

$$M_1 \sim M_2 = \left[\begin{array}{cc|cccc} 1 & 0 & 1 & 1 & \cdots & 1 & 1 \\ 0 & 0 & 0 & 0 & \cdots & 0 & 0 \\ \hline 0 & 1 & 1 & 0 & \cdots & 0 & 0 \\ 0 & 1 & 0 & 1 & \cdots & 0 & 0 \\ \vdots & \vdots & \vdots & \vdots & \ddots & \vdots & \vdots \\ 0 & 1 & 0 & 0 & \cdots & 1 & 0 \\ 0 & 1 & 0 & 0 & \cdots & 0 & 1 \end{array} \right].$$

Finally, for all $3 \leq i \leq (p-1)$, replacing R_i by $R_i + R_p$ and $R_2 \leftrightarrow R_p$ in the matrix M_2 results in the following matrix M_3 :

$$M_2 \sim M_3 = \left[\begin{array}{cc|cccc} 1 & 0 & 1 & 1 & \cdots & 1 & 1 \\ 0 & 1 & 0 & 0 & \cdots & 0 & 1 \\ \hline 0 & 0 & 1 & 0 & \cdots & 0 & 1 \\ 0 & 0 & 0 & 1 & \cdots & 0 & 1 \\ \vdots & \vdots & \vdots & \vdots & \ddots & \vdots & \vdots \\ 0 & 0 & 0 & 0 & \cdots & 1 & 1 \\ 0 & 0 & 0 & 0 & \cdots & 0 & 0 \end{array} \right].$$

From the above matrix, it is straightforward that $\text{gfrank}(M) = (p-1)$. This completes the proof. \square

Theorem 6. *Let \mathcal{C} be a classical QC-LDPC code with the parity-check matrix H that contains ℓ distinct number of block rows from the matrix \mathbf{A}_M such that $2\ell < p$. Then, there exists an entanglement-assisted quantum QC-LDPC code with the parameters $[[p^2, (p-1)(p-\ell+1); p+(\ell-1)(p-1)]]_2$. Moreover, the Tanner graph of the code \mathcal{C} has girth > 4 .*

Proof. By employing Corollary 3, we can obtain $\text{gfrank}(H)$. Let i^{th} block row of H be $(P^{k_i x_0}, P^{k_i x_1}, \dots, P^{k_i x_{(p-1)}})$, where $k_i \in \mathbb{F}_p$ for all $0 \leq i \leq (\ell-1)$. Then the (i, j) -th entry of the matrix HH^T is $P^{(k_i - k_j)x_0} + P^{(k_i - k_j)x_1} + \dots + P^{(k_i - k_j)x_{(p-1)}}$. Therefore,

$$HH^T = \begin{bmatrix} I_p & J_p & \cdots & J_p & J_p \\ J_p & I_p & \cdots & J_p & J_p \\ \vdots & \vdots & \ddots & \vdots & \vdots \\ J_p & J_p & \cdots & I_p & J_p \\ J_p & J_p & \cdots & J_p & I_p \end{bmatrix}_{(\ell p) \times (\ell p)},$$

where J_p is the $p \times p$ all-ones matrix and I_p is the $p \times p$ identity matrix. For each $0 \leq u \leq (p-1)$ and $1 \leq v \leq (\ell-1)$, we replace $R_u^{(v)}$ ⁵ by $(R_u^{(v)} + \sum_{u=0}^{(p-1)} R_u^{(0)})$ in the matrix HH^T to obtain

$$\begin{bmatrix} I_p & J_p & \cdots & J_p & J_p \\ \mathbf{0} & I_p + J_p & \cdots & \mathbf{0} & \mathbf{0} \\ \vdots & \vdots & \ddots & \vdots & \vdots \\ \mathbf{0} & \mathbf{0} & \cdots & I_p + J_p & \mathbf{0} \\ \mathbf{0} & \mathbf{0} & \cdots & \mathbf{0} & I_p + J_p \end{bmatrix}_{(\ell p) \times (\ell p)},$$

⁵ $R_u^{(v)}$ represents u^{th} row of v^{th} block row of the matrix HH^T .

where $\mathbf{0}$ represents the $p \times p$ zero matrix. By Lemma 4, one can easily conclude that $\text{gfrank}(HH^T)$ is $p + (\ell - 1)(p - 1)$. By construction, the Tanner graph of the code \mathcal{C} has girth > 4 ; hence, proved. \square

4.2 Entanglement-Assisted Quasi-Cyclic Spatially-Coupled LDPC Codes

In this subsection, we discuss the construction of entanglement-assisted quasi-cyclic spatially-coupled LDPC codes. Based on Theorem 2, we construct two families of EA quantum QC-SC-LDPC codes. Specifically, when the EA quantum QC-SC-LDPC code is constructed using two different classical QC-SC-LDPC codes, the overall Tanner graph has a girth greater than 4. Before presenting the main results of this subsection, we first state the following lemma.

Lemma 5. *For a prime $p > 3$, let J_p denote the $p \times p$ all-ones matrix, and let I_p and $\mathbf{0}$ represent the $p \times p$ identity matrix and the $p \times p$ zero matrix, respectively. We define a block matrix M with γ block rows and γ block columns as follows:*

$$M = \begin{bmatrix} \mathbf{0} & I_p + J_p & I_p + J_p & \cdots & I_p + J_p & I_p + J_p \\ I_p + J_p & \mathbf{0} & I_p + J_p & \cdots & I_p + J_p & I_p + J_p \\ I_p + J_p & I_p + J_p & \mathbf{0} & \cdots & I_p + J_p & I_p + J_p \\ \vdots & \vdots & \vdots & \ddots & \vdots & \vdots \\ I_p + J_p & I_p + J_p & I_p + J_p & \cdots & \mathbf{0} & I_p + J_p \\ I_p + J_p & I_p + J_p & I_p + J_p & \cdots & I_p + J_p & \mathbf{0} \end{bmatrix}. \quad (23)$$

Then, $\text{gfrank}(M) = (\gamma - 1)(p - 1)$ if γ is odd and $\text{gfrank}(M) = \gamma(p - 1)$ otherwise.

Proof. For simplicity, we divide the proof into two cases depending upon γ : whether γ is even or odd. We will focus on proving the result for odd γ , as similar arguments can be applied to the case when γ is even.

For all $3 \leq i \leq \gamma$, replacing R_i by $R_i + R_2$ in the given block matrix M results in the following matrix M_1 :

$$M \sim M_1 = \left[\begin{array}{cc|cccccc} \mathbf{0} & I_p + J_p & I_p + J_p & I_p + J_p & \cdots & I_p + J_p & I_p + J_p \\ I_p + J_p & \mathbf{0} & I_p + J_p & I_p + J_p & \cdots & I_p + J_p & I_p + J_p \\ \hline \mathbf{0} & I_p + J_p & I_p + J_p & \mathbf{0} & \cdots & \mathbf{0} & \mathbf{0} \\ \mathbf{0} & I_p + J_p & \mathbf{0} & I_p + J_p & \cdots & \mathbf{0} & \mathbf{0} \\ \vdots & \vdots & \vdots & \vdots & \ddots & \vdots & \vdots \\ \mathbf{0} & I_p + J_p & \mathbf{0} & \mathbf{0} & \cdots & I_p + J_p & \mathbf{0} \\ \mathbf{0} & I_p + J_p & \mathbf{0} & \mathbf{0} & \cdots & \mathbf{0} & I_p + J_p \end{array} \right].$$

Next, replacing R_1 by $R_1 + \sum_{i=3}^{\gamma} R_i$ followed by $R_2 \leftrightarrow R_1$ in the above matrix M_1 results in the following matrix M_2 :

$$M_1 \sim M_2 = \left[\begin{array}{cc|cccccc} I_p + J_p & \mathbf{0} & I_p + J_p & I_p + J_p & \cdots & I_p + J_p & I_p + J_p \\ \mathbf{0} & \mathbf{0} & \mathbf{0} & \mathbf{0} & \cdots & \mathbf{0} & \mathbf{0} \\ \hline \mathbf{0} & I_p + J_p & I_p + J_p & \mathbf{0} & \cdots & \mathbf{0} & \mathbf{0} \\ \mathbf{0} & I_p + J_p & \mathbf{0} & I_p + J_p & \cdots & \mathbf{0} & \mathbf{0} \\ \vdots & \vdots & \vdots & \vdots & \ddots & \vdots & \vdots \\ \mathbf{0} & I_p + J_p & \mathbf{0} & \mathbf{0} & \cdots & I_p + J_p & \mathbf{0} \\ \mathbf{0} & I_p + J_p & \mathbf{0} & \mathbf{0} & \cdots & \mathbf{0} & I_p + J_p \end{array} \right].$$

Finally, for all $3 \leq i \leq (\gamma - 1)$, replacing R_i with $R_i + R_\gamma$ and swapping $R_2 \leftrightarrow R_\gamma$ in the matrix M_2 , we obtain the following matrix M_3 :

$$M_2 \sim M_3 = \left[\begin{array}{cc|ccccc} I_p + J_p & \mathbf{0} & I_p + J_p & I_p + J_p & \cdots & I_p + J_p & I_p + J_p \\ \mathbf{0} & I_p + J_p & \mathbf{0} & \mathbf{0} & \cdots & \mathbf{0} & I_p + J_p \\ \hline \mathbf{0} & \mathbf{0} & I_p + J_p & \mathbf{0} & \cdots & \mathbf{0} & I_p + J_p \\ \mathbf{0} & \mathbf{0} & \mathbf{0} & I_p + J_p & \cdots & \mathbf{0} & I_p + J_p \\ \vdots & \vdots & \vdots & \vdots & \ddots & \vdots & \vdots \\ \mathbf{0} & \mathbf{0} & \mathbf{0} & \mathbf{0} & \cdots & I_p + J_p & I_p + J_p \\ \mathbf{0} & \mathbf{0} & \mathbf{0} & \mathbf{0} & \cdots & \mathbf{0} & \mathbf{0} \end{array} \right].$$

By Lemma 4, we have $\text{gfrank}(M) = (\gamma - 1) \times \text{gfrank}(I_p + J_p) = (\gamma - 1)(p - 1)$, which completes the proof for odd γ . Following the similar arguments used to prove the result for odd γ , one can easily prove the result for even γ . \square

Having proved the above lemma, we are now ready to present and prove the main results of this subsection, accompanied by detailed examples.

Let $z = p \geq 5$, $2 \leq \gamma \leq \frac{(p-1)}{2}$, $\kappa = (p - 1)$, $m = 1$, and $L = 4$. Now, we define a base matrix \mathbf{B} and a partitioning matrix \mathbf{P} of size $\gamma \times \kappa$ as follows:

$$\mathbf{B} = \begin{bmatrix} 1 & 1 & \cdots & 1 & 1 \\ 1 & 1 & \cdots & 1 & 1 \\ \vdots & \vdots & \ddots & \vdots & \vdots \\ 1 & 1 & \cdots & 1 & 1 \\ 1 & 1 & \cdots & 1 & 1 \end{bmatrix}, \quad \mathbf{P} = \begin{bmatrix} 0 & 1 & \cdots & 0 & 1 \\ 0 & 1 & \cdots & 0 & 1 \\ \vdots & \vdots & \ddots & \vdots & \vdots \\ 0 & 1 & \cdots & 0 & 1 \\ 0 & 1 & \cdots & 0 & 1 \end{bmatrix}.$$

Next, we define two different lifting matrices \mathbf{L}_1 and \mathbf{L}_2 as follows:

$$\mathbf{L}_1 = \begin{bmatrix} l_{1,1} & l_{1,2} & \cdots & l_{1,\kappa} \\ l_{2,1} & l_{2,2} & \cdots & l_{2,\kappa} \\ \vdots & \vdots & \ddots & \vdots \\ l_{\gamma-1,1} & l_{\gamma-1,2} & \cdots & l_{\gamma-1,\kappa} \\ l_{\gamma,1} & l_{\gamma,2} & \cdots & l_{\gamma,\kappa} \end{bmatrix}, \quad \mathbf{L}_2 = \begin{bmatrix} l_{\gamma+1,1} & l_{\gamma+1,2} & \cdots & l_{\gamma+1,\kappa} \\ l_{\gamma+2,1} & l_{\gamma+2,2} & \cdots & l_{\gamma+2,\kappa} \\ \vdots & \vdots & \ddots & \vdots \\ l_{2\gamma-1,1} & l_{2\gamma-1,2} & \cdots & l_{2\gamma-1,\kappa} \\ l_{2\gamma,1} & l_{(2\gamma),2} & \cdots & l_{2\gamma,\kappa} \end{bmatrix},$$

where $l_{i,j} = ij \pmod{p}$. The protograph $\mathbf{H}^{(P)}$ specified by \mathbf{B} and \mathbf{P} is given by:

$$\mathbf{H}^{(P)} = \begin{bmatrix} \mathbf{H}_0^{(P)} & \mathbf{0} & \mathbf{0} & \mathbf{H}_1^{(P)} \\ \mathbf{H}_1^{(P)} & \mathbf{H}_0^{(P)} & \mathbf{0} & \mathbf{0} \\ \mathbf{0} & \mathbf{H}_1^{(P)} & \mathbf{H}_0^{(P)} & \mathbf{0} \\ \mathbf{0} & \mathbf{0} & \mathbf{H}_1^{(P)} & \mathbf{H}_0^{(P)} \end{bmatrix}, \quad \text{where}$$

$$\mathbf{H}_0^{(P)} = \begin{bmatrix} 1 & 0 & \cdots & 1 & 0 \\ 1 & 0 & \cdots & 1 & 0 \\ \vdots & \vdots & \ddots & \vdots & \vdots \\ 1 & 0 & \cdots & 1 & 0 \\ 1 & 0 & \cdots & 1 & 0 \end{bmatrix} \quad \text{and} \quad \mathbf{H}_1^{(P)} = \begin{bmatrix} 0 & 1 & \cdots & 0 & 1 \\ 0 & 1 & \cdots & 0 & 1 \\ \vdots & \vdots & \ddots & \vdots & \vdots \\ 0 & 1 & \cdots & 0 & 1 \\ 0 & 1 & \cdots & 0 & 1 \end{bmatrix}.$$

The parity-check matrices \mathbf{H} and \mathbf{G} lifted from $\mathbf{H}^{(P)}$ with respect to \mathbf{L}_1 and \mathbf{L}_2 , respectively, are given by:

$$\mathbf{H} = \begin{bmatrix} \mathbf{H}_0 & \mathbf{0} & \mathbf{0} & \mathbf{H}_1 \\ \mathbf{H}_1 & \mathbf{H}_0 & \mathbf{0} & \mathbf{0} \\ \mathbf{0} & \mathbf{H}_1 & \mathbf{H}_0 & \mathbf{0} \\ \mathbf{0} & \mathbf{0} & \mathbf{H}_1 & \mathbf{H}_0 \end{bmatrix}, \quad \mathbf{G} = \begin{bmatrix} \mathbf{G}_0 & \mathbf{0} & \mathbf{0} & \mathbf{G}_1 \\ \mathbf{G}_1 & \mathbf{G}_0 & \mathbf{0} & \mathbf{0} \\ \mathbf{0} & \mathbf{G}_1 & \mathbf{G}_0 & \mathbf{0} \\ \mathbf{0} & \mathbf{0} & \mathbf{G}_1 & \mathbf{G}_0 \end{bmatrix}, \quad \text{where} \quad (24)$$

$$\mathbf{H}_0 = \begin{bmatrix} P^1 & \mathbf{0} & \dots & P^{(\kappa-1)} & \mathbf{0} \\ P^{2 \cdot 1} & \mathbf{0} & \dots & P^{2 \cdot (\kappa-1)} & \mathbf{0} \\ \vdots & \vdots & \ddots & \vdots & \vdots \\ P^{(\gamma-1) \cdot 1} & \mathbf{0} & \dots & P^{(\gamma-1) \cdot (\kappa-1)} & \mathbf{0} \\ P^{\gamma \cdot 1} & \mathbf{0} & \dots & P^{\gamma \cdot (\kappa-1)} & \mathbf{0} \end{bmatrix}, \quad \mathbf{H}_1 = \begin{bmatrix} \mathbf{0} & P^{1 \cdot 2} & \dots & \mathbf{0} & P^{1 \cdot \kappa} \\ \mathbf{0} & P^{2 \cdot 2} & \dots & \mathbf{0} & P^{2 \cdot \kappa} \\ \vdots & \vdots & \ddots & \vdots & \vdots \\ \mathbf{0} & P^{(\gamma-1) \cdot 2} & \dots & \mathbf{0} & P^{(\gamma-1) \cdot \kappa} \\ \mathbf{0} & P^{\gamma \cdot 2} & \dots & \mathbf{0} & P^{\gamma \cdot \kappa} \end{bmatrix},$$

$$\mathbf{G}_0 = \begin{bmatrix} P^{(\gamma+1)} & \mathbf{0} & \dots & P^{(\gamma+1) \cdot (\kappa-1)} & \mathbf{0} \\ P^{(\gamma+2) \cdot 1} & \mathbf{0} & \dots & P^{(\gamma+2) \cdot (\kappa-1)} & \mathbf{0} \\ \vdots & \vdots & \ddots & \vdots & \vdots \\ P^{(2\gamma-1) \cdot 1} & \mathbf{0} & \dots & P^{(2\gamma-1) \cdot (\kappa-1)} & \mathbf{0} \\ P^{(2\gamma) \cdot 1} & \mathbf{0} & \dots & P^{(2\gamma) \cdot (\kappa-1)} & \mathbf{0} \end{bmatrix}, \quad \mathbf{G}_1 = \begin{bmatrix} \mathbf{0} & P^{(\gamma+1) \cdot 2} & \dots & \mathbf{0} & P^{(\gamma+1) \cdot \kappa} \\ \mathbf{0} & P^{(\gamma+2) \cdot 2} & \dots & \mathbf{0} & P^{(\gamma+2) \cdot \kappa} \\ \vdots & \vdots & \ddots & \vdots & \vdots \\ \mathbf{0} & P^{(2\gamma-1) \cdot 2} & \dots & \mathbf{0} & P^{(2\gamma-1) \cdot \kappa} \\ \mathbf{0} & P^{(2\gamma) \cdot 2} & \dots & \mathbf{0} & P^{(2\gamma) \cdot \kappa} \end{bmatrix},$$

and the powers of the permutation matrix P are computed under mod (p) . Now, by using above construction, we propose a class of entanglement-assisted quantum QC-SC-LDPC codes in the following theorem.

Theorem 7. *Let \mathbf{H} and \mathbf{G} , defined by (24), be the parity-check matrices of two classical QC-SC-LDPC codes. Then there exists an entanglement-assisted quantum QC-SC-LDPC code with the parameters $[[4p(p-1), k_1 + k_2 - 4p(p-1) + (p-1); (p-1)]]_2$, where $k_1, k_2 \geq 4p(p-2) - 4(\gamma-1)(p-1)$. Moreover, the overall Tanner graph of the constructed code does not have 4-cycles.*

Proof. The length of the code and the bound on its dimension can be easily derived. Therefore, the main focus of the proof will be to determine the minimum number of maximally entangled bits required. It is straightforward to verify that

$$\mathbf{H}\mathbf{G}^T = \begin{bmatrix} \sum_{i=0}^1 \mathbf{H}_i \mathbf{G}_i^T & \mathbf{H}_0 \mathbf{G}_1^T & \mathbf{0} & \mathbf{H}_1 \mathbf{G}_0^T \\ \mathbf{H}_1 \mathbf{G}_0^T & \sum_{i=0}^1 \mathbf{H}_i \mathbf{G}_i^T & \mathbf{H}_0 \mathbf{G}_1^T & \mathbf{0} \\ \mathbf{0} & \mathbf{H}_1 \mathbf{G}_0^T & \sum_{i=0}^1 \mathbf{H}_i \mathbf{G}_i^T & \mathbf{H}_0 \mathbf{G}_1^T \\ \mathbf{H}_0 \mathbf{G}_1^T & \mathbf{0} & \mathbf{H}_1 \mathbf{G}_0^T & \sum_{i=0}^1 \mathbf{H}_i \mathbf{G}_i^T \end{bmatrix}$$

$$= \begin{bmatrix} \sum_{i=0}^1 \mathbf{H}_i \mathbf{G}_i^T & \mathbf{0} & \mathbf{0} & \mathbf{0} \\ \mathbf{0} & \sum_{i=0}^1 \mathbf{H}_i \mathbf{G}_i^T & \mathbf{0} & \mathbf{0} \\ \mathbf{0} & \mathbf{0} & \sum_{i=0}^1 \mathbf{H}_i \mathbf{G}_i^T & \mathbf{0} \\ \mathbf{0} & \mathbf{0} & \mathbf{0} & \sum_{i=0}^1 \mathbf{H}_i \mathbf{G}_i^T \end{bmatrix} \quad (\text{since } \mathbf{H}_0 \mathbf{G}_1^T = \mathbf{H}_1 \mathbf{G}_0^T = \mathbf{0}).$$

Further, it can also be easily checked that

$$\begin{aligned}
\sum_{i=0}^1 \mathbf{H}_i \mathbf{G}_i^T &= (\mathbf{H}_0 + \mathbf{H}_1)(\mathbf{G}_0 + \mathbf{G}_1)^T \quad (\text{since } \mathbf{H}_0 \mathbf{G}_1^T = \mathbf{H}_1 \mathbf{G}_0^T = \mathbf{0}) \\
&= \begin{bmatrix} P^1 & P^2 & \dots & P^\kappa \\ P^{2 \cdot 1} & P^{2 \cdot 2} & \dots & P^{2 \cdot \kappa} \\ \vdots & \vdots & \ddots & \vdots \\ P^{(\gamma-1) \cdot 1} & P^{(\gamma-1) \cdot 2} & \dots & P^{(\gamma-1) \cdot \kappa} \\ P^{\gamma \cdot 1} & P^{\gamma \cdot 2} & \dots & P^{\gamma \cdot \kappa} \end{bmatrix} \begin{bmatrix} P^{(\gamma+1) \cdot 1} & P^{(\gamma+1) \cdot 2} & \dots & P^{(\gamma+1) \cdot \kappa} \\ P^{(\gamma+2) \cdot 1} & P^{(\gamma+2) \cdot 2} & \dots & P^{(\gamma+2) \cdot \kappa} \\ \vdots & \vdots & \ddots & \vdots \\ P^{(2\gamma-1) \cdot 1} & P^{(2\gamma-1) \cdot 2} & \dots & P^{(2\gamma-1) \cdot \kappa} \\ P^{(2\gamma) \cdot 1} & P^{(2\gamma) \cdot 2} & \dots & P^{(2\gamma) \cdot \kappa} \end{bmatrix}^T \\
&= \begin{bmatrix} \sum_{i=1}^{p-1} P^i & \sum_{i=1}^{p-1} P^i & \dots & \sum_{i=1}^{p-1} P^i & \sum_{i=1}^{p-1} P^i \\ \sum_{i=1}^{p-1} P^i & \sum_{i=1}^{p-1} P^i & \dots & \sum_{i=1}^{p-1} P^i & \sum_{i=1}^{p-1} P^i \\ \vdots & \vdots & \ddots & \vdots & \vdots \\ \sum_{i=1}^{p-1} P^i & \sum_{i=1}^{p-1} P^i & \dots & \sum_{i=1}^{p-1} P^i & \sum_{i=1}^{p-1} P^i \\ \sum_{i=1}^{p-1} P^i & \sum_{i=1}^{p-1} P^i & \dots & \sum_{i=1}^{p-1} P^i & \sum_{i=1}^{p-1} P^i \end{bmatrix} \\
&= \begin{bmatrix} I_p + J_p & I_p + J_p & \dots & I_p + J_p & I_p + J_p \\ I_p + J_p & I_p + J_p & \dots & I_p + J_p & I_p + J_p \\ \vdots & \vdots & \ddots & \vdots & \vdots \\ I_p + J_p & I_p + J_p & \dots & I_p + J_p & I_p + J_p \\ I_p + J_p & I_p + J_p & \dots & I_p + J_p & I_p + J_p \end{bmatrix},
\end{aligned}$$

where J_p is the $p \times p$ all-ones matrix and I is the $p \times p$ identity matrix. From the above, we conclude that $\text{gfrank}(\mathbf{H}\mathbf{G}^T) = 4 \times \text{gfrank}\left(\sum_{i=0}^1 \mathbf{H}_i \mathbf{G}_i^T\right)$, and by Lemma 4, we have $\text{gfrank}\left(\sum_{i=0}^1 \mathbf{H}_i \mathbf{G}_i^T\right) = \text{gfrank}(I_p + J_p) = p - 1$. Theorem 2, completes the desired result. \square

Example 11. Let $p = 5$, $\gamma = 2$, $\kappa = 4$, $m = 1$, and $L = 4$. Now, we define base matrix \mathbf{B} and partitioning matrix \mathbf{P} of size 2×4 as follows:

$$\mathbf{B} = \begin{bmatrix} 1 & 1 & 1 & 1 \\ 1 & 1 & 1 & 1 \end{bmatrix}, \quad \mathbf{P} = \begin{bmatrix} 0 & 1 & 0 & 1 \\ 0 & 1 & 0 & 1 \end{bmatrix}.$$

Next, we define two different lifting matrices \mathbf{L}_1 and \mathbf{L}_2 as follows:

$$\mathbf{L}_1 = \begin{bmatrix} 1 & 2 & 3 & 4 \\ 2 & 4 & 1 & 3 \end{bmatrix}, \quad \mathbf{L}_2 = \begin{bmatrix} 3 & 1 & 4 & 2 \\ 4 & 3 & 2 & 1 \end{bmatrix}.$$

The protograph $\mathbf{H}^{(P)}$ specified by \mathbf{B} and \mathbf{P} is given by:

$$\mathbf{H}^{(P)} = \begin{bmatrix} \mathbf{H}_0^{(P)} & \mathbf{0} & \mathbf{0} & \mathbf{H}_1^{(P)} \\ \mathbf{H}_1^{(P)} & \mathbf{H}_0^{(P)} & \mathbf{0} & \mathbf{0} \\ \mathbf{0} & \mathbf{H}_1^{(P)} & \mathbf{H}_0^{(P)} & \mathbf{0} \\ \mathbf{0} & \mathbf{0} & \mathbf{H}_1^{(P)} & \mathbf{H}_0^{(P)} \end{bmatrix}, \quad \text{where}$$

$$\mathbf{H}_0^{(P)} = \begin{bmatrix} 1 & 0 & 1 & 0 \\ 1 & 0 & 1 & 0 \end{bmatrix} \text{ and } \mathbf{H}_1^{(P)} = \begin{bmatrix} 0 & 1 & 0 & 1 \\ 0 & 1 & 0 & 1 \end{bmatrix}.$$

The parity-check matrices \mathbf{H} and \mathbf{G} lifted from $\mathbf{H}^{(P)}$ with respect to \mathbf{L}_1 and \mathbf{L}_2 , respectively, are given by:

$$\mathbf{H} = \begin{bmatrix} \mathbf{H}_0 & \mathbf{0} & \mathbf{0} & \mathbf{H}_1 \\ \mathbf{H}_1 & \mathbf{H}_0 & \mathbf{0} & \mathbf{0} \\ \mathbf{0} & \mathbf{H}_1 & \mathbf{H}_0 & \mathbf{0} \\ \mathbf{0} & \mathbf{0} & \mathbf{H}_1 & \mathbf{H}_0 \end{bmatrix}, \quad \mathbf{G} = \begin{bmatrix} \mathbf{G}_0 & \mathbf{0} & \mathbf{0} & \mathbf{G}_1 \\ \mathbf{G}_1 & \mathbf{G}_0 & \mathbf{0} & \mathbf{0} \\ \mathbf{0} & \mathbf{G}_1 & \mathbf{G}_0 & \mathbf{0} \\ \mathbf{0} & \mathbf{0} & \mathbf{G}_1 & \mathbf{G}_0 \end{bmatrix}, \text{ where} \quad (25)$$

$$\mathbf{H}_0 = \begin{bmatrix} P^1 & \mathbf{0} & P^3 & \mathbf{0} \\ P^2 & \mathbf{0} & P^1 & \mathbf{0} \end{bmatrix}, \quad \mathbf{H}_1 = \begin{bmatrix} \mathbf{0} & P^2 & \mathbf{0} & P^4 \\ \mathbf{0} & P^4 & \mathbf{0} & P^3 \end{bmatrix}$$

$$\mathbf{G}_0 = \begin{bmatrix} P^3 & \mathbf{0} & P^4 & \mathbf{0} \\ P^4 & \mathbf{0} & P^2 & \mathbf{0} \end{bmatrix}, \quad \mathbf{G}_1 = \begin{bmatrix} \mathbf{0} & P^1 & \mathbf{0} & P^2 \\ \mathbf{0} & P^3 & \mathbf{0} & P^1 \end{bmatrix}.$$

Let \mathbf{H} and \mathbf{G} , defined by (25), be the parity-check matrices of two classical quasi-cyclic (QC) spatially-coupled (SC) LDPC codes. Then there exists an entanglement-assisted quantum QC-SC-LDPC code with the parameters $[[80, 12; 4]]_2$. Moreover, the overall Tanner graph of the constructed code does not have 4-cycles.

Theorem 8. Let \mathbf{H} , defined by (24), be the parity-check matrix of a classical QC-SC-LDPC code. Then there exists an entanglement-assisted quantum QC-SC-LDPC code with the following parameters

$$\begin{cases} [[4p(p-1), 2k - 4p(p-1) + 4(\gamma-1)(p-1); 4(\gamma-1)(p-1)]]_2, & \text{if } \gamma \text{ is odd,} \\ [[4p(p-1), 2k - 4p(p-1) + 4\gamma(p-1); 4\gamma(p-1)]]_2, & \text{if } \gamma \text{ is even,} \end{cases}$$

where $k \geq 4p(p-2) - 4(\gamma-1)(p-1)$. Moreover, the Tanner graph of the employed classical code does not have 4-cycles.

Proof. The length of the code and the bound on its dimension can be easily derived. Thus, the primary focus of the proof will be to find the minimum number of maximally entangled bits (ebits) needed. One can easily check that

$$\begin{aligned} \mathbf{H}\mathbf{H}^T &= \begin{bmatrix} \sum_{i=0}^1 \mathbf{H}_i \mathbf{H}_i^T & \mathbf{H}_0 \mathbf{H}_1^T & \mathbf{0} & \mathbf{H}_1 \mathbf{H}_0^T \\ \mathbf{H}_1 \mathbf{H}_0^T & \sum_{i=0}^1 \mathbf{H}_i \mathbf{H}_i^T & \mathbf{H}_0 \mathbf{H}_1^T & \mathbf{0} \\ \mathbf{0} & \mathbf{H}_1 \mathbf{H}_0^T & \sum_{i=0}^1 \mathbf{H}_i \mathbf{H}_i^T & \mathbf{H}_0 \mathbf{H}_1^T \\ \mathbf{H}_0 \mathbf{H}_1^T & \mathbf{0} & \mathbf{H}_1 \mathbf{H}_0^T & \sum_{i=0}^1 \mathbf{H}_i \mathbf{H}_i^T \end{bmatrix} \\ &= \begin{bmatrix} \sum_{i=0}^1 \mathbf{H}_i \mathbf{H}_i^T & \mathbf{0} & \mathbf{0} & \mathbf{0} \\ \mathbf{0} & \sum_{i=0}^1 \mathbf{H}_i \mathbf{H}_i^T & \mathbf{0} & \mathbf{0} \\ \mathbf{0} & \mathbf{0} & \sum_{i=0}^1 \mathbf{H}_i \mathbf{H}_i^T & \mathbf{0} \\ \mathbf{0} & \mathbf{0} & \mathbf{0} & \sum_{i=0}^1 \mathbf{H}_i \mathbf{H}_i^T \end{bmatrix} \quad (\text{since } \mathbf{H}_0 \mathbf{H}_1^T = \mathbf{H}_1 \mathbf{H}_0^T = \mathbf{0}). \end{aligned}$$

Further, it is also straightforward to get

$$\begin{aligned}
\sum_{i=0}^1 \mathbf{H}_i \mathbf{H}_i^T &= (\mathbf{H}_0 + \mathbf{H}_1)(\mathbf{H}_0 + \mathbf{H}_1)^T \quad (\text{since } \mathbf{H}_0 \mathbf{H}_1^T = \mathbf{H}_1 \mathbf{H}_0^T = \mathbf{0}) \\
&= \begin{bmatrix} P^1 & P^2 & \dots & P^\kappa \\ P^{2 \cdot 1} & P^{2 \cdot 2} & \dots & P^{2 \cdot \kappa} \\ \vdots & \vdots & \ddots & \vdots \\ P^{(\gamma-1) \cdot 1} & P^{(\gamma-1) \cdot 2} & \dots & P^{(\gamma-1) \cdot \kappa} \\ P^{\gamma \cdot 1} & P^{\gamma \cdot 2} & \dots & P^{\gamma \cdot \kappa} \end{bmatrix} \begin{bmatrix} P^1 & P^2 & \dots & P^\kappa \\ P^{2 \cdot 1} & P^{2 \cdot 2} & \dots & P^{2 \cdot \kappa} \\ \vdots & \vdots & \ddots & \vdots \\ P^{(\gamma-1) \cdot 1} & P^{(\gamma-1) \cdot 2} & \dots & P^{(\gamma-1) \cdot \kappa} \\ P^{\gamma \cdot 1} & P^{\gamma \cdot 2} & \dots & P^{\gamma \cdot \kappa} \end{bmatrix}^T \\
&= \begin{bmatrix} \mathbf{0} & \sum_{i=0}^{p-1} P^i & \dots & \sum_{i=1}^{p-1} P^i & \sum_{i=1}^{p-1} P^i \\ \sum_{i=1}^{p-1} P^i & \mathbf{0} & \dots & \sum_{i=1}^{p-1} P^i & \sum_{i=1}^{p-1} P^i \\ \vdots & \vdots & \ddots & \vdots & \vdots \\ \sum_{i=1}^{p-1} P^i & \sum_{i=1}^{p-1} P^i & \dots & \mathbf{0} & \sum_{i=1}^{p-1} P^i \\ \sum_{i=1}^{p-1} P^i & \sum_{i=1}^{p-1} P^i & \dots & \sum_{i=1}^{p-1} P^i & \mathbf{0} \end{bmatrix} \\
&= \begin{bmatrix} \mathbf{0} & I_p + J_p & \dots & I_p + J_p & I_p + J_p \\ I_p + J_p & \mathbf{0} & \dots & I_p + J_p & I_p + J_p \\ \vdots & \vdots & \ddots & \vdots & \vdots \\ I_p + J_p & I_p + J_p & \dots & \mathbf{0} & I_p + J_p \\ I_p + J_p & I_p + J_p & \dots & I_p + J_p & \mathbf{0} \end{bmatrix},
\end{aligned}$$

where J_p is the $p \times p$ all-ones matrix and I is the $p \times p$ identity matrix.

By Lemma 5, $\text{gfrank}(\mathbf{H}\mathbf{H}^T) = 4 \times \text{gfrank}(\sum_{i=0}^1 \mathbf{H}_i \mathbf{H}_i^T) = \begin{cases} 4(\gamma-1)(p-1), & \text{if } \gamma \text{ is odd;} \\ 4\gamma(p-1), & \text{if } \gamma \text{ is even.} \end{cases}$

By applying Theorem 2, we obtain the desired result. \square

Example 12. Let $p = 7$, $\gamma = 3$, $\kappa = 6$, $m = 1$, and $L = 4$. Now, we define base matrix \mathbf{B} , partitioning matrix \mathbf{P} and lifting matrix \mathbf{L} of size 2×4 as follows:

$$\mathbf{B} = \begin{bmatrix} 1 & 1 & 1 & 1 & 1 & 1 \\ 1 & 1 & 1 & 1 & 1 & 1 \\ 1 & 1 & 1 & 1 & 1 & 1 \end{bmatrix}, \quad \mathbf{P} = \begin{bmatrix} 0 & 1 & 0 & 1 & 0 & 1 \\ 0 & 1 & 0 & 1 & 0 & 1 \\ 0 & 1 & 0 & 1 & 0 & 1 \end{bmatrix}, \quad \mathbf{L} = \begin{bmatrix} 1 & 2 & 3 & 4 & 5 & 6 \\ 2 & 4 & 6 & 1 & 3 & 5 \\ 3 & 6 & 2 & 5 & 1 & 4 \end{bmatrix}.$$

The protograph $\mathbf{H}^{(P)}$ specified by \mathbf{B} and \mathbf{P} is given by:

$$\mathbf{H}^{(P)} = \begin{bmatrix} \mathbf{H}_0^{(P)} & \mathbf{0} & \mathbf{0} & \mathbf{H}_1^{(P)} \\ \mathbf{H}_1^{(P)} & \mathbf{H}_0^{(P)} & \mathbf{0} & \mathbf{0} \\ \mathbf{0} & \mathbf{H}_1^{(P)} & \mathbf{H}_0^{(P)} & \mathbf{0} \\ \mathbf{0} & \mathbf{0} & \mathbf{H}_1^{(P)} & \mathbf{H}_0^{(P)} \end{bmatrix}, \quad \text{where}$$

$$\mathbf{H}_0^{(P)} = \begin{bmatrix} 0 & 1 & 0 & 1 & 0 & 1 \\ 0 & 1 & 0 & 1 & 0 & 1 \\ 0 & 1 & 0 & 1 & 0 & 1 \end{bmatrix} \quad \text{and} \quad \mathbf{H}_1^{(P)} = \begin{bmatrix} 0 & 1 & 0 & 1 & 0 & 1 \\ 0 & 1 & 0 & 1 & 0 & 1 \\ 0 & 1 & 0 & 1 & 0 & 1 \end{bmatrix}.$$

The parity-check matrix \mathbf{H} lifted from $\mathbf{H}^{(P)}$ with respect to \mathbf{L} is

$$\mathbf{H} = \begin{bmatrix} \mathbf{H}_0 & \mathbf{0} & \mathbf{0} & \mathbf{H}_1 \\ \mathbf{H}_1 & \mathbf{H}_0 & \mathbf{0} & \mathbf{0} \\ \mathbf{0} & \mathbf{H}_1 & \mathbf{H}_0 & \mathbf{0} \\ \mathbf{0} & \mathbf{0} & \mathbf{H}_1 & \mathbf{H}_0 \end{bmatrix}, \text{ where} \quad (26)$$

$$\mathbf{H}_0 = \begin{bmatrix} P^1 & \mathbf{0} & P^3 & \mathbf{0} & P^5 & \mathbf{0} \\ P^2 & \mathbf{0} & P^6 & \mathbf{0} & P^3 & \mathbf{0} \\ P^3 & \mathbf{0} & P^2 & \mathbf{0} & P^1 & \mathbf{0} \end{bmatrix} \text{ and } \mathbf{H}_1 = \begin{bmatrix} \mathbf{0} & P^2 & \mathbf{0} & P^4 & \mathbf{0} & P^6 \\ \mathbf{0} & P^4 & \mathbf{0} & P^1 & \mathbf{0} & P^5 \\ \mathbf{0} & P^6 & \mathbf{0} & P^5 & \mathbf{0} & P^4 \end{bmatrix}.$$

Let \mathbf{H} , defined by (26), be the parity-check matrix of a classical QC-SC-LDPC code. Then there exists a $[[168, 64; 48]]_2$ entanglement-assisted quantum QC-SC-LDPC code.

Let m and r be positive integers such that $1 \leq m < \frac{r}{2} \times r$. Let \mathbf{B} , \mathbf{P} , and \mathbf{L} denote the $\frac{r}{2} \times r$ base matrix, partitioning matrix, and lifting matrix, respectively. The entries of \mathbf{L} are populated according to the procedure outlined in Algorithm 2. Let L represent the coupling length. Any positive integer t that results in the construction of the lifting matrix L corresponds to the size of the right circulant permutation matrix. Consider the following tail-biting parity check matrix for a classical QC-SC-LDPC code:

$$\mathbf{H}_{\text{TB}} = \begin{bmatrix} \mathbf{H}_0 & \mathbf{0} & \cdots & \mathbf{0} & \mathbf{H}_m & \cdots & \mathbf{H}_1 \\ \mathbf{H}_1 & \mathbf{H}_0 & \mathbf{0} & \cdots & \mathbf{0} & \ddots & \vdots \\ \vdots & \mathbf{H}_1 & \mathbf{H}_0 & \ddots & \ddots & \ddots & \mathbf{H}_m \\ \mathbf{H}_m & \vdots & \ddots & \ddots & \mathbf{0} & \ddots & \mathbf{0} \\ \mathbf{0} & \mathbf{H}_m & \cdots & \mathbf{H}_1 & \mathbf{H}_0 & \ddots & \vdots \\ \vdots & \ddots & \ddots & \vdots & \ddots & \ddots & \mathbf{0} \\ \mathbf{0} & \cdots & \mathbf{0} & \mathbf{H}_m & \cdots & \mathbf{H}_1 & \mathbf{H}_0 \end{bmatrix}. \quad (27)$$

By applying Theorem 2, one can construct an entanglement-assisted quantum QC-SC-LDPC code with the parameters $[[n, 2k - n + c; c]]_2$, where $n = rtL$ and rest of the parameters depends on the forms of \mathbf{B} , \mathbf{P} , \mathbf{L} , and \mathbf{H}_{TB} . Moreover, the Tanner graph associated with \mathbf{H}_{TB} is devoid of short cycles.

5 Entanglement-assisted quantum QC-LDPC code with Tanner graph of girth greater than 6

In this section, we present the construction of EA quantum QC-LDPC codes of girth > 6 . This section has been divided into two subsections, namely Subsection 5.1 and Subsection 5.2. First, in Subsection 5.1, we introduce an entanglement-assisted quantum QC-LDPC code with a parity-check matrix that has a uniform column weight of 3. Subsequently, in Subsection 5.2, we present an EA quantum QC-LDPC code with a parity check matrix having a uniform column weight of 4.

5.1 Entanglement-assisted quantum QC-LDPC codes with parity-check matrix that has a uniform column weight of 3

In the following theorem, we have proposed a class of entanglement-assisted quantum QC-LDPC codes.

Theorem 9. Let P be a right circulant permutation matrix of order $w^\ell + 1$, where $\ell \geq 6$ and $w \geq 2$ are positive integers. Let

$$M = \begin{bmatrix} 0 & 0 & \cdots & 0 \\ w^1 & w^2 & \cdots & w^\ell \\ -w^1 & -w^2 & \cdots & -w^\ell \end{bmatrix}$$

be a model matrix associated with the parity-check matrix H , where $-w^x$ stands for additive inverse of w^x in $\mathbb{Z}_{(w^\ell+1)}$. Then, there exists an entanglement-assisted quantum QC LDPC codes with the parameters $[[(w^\ell + 1)\ell, 2k - (w^\ell + 1)\ell + c; c]_2$, where $k \geq (\ell - 3)(w^\ell + 1) + 2$ and $c \leq 3(w^\ell + 1) - 2$. In addition, the Tanner graph of H is of girth greater than 6.

Proof. The length is straightforward to determine, and the lower bound on the dimension k can easily be obtained using Theorem 4. Now, we will show that our construction is free from cycles of length 4. The existence of 4-cycle requires two columns and two rows from the matrix M . Each nonzero row in M contains distinct entries under modulo $(w^\ell + 1)$; thus, by Proposition 1, the presence of a 4-cycle is not possible for one zero row and one nonzero row. Consequently, the presence of a 4-cycle is possible only for two nonzero rows. By Corollary 1, there exists a 4-cycle in two nonzero rows if and only if the following holds:

$$\begin{aligned} w^a + w^a &= w^b + w^b \pmod{(w^\ell + 1)}, \text{ for some } 1 \leq a, b \leq \ell, \text{ where } a \neq b \\ \iff 2w^a &= 2w^b \pmod{(w^\ell + 1)} \\ \iff 2 &= 2w^{b-a} \pmod{(w^\ell + 1)} \quad (\text{since } \gcd(w^a, w^\ell + 1) = 1), \end{aligned}$$

which leads to a contradiction. Hence, there is no cycle of length 4 in the Tanner graph of H .

Next, we show that the Tanner graph of H is devoid of cycles of length 6. To prove that, consider any three columns from the matrix M as follows

$$\begin{bmatrix} \cdots & 0 & \cdots & 0 & \cdots & 0 & \cdots \\ \cdots & w^a & \cdots & w^b & \cdots & w^c & \cdots \\ \cdots & -w^a & \cdots & -w^b & \cdots & -w^c & \cdots \end{bmatrix}, \quad (28)$$

where $1 \leq a < b < c \leq \ell$. We examine the presence of all possible 6-cycles, as illustrated in Figure 2, in the segment of the Tanner graph corresponding to a portion of the model matrix defined by Equation (28).

1. **Existence of Type-I 6-cycle:** A Type-I cycle of length 6 exists in the Tanner graph of H if and only if the following condition is satisfied:

$$\begin{aligned} -w^a &= -w^c - w^c + w^b \pmod{(w^\ell + 1)} \\ \implies 2w^c &= w^b + w^a \pmod{(w^\ell + 1)} \\ \implies 2w^{c-1} &= w^{b-1} + w^{a-1} \pmod{(w^\ell + 1)} \quad (\text{since } \gcd(w, w^\ell + 1) = 1). \end{aligned}$$

This leads to a contradiction, as the value on the left is greater than the value on the right.

2. **Existence of Type-II 6-cycle:** A Type-II 6-cycle exists if and only if $-w^a = -w^b - w^b + w^c$ under mod $(w^\ell + 1)$, which implies $w^c = 2w^b - w^a$ under mod $(w^\ell + 1)$. However, this leads to a contradiction, as the value on the left is greater than the value on the right.

3. **Existence of Type-III 6-cycle:** There exists Type-III 6-cycle if and only if the following holds:

$$\begin{aligned} -w^c &= -w^a - w^a + w^b \pmod{(w^\ell + 1)} \\ \implies 2w^a &= w^c + w^b \pmod{(w^\ell + 1)} \\ \implies 2w^{a-1} &= w^{c-1} + w^{b-1} \pmod{(w^\ell + 1)} \quad (\text{since } \gcd(w, w^\ell + 1) = 1). \end{aligned}$$

This is a contradiction since the number on the left is less than on the right.

4. **Existence of Type-IV 6-cycle:** A Type-IV 6-cycle exists if and only if the following condition holds: $-w^c = -w^b - w^b + w^a \pmod{(w^\ell + 1)}$, which implies $w^c = 2w^b - w^a \pmod{(w^\ell + 1)}$. However, this leads to a contradiction, as the number on the left is greater than the number on the right.

5. **Existence of Type-V 6-cycle:** There exists Type-V 6-cycle if and only if the following holds:

$$\begin{aligned} -w^b &= -w^a - w^a + w^c \pmod{(w^\ell + 1)} \\ \implies 2w^a &= w^c + w^b \pmod{(w^\ell + 1)} \\ \implies 2w^{a-1} &= w^{c-1} + w^{b-1} \pmod{(w^\ell + 1)} \quad (\text{since } \gcd(w, w^\ell + 1) = 1). \end{aligned}$$

This is a contradiction since the number on the left is less than on the right.

6. **Existence of Type-VI 6-cycle:** There exists a Type VI 6-cycle if and only if the following holds:

$$\begin{aligned} -w^b &= -w^c - w^c + w^a \pmod{(w^\ell + 1)} \\ \implies 2w^c &= w^b + w^a \pmod{(w^\ell + 1)} \\ \implies 2w^{c-1} &= w^{b-1} + w^{a-1} \pmod{(w^\ell + 1)} \quad (\text{since } \gcd(w, w^\ell + 1) = 1), \end{aligned}$$

which leads to a contradiction since the number on the left is greater than on the right.

The minimum number of required maximally entangled bits is given by

$$c = \text{gfrank}(HH^T),$$

where

$$\begin{aligned} HH^T &= \begin{bmatrix} I & I & \cdots & I \\ P^w & P^{w^2} & \cdots & P^{w^\ell} \\ P^{-w} & P^{-w^2} & \cdots & P^{-w^\ell} \end{bmatrix} \begin{bmatrix} I & P^{-w} & P^w \\ I & P^{-w^2} & P^{w^2} \\ \vdots & \vdots & \vdots \\ I & P^{-w^\ell} & P^{w^\ell} \end{bmatrix} \\ &= \begin{bmatrix} \ell I & \sum_{i=1}^{\ell} P^{-w^i} & \sum_{i=1}^{\ell} P^{w^i} \\ \sum_{i=1}^{\ell} P^{w^i} & \ell I & \sum_{i=2}^{\ell} P^{w^i} + P^{w^{\ell-1}} \\ \sum_{i=1}^{\ell} P^{-w^i} & \sum_{i=2}^{\ell} P^{-w^i} + P^w & \ell I \end{bmatrix}. \end{aligned}$$

It is easy to verify that the $\text{gfrank}(HH^T) \leq 3(w^\ell + 1) - 2$, since the vector sum of each block row is a vector whose all entries are either 1 or 0, depending on whether ℓ is even or odd. This completes the proof. \square

Example 13. For $\ell = 6$ and $w = 2$, we define the parity-check matrix H and the associated model matrix M as follows:

$$H = \begin{bmatrix} I & I & I & I & I & I \\ P^2 & P^4 & P^8 & P^{16} & P^{32} & P^{64} \\ P^{63} & P^{61} & P^{57} & P^{49} & P^{33} & P \end{bmatrix},$$

$$M = \begin{bmatrix} 0 & 0 & 0 & 0 & 0 & 0 \\ 2 & 4 & 8 & 16 & 32 & 64 \\ 63 & 61 & 57 & 49 & 33 & 1 \end{bmatrix},$$

where P is the right circulant permutation matrix of order 65. Then there exists an entanglement-assisted quantum QC-LDPC code with the parameters $[[390, 2k - 390 + c; c]]_2$, where $k \geq 197$ and $c \leq 193$.

Remark 3. Since $2 + 63 = 64 + 1$, the entries in M do not form a Sidon sequence.

5.2 Entanglement-assisted quantum QC-LDPC codes with parity-check matrix that has a uniform column weight of 4

In the following theorem, we propose a class of entanglement-assisted quantum QC-LDPC codes, constructed using classical QC-LDPC codes which is characterized by Tanner graph of girth greater than 6.

Theorem 10. Let $S = \{a_1, a_2, a_3, \dots, a_t\}$, where $2 \leq a_1 < a_2 < a_3 \dots < a_t$ and for any $p < q < r$, $a_q - a_p = a_r - a_q = 1$ does not hold. Let P be a right circulant permutation matrix of order $(w^{a_t+1} - 1)$, where $a_t \geq 8$ is an integer and $w \geq 2$ is an even integer, and let

$$M = \begin{bmatrix} 0 & 0 & \dots & 0 \\ w^{a_1} & w^{a_2} & \dots & w^{a_t} \\ w^{a_1-1} & w^{a_2-1} & \dots & w^{a_t-1} \\ w^{a_1-2} & w^{a_2-2} & \dots & w^{a_t-2} \end{bmatrix}$$

be a model matrix associated with the parity-check matrix H . Then there exists an entanglement assisted quantum QC-LDPC code with parameters $[[n, 2k - n + c; c]]_2$, where $n = (w^{a_t+1} - 1)t$, $k \geq (w^{a_t+1} - 1)(t - 4) + 3$ and $c \leq 4(w^{a_t+1} - 1) - 3$. In addition, the Tanner graph of the parity-check matrix H is of girth greater than 6.

Proof. The length of the code is obvious to determine, and the lower bound on the dimension k can easily be obtained using Theorem 4. We will show that the Tanner graph of H is free from 4-cycles. Verifying that each nonzero row contains different elements from $\mathbb{Z}_{(w^{a_t+1}-1)}$ is easy. Therefore, by Proposition 1, the presence of a 4-cycle is not possible for one zero row and one nonzero row. Consider any two non-zero rows from the matrix M . Then there exists a 4-cycle in the Tanner graph of H if and only if there exist $p, q \in \{1, 2, \dots, t\}$, where $p < q$, such that

$$w^{a_p-\ell_1} - w^{a_p-\ell_2} = w^{a_q-\ell_1} - w^{a_q-\ell_2} \pmod{(w^{a_t+1} - 1)}, \quad (29)$$

where $\ell_1 \in \{0, 1\}$, $\ell_2 \in \{1, 2\}$ and $\ell_1 < \ell_2$. The Equation (29) holds if and only if

$$\begin{aligned} (w^{(\ell_2-\ell_1)} - 1)w^{a_p-\ell_2} &= (w^{(\ell_2-\ell_1)} - 1)w^{a_q-\ell_2} \pmod{(w^{a_t+1} - 1)} \\ \iff (w^{(\ell_2-\ell_1)} - 1) &= (w^{(\ell_2-\ell_1)} - 1)w^{(a_q-a_p)} \quad (\text{since } \gcd(w^{a_p-\ell_2}, w^{a_t+1} - 1) = 1), \end{aligned}$$

which leads to a contradiction since the number on the left is odd whereas the number on the right is even.

Next, we will prove that the graphical representation of H does not have cycles of length 6. To avoid repetition in the proof, we will consider only two cases. In the first case, we have one zero row and two nonzero rows, and in the second case, we have all nonzero rows.

Consider the following three rows and three arbitrary columns from the matrix M :

$$\begin{bmatrix} \dots & 0 & \dots & 0 & \dots & 0 & \dots \\ \dots & w^{a_p} & \dots & w^{a_q} & \dots & w^{a_r} & \dots \\ \dots & w^{a_p-1} & \dots & w^{a_q-1} & \dots & w^{a_r-1} & \dots \end{bmatrix}, \quad (30)$$

where $a_1 \leq a_p < a_q < a_r \leq a_t$. We investigate the existence of all possible 6-cycles, as shown in Figure 2, within the segment of the Tanner graph that corresponds to a portion of the model matrix defined by Equation (30).

1. **Existence of Type-I 6-cycle:** There exists Type-I 6-cycle if and only if the following holds:

$$\begin{aligned} w^{a_p-1} &= w^{a_r-1} - w^{a_r} + w^{a_q} \pmod{w^{a_t+1} - 1} \\ \implies w^{a_r} - w^{a_q} &= w^{a_r-1} - w^{a_p-1} \pmod{w^{a_t+1} - 1} \\ \implies w^{a_q}(w^{a_r-a_q} - 1) &= w^{a_p-1}(w^{a_r-a_p} - 1) \pmod{w^{a_t+1} - 1} \\ \implies w^{a_q-a_p+1}(w^{a_r-a_q} - 1) &= (w^{a_r-a_p} - 1) \pmod{w^{a_t+1} - 1}, \end{aligned}$$

since $\gcd(w^{a_p-1}, w^{a_t+1} - 1) = 1$. This is a contradiction, as the number on the left is even, while the number on the right is odd.

2. **Existence of Type-II 6-cycle:** A Type-II 6-cycle exists if and only if $w^{a_p-1} = w^{a_q-1} - w^{a_q} + w^{a_r} \pmod{w^{a_t+1} - 1}$ if and only if $w^{a_p-1} + w^{a_q} = w^{a_q-1} + w^{a_r} \pmod{w^{a_t+1} - 1}$ which leads to a contradiction, as the left-hand side is smaller than the right-hand side.
3. **Existence of Type-III 6-cycle:** There exists Type-III 6-cycle if and only if the following holds:

$$\begin{aligned} w^{a_r-1} &= w^{a_p-1} - w^{a_p} + w^{a_q} \pmod{w^{a_t+1} - 1} \\ \implies w^{a_r-1} - w^{a_p-1} &= w^{a_q} - w^{a_p} \pmod{w^{a_t+1} - 1} \\ \implies w^{a_p-1}(w^{a_r-a_p} - 1) &= w^{a_p}(w^{a_q-a_p} - 1) \pmod{w^{a_t+1} - 1} \\ \implies (w^{a_r-a_p} - 1) &= w(w^{a_q-a_p} - 1) \pmod{w^{a_t+1} - 1}, \end{aligned}$$

since $\gcd(w^{a_p-1}, w^{a_t+1} - 1) = 1$. Which is a contradiction since the number on the left is odd whereas the number on the right is even.

4. **Existence of Type-IV 6-cycle:** A Type-IV 6-cycle exists if and only if $w^{a_r-1} = w^{a_q-1} - w^{a_q} + w^{a_p} \pmod{w^{a_t+1} - 1}$, which implies $w^{a_r-1} + w^{a_q} = w^{a_q-1} + w^{a_p} \pmod{w^{a_t+1} - 1}$ and leads to a contradiction, as the left-hand side is greater than the right-hand side.

5. **Existence of Type-V 6-cycle:** A Type-V 6-cycle exists if and only if the following condition holds:

$$\begin{aligned}
w^{a_q-1} &= w^{a_p-1} - w^{a_p} + w^{a_r} \pmod{(w^{a_t+1} - 1)} \\
\implies w^{a_q-1} - w^{a_p-1} &= w^{a_r} - w^{a_p} \pmod{(w^{a_t+1} - 1)} \\
\implies w^{a_p-1}(w^{a_q-a_p} - 1) &= w^{a_p}(w^{a_r-a_p} - 1) \pmod{(w^{a_t+1} - 1)} \\
\implies (w^{a_q-a_p} - 1) &= w(w^{a_r-a_p} - 1) \pmod{(w^{a_t+1} - 1)},
\end{aligned}$$

since $\gcd(w^{a_p-1}, w^{a_t+1} - 1) = 1$. Which leads to a contradiction since the number on the left is odd whereas the number on the right is even.

6. **Existence of Type-VI 6-cycle:** There exists a Type VI 6-cycle if and only if the following holds:

$$\begin{aligned}
w^{a_q-1} &= w^{a_r-1} - w^{a_r} + w^{a_p} \pmod{(w^{a_t+1} - 1)} \\
\implies w^{a_r-1} - w^{a_q-1} &= w^{a_r} - w^{a_p} \pmod{(w^{a_t+1} - 1)} \\
\implies w^{a_q-1}(w^{a_r-a_q} - 1) &= w^{a_p}(w^{a_r-a_p} - 1) \pmod{(w^{a_t+1} - 1)} \\
\implies w^{a_q-a_p-1}(w^{a_r-a_q} - 1) &= (w^{a_r-a_p} - 1) \pmod{(w^{a_t+1} - 1)},
\end{aligned}$$

since $\gcd(w^{a_p}, w^{a_t+1} - 1) = 1$. This is a contradiction since the number on the left is even whereas the number on the right is odd unless $a_q - a_p = 1$. If $a_q - a_p = 1$, then $(w^{a_r-a_q} - 1) = (w^{a_r-a_p} - 1) \pmod{(w^{a_t+1} - 1)}$ if and only if $a_p = a_q$ which is a contradiction to the fact that $a_p < a_q$.

Consider the following three rows and three columns from the above matrix M :

$$\begin{bmatrix} \dots & w^{a_p} & \dots & w^{a_q} & \dots & w^{a_r} & \dots \\ \dots & w^{a_p-1} & \dots & w^{a_q-1} & \dots & w^{a_r-1} & \dots \\ \dots & w^{a_p-2} & \dots & w^{a_q-2} & \dots & w^{a_r-2} & \dots \end{bmatrix}, \quad (31)$$

where $a_1 \leq a_p < a_q < a_r \leq a_t$. We explore the presence of all possible 6-cycles, as depicted in Figure 2, in the segment of the Tanner graph that corresponds to a portion of the model matrix defined by Equation (31).

1. **Existence of Type-I 6-cycle:** There exists Type-I 6-cycle if and only if the following condition holds:

$$\begin{aligned}
w^{a_p-2} - w^{a_p} &= w^{a_r-2} - w^{a_r-1} + w^{a_q-1} - w^{a_q} \pmod{(w^{a_t+1} - 1)} \\
\implies (1 - w^2)w^{a_p-2} &= w^{a_r-2}(1 - w) + (1 - w)w^{a_q-1} \pmod{(w^{a_t+1} - 1)} \\
\implies w^{a_p-2} + w^{a_p-1} &= w^{a_r-2} + w^{a_q-1} \pmod{\left(\frac{w^{a_t+1} - 1}{w - 1}\right)},
\end{aligned}$$

which is a contradiction since the number on the left is less than the number on the right.

2. **Existence of Type-II 6-cycle:** A Type-II cycle of length 6 exists if and only if the following condition is satisfied:

$$\begin{aligned}
w^{a_p-2} - w^{a_p} &= w^{a_q-2} - w^{a_q-1} + w^{a_r-1} - w^{a_r} \pmod{(w^{a_t+1} - 1)} \\
\implies (1 - w^2)w^{a_p-2} &= w^{a_q-2}(1 - w) + (1 - w)w^{a_r-1} \pmod{(w^{a_t+1} - 1)}
\end{aligned}$$

$$\implies w^{a_p-2} + w^{a_p-1} = w^{a_r-2} + w^{a_q-1} \pmod{\left(\frac{w^{a_t+1}-1}{w-1}\right)}.$$

This leads to a contradiction, as the number on the left is less than the number on the right.

3. **Existence of Type-III 6-cycle:** There exists Type-III 6-cycle if and only if the following condition is satisfied:

$$\begin{aligned} w^{a_r-2} - w^{a_r} &= w^{a_p-2} - w^{a_p-1} + w^{a_q-1} - w^{a_q} \pmod{(w^{a_t+1}-1)} \\ \implies (1-w^2)w^{a_r-2} &= w^{a_p-2}(1-w) + w^{a_q-1}(1-w) \pmod{(w^{a_t+1}-1)} \\ \implies w^{a_r-2} + w^{a_r-1} &= w^{a_p-2} + w^{a_q-1} \pmod{\left(\frac{w^{a_t+1}-1}{w-1}\right)}, \end{aligned}$$

which is a contradiction since the number on the left is greater than the number on the right.

4. **Existence of Type-IV 6-cycle:** A Type-IV cycle of length 6 exists if and only if the following condition is satisfied:"

$$\begin{aligned} w^{a_r-2} - w^{a_r} &= w^{a_q-2} - w^{a_q-1} + w^{a_p-1} - w^{a_p} \pmod{(w^{a_t+1}-1)} \\ \implies (1-w^2)w^{a_r-2} &= w^{a_q-2}(1-w) + w^{a_p-1}(1-w) \pmod{(w^{a_t+1}-1)} \\ \implies w^{a_r-2} + w^{a_r-1} &= w^{a_q-2} + w^{a_p-1} \pmod{\left(\frac{w^{a_t+1}-1}{w-1}\right)}. \end{aligned}$$

This leads to a contradiction, as the number on the left is greater than the number on the right.

5. **Existence of Type-V 6-cycle:** There exists Type-V 6-cycle if and only if the following condition holds:

$$\begin{aligned} w^{a_q-2} - w^{a_q} &= w^{a_p-2} - w^{a_p-1} + w^{a_r-1} - w^{a_r} \pmod{(w^{a_t+1}-1)} \\ \implies (1-w^2)w^{a_q-2} &= w^{a_p-2}(1-w) + (1-w)w^{a_r-1} \pmod{(w^{a_t+1}-1)} \\ \implies w^{a_q-2} + w^{a_q-1} &= w^{a_p-2} + w^{a_r-1} \pmod{\left(\frac{w^{a_t+1}-1}{w-1}\right)}, \end{aligned}$$

which is a contradiction since the number on the left is less than the number on the right.

6. **Existence of Type-VI 6-cycle:** A Type VI 6-cycle exists if and only if the following condition is satisfied:

$$\begin{aligned} w^{a_q-2} - w^{a_q} &= w^{a_r-2} - w^{a_r-1} + w^{a_p-1} - w^{a_p} \pmod{(w^{a_t+1}-1)} \\ \implies (1-w^2)w^{a_q-2} &= w^{a_r-2}(1-w) + (1-w)w^{a_p-1} \pmod{(w^{a_t+1}-1)} \\ \implies w^{a_q-2} + w^{a_q-1} &= w^{a_r-2} + w^{a_p-1} \pmod{\left(\frac{w^{a_t+1}-1}{w-1}\right)} \\ \implies (w^{a_q-a_p} - 1)w^{a_p-1} &= (w^{a_r-a_q} - 1)w^{a_q-2} \pmod{\left(\frac{w^{a_t+1}-1}{w-1}\right)} \\ \implies (w^{a_q-a_p} - 1) &= (w^{a_r-a_q} - 1)w^{a_q-a_p-1} \pmod{\left(\frac{w^{a_t+1}-1}{w-1}\right)}. \end{aligned}$$

This leads to a contradiction, as the number on the left is odd while the number on the right is even, unless $a_q - a_p = 1$. If $a_q - a_p = 1$, then the condition $(w^{a_q - a_p} - 1) = (w^{a_r - a_q} - 1) \pmod{(w^{a_t + 1} - 1)}$ holds if and only if $a_q - a_p = a_r - a_q = 1$, which leads to a contradiction with the original assumptions.

The minimum number of required maximally entangled bits is given by

$$c = \text{gfrank}(HH^T),$$

where

$$HH^T = \begin{bmatrix} I & I & \dots & I \\ P(w^{a_1}) & P(w^{a_2}) & \dots & P(w^{a_t}) \\ P(w^{a_1-1}) & P(w^{a_2-1}) & \dots & P(w^{a_t-1}) \\ P(w^{a_1-2}) & P(w^{a_2-2}) & \dots & P(w^{a_t-2}) \end{bmatrix} \begin{bmatrix} I & I & \dots & I \\ P(w^{a_1}) & P(w^{a_2}) & \dots & P(w^{a_t}) \\ P(w^{a_1-1}) & P(w^{a_2-1}) & \dots & P(w^{a_t-1}) \\ P(w^{a_1-2}) & P(w^{a_2-2}) & \dots & P(w^{a_t-2}) \end{bmatrix}^T$$

$$= \begin{bmatrix} tI & \sum_{i=1}^t P^{-w^{a_i}} & \sum_{i=1}^t P^{-(w^{a_i-1})} & \sum_{i=1}^t P^{-(w^{a_i-2})} \\ \sum_{i=1}^t P^{w^{a_i}} & tI & \sum_{i=1}^t P^{(w^{a_i-1})} & \sum_{i=1}^t P^{3 \cdot w^{a_i-2}} \\ \sum_{i=1}^t P^{w^{a_i-1}} & \sum_{i=1}^t P^{-w^{a_i-1}} & tI & \sum_{i=1}^t P^{w^{a_i-2}} \\ \sum_{i=1}^t P^{(w^{a_i-2})} & \sum_{i=1}^t P^{-3 \cdot w^{a_i-2}} & \sum_{i=1}^t P^{-w^{a_i-2}} & tI \end{bmatrix}.$$

It is easy to verify that the $\text{gfrank}(HH^T) \leq 4(w^{a_t+1} - 1) - 3$ since the vector sum of each block row is either all-ones vector or zero-vector depending on whether t is even or odd, completing the proof. \square

Theorem 11. *Let $S = \{a_1, a_2, a_3, \dots, a_t\}$, where $2 \leq a_1 < a_2 < a_3 \dots < a_t$ and for any $1 \leq p < q \leq t$, $a_q - a_p \geq 2$. Let P be a right circulant permutation matrix of order $(w^{a_t+1} - 1)$, where $a_t \geq 8, w \geq 2$ are integers, and let*

$$M = \begin{bmatrix} 0 & 0 & \dots & 0 \\ w^{a_1} & w^{a_2} & \dots & w^{a_t} \\ w^{a_1-1} & w^{a_2-1} & \dots & w^{a_t-1} \\ w^{a_1-2} & w^{a_2-2} & \dots & w^{a_t-2} \end{bmatrix}$$

be a model matrix associated with the parity-check matrix H . Then there exists an entanglement assisted quantum QC-LDPC code with parameters $[[n, 2k - n + c; c]]_2$, where $n = (w^{a_t+1} - 1)t$, $k \geq (w^{a_t+1} - 1)(t - 4) + 3$ and $c \leq 4(w^{a_t+1} - 1) - 3$. In addition, the Tanner graph of the parity-check matrix H is of girth greater than 6.

Proof. The length of the code is straightforward to determine, and the lower bound on the dimension k can be easily derived using Theorem 4. Following similar arguments used in proving Theorem 10, one can easily show that the Tanner graph of H is free from 4-cycles.

Next, we will prove that the graphical representation of H does not contain cycles of length 6. To streamline the proof and avoid repetition, we will consider two cases. In the first case, we have one zero row and two nonzero rows, while in the second case, all rows are nonzero. Consider the following three rows and three arbitrary columns from the matrix M :

$$\begin{bmatrix} \dots & 0 & \dots & 0 & \dots & 0 & \dots \\ \dots & w^{a_p} & \dots & w^{a_q} & \dots & w^{a_r} & \dots \\ \dots & w^{a_p-1} & \dots & w^{a_q-1} & \dots & w^{a_r-1} & \dots \end{bmatrix}, \quad (32)$$

Algorithm 3 Syndrome-based binary Sum-Product Decoding

- 1: **procedure** SYNDROME SUM PRODUCT DECODING
- 2: **Input:** Syndrome S , parity-check matrix $H_{\rho \times n}$, maximum allowable iterations l_{\max} , depolarizing probability p_d .
- 3: **Output:** Estimated error vector \tilde{e} .
- 4: Create a Tanner graph using the matrix H with n variable nodes and ρ check nodes.
- 5: Initialize LLRs for all variable nodes:

$$L_i = \ln \left(\frac{1-p_d}{p_d} \right), \quad \forall i \in \{1, 2, \dots, n\}.$$

- 6: Pass initialized LLRs to the check nodes connected to the variable nodes.
- 7: **for** each check node j **do**
- 8: Compute the message to variable node i :

$$\mu_{j \rightarrow i} = 2(-1)^{S_j} \tanh^{-1} \left(\prod_{k \in \mathcal{N}_j^{(c)} \setminus \{i\}} \tanh \left(\frac{\nu_{k \rightarrow j}}{2} \right) \right).$$

- 9: **end for**
- 10: **for** each variable node i **do**
- 11: Compute the message to check node j :

$$\nu_{i \rightarrow j} = L_i + \sum_{k \in \mathcal{N}_i^{(v)} \setminus \{j\}} \mu_{k \rightarrow i}.$$

- 12: **end for**
- 13: Compute posterior probabilities for each variable node:

$$P_i = L_i + \sum_{j \in \mathcal{N}_i^{(v)}} \mu_{j \rightarrow i}.$$

- 14: Determine estimated error vector \tilde{e} using:

$$\tilde{e}_i = \begin{cases} 0, & \text{if } P_i > 0, \\ 1, & \text{if } P_i \leq 0. \end{cases}$$

- 15: Check convergence:
 - 16: **if** $\tilde{S} = H\tilde{e}^T$ or iterations reach l_{\max} **then**
 - 17: **return** \tilde{e}
 - 18: **else**
 - 19: Go to step 7
 - 20: **end if**
 - 21: **end procedure**
-

where $a_1 \leq a_p < a_q < a_r \leq a_t$. We investigate the existence of all possible 6-cycles, as shown in Figure 2, within the segment of the Tanner graph that corresponds to a portion of the model matrix defined by Equation (32).

1. **Existence of Type-I 6-cycle:** There exists Type-I 6-cycle if and only if the fol-
-

lowing holds:

$$\begin{aligned}
w^{a_p-1} &= w^{a_r-1} - w^{a_r} + w^{a_q} \pmod{(w^{a_t+1} - 1)} \\
\implies w^{a_r} - w^{a_q} &= w^{a_r-1} - w^{a_p-1} \pmod{(w^{a_t+1} - 1)} \\
\implies (w-1)w^{a_r-1} + (w^{a_r-1} - w^{a_q}) &= w^{a_r-1} - w^{a_p-1} \pmod{(w^{a_t+1} - 1)}.
\end{aligned}$$

This is a contradiction, as the number on the left is greater than the number on the right.

2. **Existence of Type-II 6-cycle:** A Type-II 6-cycle exists if and only if $w^{a_p-1} = w^{a_q-1} - w^{a_q} + w^{a_r} \pmod{(w^{a_t+1} - 1)}$ if and only if $w^{a_p-1} + w^{a_q} = w^{a_q-1} + w^{a_r} \pmod{(w^{a_t+1} - 1)}$ which leads to a contradiction, as the left-hand side is smaller than the right-hand side.
3. **Existence of Type-III 6-cycle:** There exists Type-III 6-cycle if and only if the following holds:

$$\begin{aligned}
w^{a_r-1} &= w^{a_p-1} - w^{a_p} + w^{a_q} \pmod{(w^{a_t+1} - 1)} \\
\implies w^{a_r-1} - w^{a_p-1} &= w^{a_q} - w^{a_p} \pmod{(w^{a_t+1} - 1)} \\
\implies (w-1)w^{a_r-2} + (w^{a_r-2} - w^{a_p-1}) &= w^{a_q} - w^{a_p} \pmod{(w^{a_t+1} - 1)},
\end{aligned}$$

which is a contradiction since the number on the right is less than the number on the left.

4. **Existence of Type-IV 6-cycle:** A Type-IV 6-cycle exists if and only if $w^{a_r-1} = w^{a_q-1} - w^{a_q} + w^{a_p} \pmod{(w^{a_t+1} - 1)}$, which implies $w^{a_r-1} + w^{a_q} = w^{a_q-1} + w^{a_p} \pmod{(w^{a_t+1} - 1)}$ and leads to a contradiction, as the left-hand side is greater than the right-hand side.
5. **Existence of Type-V 6-cycle:** A Type-V 6-cycle exists if and only if the following condition holds:

$$\begin{aligned}
w^{a_q-1} &= w^{a_p-1} - w^{a_p} + w^{a_r} \pmod{(w^{a_t+1} - 1)} \\
\implies w^{a_q-1} - w^{a_p-1} &= w^{a_r} - w^{a_p} \pmod{(w^{a_t+1} - 1)} \\
\implies w^{a_q-1} - w^{a_p-1} &= (w-1)w^{a_r-1} + (w^{a_r-1} - w^{a_p}) \pmod{(w^{a_t+1} - 1)},
\end{aligned}$$

which is a contradiction since the number on the left is less than the number on the right.

6. **Existence of Type-VI 6-cycle:** There exists a Type VI 6-cycle if and only if the following holds:

$$\begin{aligned}
w^{a_q-1} &= w^{a_r-1} - w^{a_r} + w^{a_p} \pmod{(w^{a_t+1} - 1)} \\
\implies w^{a_r-1} - w^{a_q-1} &= w^{a_r} - w^{a_p} \pmod{(w^{a_t+1} - 1)} \\
\implies w^{a_r-1} - w^{a_q-1} &= (w-1)w^{a_r-1} + (w^{a_r-1} - w^{a_p}) \pmod{(w^{a_t+1} - 1)},
\end{aligned}$$

which is a contradiction since the number on the right is greater than the number the number on the left.

Consider the following three rows and three columns from the above matrix M :

$$\begin{bmatrix} \dots & w^{a_p} & \dots & w^{a_q} & \dots & w^{a_r} & \dots \\ \dots & w^{a_p-1} & \dots & w^{a_q-1} & \dots & w^{a_r-1} & \dots \\ \dots & w^{a_p-2} & \dots & w^{a_q-2} & \dots & w^{a_r-2} & \dots \end{bmatrix}, \quad (33)$$

where $a_1 \leq a_p < a_q < a_r \leq a_t$. We investigate the existence of all possible 6-cycles, as shown in Figure 2, within the segment of the Tanner graph that corresponds to a portion of the model matrix defined by Equation (33).

1. **Existence of Type-I 6-cycle:** There exists Type-I 6-cycle if and only if the following condition holds:

$$\begin{aligned} w^{a_p-2} - w^{a_p} &= w^{a_r-2} - w^{a_r-1} + w^{a_q-1} - w^{a_q} \pmod{(w^{a_t+1} - 1)} \\ \implies (1 - w^2)w^{a_p-2} &= w^{a_r-2}(1 - w) + (1 - w)w^{a_q-1} \pmod{(w^{a_t+1} - 1)} \\ \implies w^{a_p-2} + w^{a_p-1} &= w^{a_r-2} + w^{a_q-1} \pmod{\left(\frac{w^{a_t+1} - 1}{w - 1}\right)}, \end{aligned}$$

which is a contradiction since the number on the left is less than the number on the right.

2. **Existence of Type-II 6-cycle:** A Type-II cycle of length 6 exists if and only if the following condition is satisfied:

$$\begin{aligned} w^{a_p-2} - w^{a_p} &= w^{a_q-2} - w^{a_q-1} + w^{a_r-1} - w^{a_r} \pmod{(w^{a_t+1} - 1)} \\ \implies (1 - w^2)w^{a_p-2} &= w^{a_q-2}(1 - w) + (1 - w)w^{a_r-1} \pmod{(w^{a_t+1} - 1)} \\ \implies w^{a_p-2} + w^{a_p-1} &= w^{a_r-2} + w^{a_q-1} \pmod{\left(\frac{w^{a_t+1} - 1}{w - 1}\right)}. \end{aligned}$$

This leads to a contradiction, as the number on the left is less than the number on the right.

3. **Existence of Type-III 6-cycle:** There exists Type-III 6-cycle if and only if the following condition is satisfied:

$$\begin{aligned} w^{a_r-2} - w^{a_r} &= w^{a_p-2} - w^{a_p-1} + w^{a_q-1} - w^{a_q} \pmod{(w^{a_t+1} - 1)} \\ \implies (1 - w^2)w^{a_r-2} &= w^{a_p-2}(1 - w) + w^{a_q-1}(1 - w) \pmod{(w^{a_t+1} - 1)} \\ \implies w^{a_r-2} + w^{a_r-1} &= w^{a_p-2} + w^{a_q-1} \pmod{\left(\frac{w^{a_t+1} - 1}{w - 1}\right)}, \end{aligned}$$

which is a contradiction since the number on the left is greater than the number on the right.

4. **Existence of Type-IV 6-cycle:** A Type-IV cycle of length 6 exists if and only if the following condition is satisfied:"

$$\begin{aligned} w^{a_r-2} - w^{a_r} &= w^{a_q-2} - w^{a_q-1} + w^{a_p-1} - w^{a_p} \pmod{(w^{a_t+1} - 1)} \\ \implies (1 - w^2)w^{a_r-2} &= w^{a_q-2}(1 - w) + w^{a_p-1}(1 - w) \pmod{(w^{a_t+1} - 1)} \\ \implies w^{a_r-2} + w^{a_r-1} &= w^{a_q-2} + w^{a_p-1} \pmod{\left(\frac{w^{a_t+1} - 1}{w - 1}\right)}. \end{aligned}$$

This leads to a contradiction, as the number on the left is greater than the number on the right.

5. **Existence of Type-V 6-cycle:** There exists Type-V 6-cycle if and only if the following condition holds:

$$\begin{aligned}
& w^{a_q-2} - w^{a_q} = w^{a_p-2} - w^{a_p-1} + w^{a_r-1} - w^{a_r} \pmod{(w^{a_t+1} - 1)} \\
\implies & (1 - w^2)w^{a_q-2} = w^{a_p-2}(1 - w) + (1 - w)w^{a_r-1} \pmod{(w^{a_t+1} - 1)} \\
\implies & w^{a_q-2} + w^{a_q-1} = w^{a_p-2} + w^{a_r-1} \pmod{\left(\frac{w^{a_t+1} - 1}{w - 1}\right)},
\end{aligned}$$

which is a contradiction since the number on the left is less than the number on the right.

6. **Existence of Type-VI 6-cycle:** A Type VI 6-cycle exists if and only if the following condition is satisfied:

$$\begin{aligned}
& w^{a_q-2} - w^{a_q} = w^{a_r-2} - w^{a_r-1} + w^{a_p-1} - w^{a_p} \pmod{(w^{a_t+1} - 1)} \\
\implies & (1 - w^2)w^{a_q-2} = w^{a_r-2}(1 - w) + (1 - w)w^{a_p-1} \pmod{(w^{a_t+1} - 1)} \\
\implies & w^{a_q-2} + w^{a_q-1} = w^{a_r-2} + w^{a_p-1} \pmod{\left(\frac{w^{a_t+1} - 1}{w - 1}\right)} \\
\implies & w^{a_q-2} + w^{a_q-1} = (w - 1)w^{a_r-3} + (w^{a_r-3} + w^{a_p-1}) \pmod{\left(\frac{w^{a_t+1} - 1}{w - 1}\right)}.
\end{aligned}$$

This leads to a contradiction, as the number on the left is less the number on the right.

The minimum number of required maximally entangled bits is given by

$$c = \text{gfrank}(HH^T),$$

where

$$\begin{aligned}
HH^T &= \begin{bmatrix} I & I & \dots & I \\ P(w^{a_1}) & P(w^{a_2}) & \dots & P(w^{a_t}) \\ P(w^{a_1-1}) & P(w^{a_2-1}) & \dots & P(w^{a_t-1}) \\ P(w^{a_1-2}) & P(w^{a_2-2}) & \dots & P(w^{a_t-2}) \end{bmatrix} \begin{bmatrix} I & I & \dots & I \\ P(w^{a_1}) & P(w^{a_2}) & \dots & P(w^{a_t}) \\ P(w^{a_1-1}) & P(w^{a_2-1}) & \dots & P(w^{a_t-1}) \\ P(w^{a_1-2}) & P(w^{a_2-2}) & \dots & P(w^{a_t-2}) \end{bmatrix}^T \\
&= \begin{bmatrix} tI & \sum_{i=1}^t P^{-w^{a_i}} & \sum_{i=1}^t P^{-(w^{a_i-1})} & \sum_{i=1}^t P^{-(w^{a_i-2})} \\ \sum_{i=1}^t Pw^{a_i} & tI & \sum_{i=1}^t P(w^{a_i-1}) & \sum_{i=1}^t P3.w^{a_i-2} \\ \sum_{i=1}^t Pw^{a_i-1} & \sum_{i=1}^t P^{-w^{a_i-1}} & tI & \sum_{i=1}^t Pw^{a_i-2} \\ \sum_{i=1}^t P(w^{a_i-2}) & \sum_{i=1}^t P^{-3.w^{a_i-2}} & \sum_{i=1}^t P^{-w^{a_i-2}} & tI \end{bmatrix}.
\end{aligned}$$

It is easy to verify that the $\text{gfrank}(HH^T) \leq 4(w^{a_t+1} - 1) - 3$ since the vector sum of each block row is either all-ones vector or zero-vector depending on whether t is even or odd, completing the proof. \square

6 Code Performance over Markovian correlated quantum channels

Consider a quantum state ρ consisting of l -qubits, which is transmitted over a quantum channel exhibiting Markovian correlations, as studied in prior works for quantum error

correction in burst errors and correlated channels [83, 84]. The channel model assumes a depolarizing noise process, denoted by $\pi(p_d)$, that acts independently on each qubit. When applied to a single qubit state σ , the channel introduces a Pauli error with probability p_d as follows: $\sigma \rightarrow (1 - p_d)\sigma + \frac{p_d}{3}(X\sigma X + Y\sigma Y + Z\sigma Z)$, where X , Y , and Z represent the Pauli matrices acting on the state σ .

In this model, the Pauli error E_i on the i^{th} qubit can be an element from the set $\{I, X, Y, Z\}$. Due to Markovian correlations in the channel, an error E_i occurring on the i^{th} qubit influences the likelihood of an error E_j on an adjacent qubit j , where $j = i + 1$. This influence is governed by a correlation parameter η , under a first-order Markov process, and is mathematically described by the conditional probability:

$$P(E_j|E_i) = (1 - \eta)P(E_j) + \eta \delta_{E_i, E_j},$$

where δ_{E_i, E_j} is an indicator function given by

$$\delta_{E_i, E_j} = \begin{cases} 1, & \text{if } E_i = E_j, \\ 0, & \text{if } E_i \neq E_j. \end{cases}$$

For each qubit $i \in \{1, 2, \dots, l\}$, the probability distribution for the error E_i is specified as $P(E_i = I) = 1 - p_d$ for the identity error, and $P(E_i \in \mathcal{E}) = \frac{p_d}{3}$, where $\mathcal{E} = \{X, Y, Z\}$. This model captures the correlated nature of errors in the quantum channel, allowing us to analyze the impact of noise propagation on entangled states in a systematic way. In general, if Φ is the Markovian error applied on the l -qubit state ρ , then

$$\Phi(\rho) = \sum_{E_1, \dots, E_l} P(E_1) \prod_{i=2}^l P(E_i|E_{i-1}) E_l \cdots E_1 \rho E_1^\dagger \cdots E_l^\dagger.$$

The classical quasi-cyclic LDPC code $\mathcal{C} = [n, k, d]$, designed using permutation matrices of order p as described in Section 3, has a burst error correction capability of at least length p [6]. The EA quantum QC-LDPC code $Q = [[n, k, d_q; c]]_2$, constructed from \mathcal{C} as detailed in Theorem 5, can correct quantum burst errors of length p because the matrices H_x and H_z , derived from H , are individually capable of correcting bursts of length at least p [85].

6.1 Binary Sum-Product Algorithm

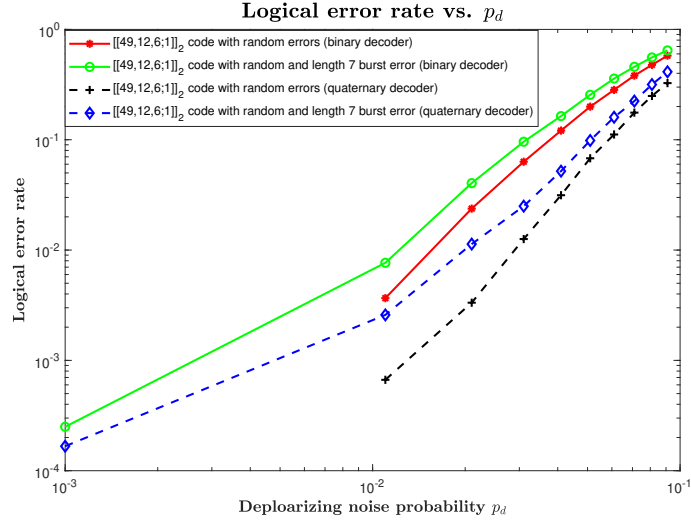
We now describe the syndrome-based sum-product algorithm with the tanh-based approach [86] over the Tanner graph derived from the following stabilizer matrix

$$H_{\text{CSS}} = \left[\begin{array}{c|c} H_x & \mathbf{0}_{(n-k_1) \times n} \\ \mathbf{0}_{(n-k_2) \times n} & H_z \end{array} \right],$$

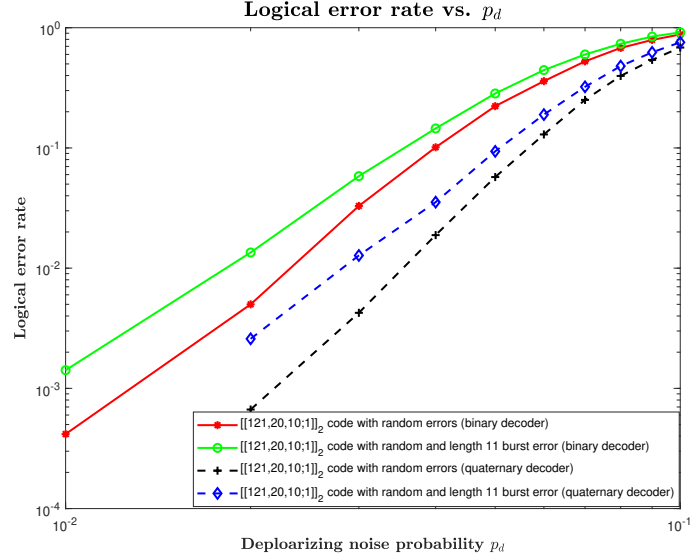
where $H_x H_z^\text{T} \equiv \mathbf{0} \pmod{2}$, for the $[[n, k_1 + k_2 - n, d_q]]_2$ quantum CSS code. This Tanner graph is divided into two separate graphs: one constructed using H_x with n variable nodes and $n - k_1$ check nodes, and another using H_z with n variable nodes and $n - k_2$ check nodes. The sum-product algorithm operates concurrently over both the Tanner graphs.

Let the syndrome $S = [S_x, S_z]$ be obtained by measuring observables isomorphic to H_x and H_z on quantum hardware. The tanh-based message-passing algorithm, detailed in Algorithm 3, is used to pass messages over each graph. For a variable node i connected to a check node j , the message from the variable node to the check node is updated as:

$$\nu_{i,j} = L_i + \sum_{k \in \mathcal{N}_i^{(v)} \setminus \{j\}} \mu_{k,i},$$



(a) Performance of the $[[49, 12, 6; 1]]_2$ code.



(b) Performance of the $[[121, 20, 10; 1]]_2$ code.

Figure 6: The performance curves for the $[[49, 12, 6; 1]]_2$ and $[[121, 20, 10; 1]]_2$ EA quantum QC-LDPC codes over the depolarizing random noise and depolarizing random noise with Markovian burst errors using the sum-product binary and quaternary decoders are shown. The logical error rate is plotted against the depolarizing probability p_d . The quaternary decoder performs better compared to the binary decoder for both random depolarizing and random depolarizing with burst errors. Figures (a) and (b) also show the performance improvement with increasing order of the tiled permutation matrices from $p = 7$ to $p = 11$.

where $L_i = \ln\left(\frac{1-p_d}{p_d}\right)$ is the log-likelihood ratio (LLR) associated with the depolarizing noise model $\pi(p_d)$, fixed for all n qubits due to uniform error likelihood.

For each check node j and its neighboring variable node i , the message from the check

node to the variable node is given by

$$\mu_{j,i} = 2(-1)^{S_j} \tanh^{-1} \left(\prod_{k \in \mathcal{N}_j^{(c)} \setminus \{i\}} \tanh \left(\frac{\nu_{k,j}}{2} \right) \right), \quad (34)$$

where $\mathcal{N}_j^{(c)}$ represents the neighboring variable nodes connected to check node j , and $\mathcal{N}_i^{(v)}$ represents the neighboring check nodes connected to variable node i . The sign of each syndrome bit S_j determines the sign of the messages at the check nodes.

The algorithm continues iterating until the estimated error vector calculated as follows: $\tilde{e}_{x,z} = \text{sign} \left(L_i + \sum_{k \in \mathcal{N}_i^{(v)}} \mu_{k,i} \right)$ reproduces the syndrome $S_{x,z}$, i.e., $\tilde{S}_x = H_x \tilde{e}_x^T$ and $\tilde{S}_z = H_z \tilde{e}_z^T$. If $\tilde{S}_x = S_x$ and $\tilde{S}_z = S_z$, or the maximum iteration count l_{\max} is reached, the algorithm terminates.

6.2 Quaternary Sum-Product Algorithm

In this subsection, we will describe the quaternary sum product algorithm [87], which takes into account the correlations between the errors X and Z , which is useful for the Markovian correlated quantum channel described in Section 6 since the binary messages are replaced with quaternary vectors, i.e., the vectors of length four, over the combined Tanner graph. The quaternary vectors contain the log-likelihoods (LLR) of the Pauli-operators on a single qubit $\{I, X, Y, Z\}$ that is passed on the combined Tanner graph such that the maximum LLR out of four LLRs in a quaternary vector will provide the most-likely Pauli-error on that particular qubit in an n -qubit codeword state.

Now, the stabilizer H_{CSS} matrix can be combined to form quaternary matrix as $H = \begin{bmatrix} \omega H_x \\ H_z \end{bmatrix}$ such that the X and Z in a stabilizer matrix are represented by ω and 1 , respectively, where $1, \omega \in \mathbb{F}_4$. The joint Tanner graph designed using the matrix H has corresponding edges labeled with ω and 1 to distinguish H_x and H_z stabilizer matrices, respectively. Consider the syndrome $S = [S_x S_z]$ is obtained by measuring the stabilizer generators of the quantum code over a depolarizing noise channel $\pi(p_d)$. The i^{th} variable node will pass the $M_{i,j}^{(t)}$ message to the j^{th} check node at the t^{th} iteration such that

$$M_{i,j}^{(t)} = F_{\max}(L_{c_1}^{(t)}, L_{c_2}^{(t)}) - F_{\max}(L_{a_1}^{(t)}, L_{a_2}^{(t)}), \quad (35)$$

where $F_{\max}(a, b) = \max\{a, b\} + \log\{1 + \exp\{-|a - b|\}\}$, $L_{c_1}^{(t)}$, $L_{c_2}^{(t)}$, $L_{a_1}^{(t)}$ and $L_{a_2}^{(t)}$ are the LLRs of the single qubit Pauli errors at the t^{th} iteration. $L_{c_1}^{(t)}$, $L_{c_2}^{(t)}$ are the LLRs of the single qubit Pauli operators that commute with an element of the single qubit Pauli operator isomorphic to element $H_{i,j}$. Similarly, $L_{a_1}^{(t)}$ and $L_{a_2}^{(t)}$ are the LLRs of the single qubit Pauli operators that anti-commute with an operator isomorphic to an element $H_{i,j}$. For example, $H_{i,j} = \omega \equiv X$ then $\{I, X\}$ will commute and $\{Y, Z\}$ anti-commute with X so the corresponding LLRs are $L_I^{(t)}$ and $L_X^{(t)}$ are LLRs for the commuting set and $L_Y^{(t)}$ and $L_Z^{(t)}$ are for the anti-commuting set.

Initially, all the variable nodes are equally likely to be susceptible to the $\{X, Y, Z\}$ Pauli-errors with probability $\frac{p}{3}$. So, the quaternary LLR vectors to the i^{th} variable nodes are given by

$$l_i^{(0)} = \left[\log \left(\frac{p_I}{p_I} \right), \log \left(\frac{p_X}{p_I} \right), \log \left(\frac{p_Y}{p_I} \right), \log \left(\frac{p_Z}{p_I} \right) \right], \forall i \in \{1, 2, \dots, n\} \quad (36)$$

Algorithm 4 Syndrome-based Quaternary Sum-Product Decoding

- 1: **procedure** SYNDROME SUM PRODUCT DECODING
- 2: **Input:** Syndrome S , parity-check matrix $H_{\rho \times n}$, maximum allowable iterations l_{\max} , depolarizing probability p_d .
- 3: **Output:** Estimated error vector \tilde{e} .
- 4: Create a Tanner graph using the matrix H with n variable nodes and ρ check nodes.
- 5: Initialize LLRs in quaternary vector form for all variable nodes:

$$l_i^{(0)} = \left[0, \log \left(\frac{p}{3(1-p)} \right), \log \left(\frac{p}{3(1-p)} \right), \log \left(\frac{p}{3(1-p)} \right) \right], \forall i \in \{1, 2, \dots, n\}.$$

Using $l_i^{(0)}$, we calculate

$$M_{i,j} = F_{\max} \left(0, \log \left(\frac{p}{3(1-p)} \right) \right) - F_{\max} \left(\log \left(\frac{p}{3(1-p)} \right), \log \left(\frac{p}{3(1-p)} \right) \right), \\ \forall i \in \{1, 2, \dots, n\} \text{ and } j \in \{1, 2, \dots, n-k\}.$$

- 6: Pass initialized $M_{i,j}$ to the check nodes connected to the variable nodes.
- 7: **for** each check node j **do**
- 8: Compute the message to variable node i :

$$\mu_{i,j} = 2(-1)^{S_j} \tanh^{-1} \left(\prod_{k \in \mathcal{N}_j^{(c)} \setminus \{i\}} \tanh \left(\frac{M_{k,j}}{2} \right) \right).$$

Using $\mu_{i,j}$, we generate a quaternary vector passed to each variable node as follows:

$$L_{i,j}^{(t)} = \begin{cases} 0, & \text{if } [P_k, H_{i,j}^{(P)}] = 0, \forall k \in \{0, 1, 2, 3\}, \\ -\mu_{i,j}, & \text{if } \{P_k, H^{(P)}\} = 0, \forall k \in \{0, 1, 2, 3\}. \end{cases}$$

- 9: **end for**
- 10: **for** each variable node i **do**
- 11: Compute the message to check node j :

$$l_{i,j}^{(t)} = l_i^{(0)} + \sum_{k \in \mathcal{N}_i^{(v)} \setminus \{j\}} L_{i,k}^{(t)}.$$

- 12: **end for**
- 13: Compute posterior probabilities for each variable node:

$$E_i = \operatorname{argmax} \left[l_i^{(0)} + \sum_{k \in \mathcal{N}_i^{(v)}} L_{i,k}^{(t)} \right].$$

Using E_i , obtain the binary vector \tilde{e}_i isomorphic to the Pauli error operator.

- 14: Check convergence:
- 15: **if** $\hat{S} = H\tilde{e}^T$ or iterations reach l_{\max} **then**
- 16: **return** \tilde{e}
- 17: **else**
- 18: Go to step 7
- 19: **end if**

20: **end procedure**

such that $p_I = 1 - p$ and $p_X = p_Y = p_Z = \frac{p}{3}$ for the depolarizing channel. Therefore, $l_i^{(0)}$ is given by

$$l_i^{(0)} = \left[0, \log \left(\frac{p}{3(1-p)} \right), \log \left(\frac{p}{3(1-p)} \right), \log \left(\frac{p}{3(1-p)} \right) \right], \forall i \in \{1, 2, \dots, n\}. \quad (37)$$

Using Equation (35), the initial message $M_{i,j}^{(1)}$ on the edge connecting the i^{th} variable node to the j^{th} check node is given by

$$M_{i,j}^{(1)} = F_{\max} \left(0, \log \left(\frac{p}{3(1-p)} \right) \right) - F_{\max} \left(\log \left(\frac{p}{3(1-p)} \right), \log \left(\frac{p}{3(1-p)} \right) \right), \\ \forall i \in \{1, 2, \dots, n\} \text{ and } j \in \{1, 2, \dots, n-k\}. \quad (38)$$

The form of initial message $M_{i,j}^{(1)}$ is due to the fact that the initial LLRs for all X , Y and Z are equal to $\log \left(\frac{p}{3(1-p)} \right)$. This implies $L_{a_1}^{(1)} = L_{a_2}^{(1)} = L_{c_2}^{(1)} = \log \left(\frac{p}{3(1-p)} \right)$ and I commutes with all single qubit Pauli operators, implying $L_{c_1}^{(1)} = 0$.

At the j^{th} check node, the message $\mu_{i,j}^{(t)}$ to the i^{th} variable node is calculated using Equation (34) as follows:

$$\mu_{i,j}^{(t)} = 2(-1)^{S_j} \tanh^{-1} \left(\prod_{k \in \mathcal{N}_j^{(c)} \setminus \{i\}} \tanh \left(\frac{M_{k,j}^{(t)}}{2} \right) \right).$$

The message $\mu_{i,j}$ can be converted to the quaternary vector corresponding to $[I, X, Y, Z] = [P_0, P_1, P_2, P_3]$ as follows:

$$L_{i,j}^{(t)} = \begin{cases} 0, & \text{if } [P_k, H_{i,j}^{(P)}] = 0, \forall k \in \{0, 1, 2, 3\}, \\ -\mu_{i,j}, & \text{if } \{P_k, H_{i,j}^{(P)}\} = 0, \forall k \in \{0, 1, 2, 3\}, \end{cases} \quad (39)$$

where $H_{i,j}^{(P)}$ is the operator isomorphic to the element of \mathbb{F}_4 in $H_{i,j}$, i.e., $H_{i,j}^{(P)} \equiv H_{i,j}$. At the i^{th} variable, the new LLR is calculated by adding the LLRs from the neighboring check nodes $\mathcal{N}_i^{(v)}$ leaving the LLR of the j^{th} check node as follows:

$$l_{i,j}^{(t)} = l_i^{(0)} + \sum_{k \in \mathcal{N}_i^{(v)} \setminus \{j\}} L_{i,k}^{(t)}. \quad (40)$$

Again, instead of transmitting $l_{i,j}^{(t)}$, $M_{i,j}^{(t)}$ is calculated using Equation (35) and transmitted on the edge to the j^{th} check-node from the i^{th} variable node. The process is repeated until the estimated error vector

$$E_i^{(t)} = \operatorname{argmax} \left(l_i^{(0)} + \sum_{k \in \mathcal{N}_i^{(v)}} L_{i,k}^{(t)} \right), \text{ for all } i \in \{1, 2, \dots, n\},$$

at the end of every t iteration generates the same syndrome as the initial syndrome S .

6.3 Performance of EA Quantum QC-LDPC Codes

In the presence of burst or correlated errors that can be modeled as a Markov process, decoding on separate Tanner graphs for X and Z stabilizer generators is suboptimal. This underperformance arises due to the classical correlations between the X and Z error components, which are not fully captured by independent decoding.

To address this, a **joint Tanner graph** can be constructed that integrates the X and Z stabilizer generators into a unified framework. This joint representation allows the decoder to account for the correlations between the X and Z error components more effectively.

The constructions of such joint graphs in a stabilizer code construction have a disadvantage of cycles of length 4, arising due to the dual containment property of the classical codes required for the construction of quantum CSS codes. However, in the **entanglement-assisted quantum error correction (EAQEC)** framework, where additional preshared entanglement between sender and receiver is available, the use of joint graphs becomes particularly advantageous. Since the entangled qubit shared with the receiver does not take active participation in the decoding process due to the consideration of noise-free qubits shared with the receiver, then cycles of length 4 are avoided since only qubits transmitted from the sender end are considered noisy. By leveraging the additional structure introduced by the shared entanglement, the decoder can exploit the correlations to achieve better error correction performance, especially under the Markovian error model where temporal and spatial correlations are prevalent.

For total number of errors m_E , the logical error rate (LER) of the quantum code is $\frac{n_E}{m_E}$. n_E counts errors where $E_2^\dagger E_1 \notin S$ or the decoder has reached its maximum iterations, where E_1 is the actual error, E_2 is the error estimated by the decoder, and S is the stabilizer group. The plot of logical error rate versus p_d , using independent syndrome-based sum product algorithms on the binary and quaternary decoders in Figures (6a) and (6b). Figures show the logical error rate vs. depolarizing error probability p_d for $\eta = 0.5$ over the Markovian error model. Monte Carlo simulations with 12,000 errors are performed to plot the logical errors to evaluate $[[121, 20, 10; 1]]_2$ and $[[49, 12, 6; 1]]_2$ EA quantum QC LDPC codes for random and burst errors. The performances of the codes against the depolarizing channel and depolarizing channel with burst errors are plotted while running the binary decoders on the separate Tanner graphs and the quaternary decoder on the combined graph.

From Figures (6a) and (6b), we can clearly see the performance improvements when using a quaternary decoder on a combined graph compared to the binary decoder on two separate graphs with maximum decoding iterations for both decoders set to $l_{\max} = 100$.

In the case of burst/correlated errors from the Markovian model described earlier, we note, from Figures (6a) and (6b), the quaternary decoder is performing better than the binary decoder while comparing the curves of quaternary decoder against depolarizing with Markovian burst and the binary decoder against the depolarizing without Markovian burst. This is due to the classical nature of decoding in the case of binary decoder on the separate Tanner graphs. Therefore, quaternary decoders are well suited for correlated quantum channels like Markovian bursts.

From Figures (6a) and (6b), we also note that the performance of the EA quantum QC LDPC codes improves with increasing p from 0.01 to 0.1 even when the length of the burst increases linearly with p . Figure 7 shows the logical error rate vs. η . For simplicity, we have considered the two EA quantum QC LDPC codes $[[25, 8, 4; 1]]_2$ and $[[49, 12, 6; 1]]_2$. From Figure 7, we observe that the logical error rate of the EA quantum QC LDPC codes becomes similar for the random errors case, as well as for a mixture of random and burst errors over higher η than otherwise, implying that the code can correct almost all bursts

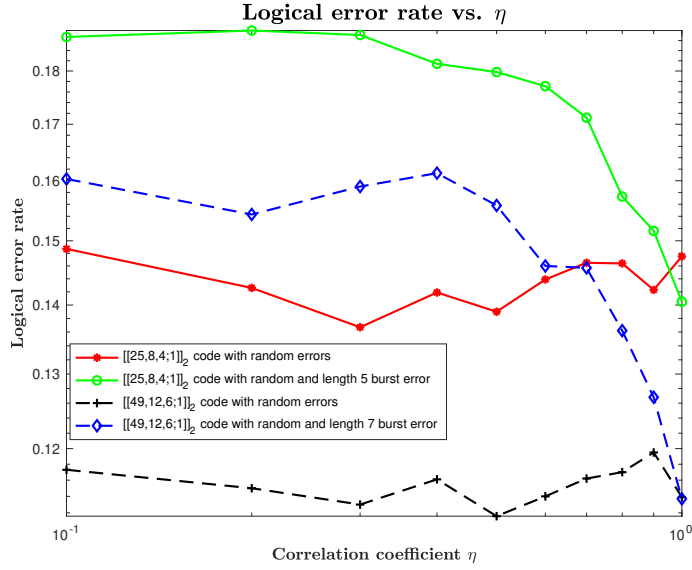


Figure 7: The LER vs. η for $p_d = 0.03$ is shown for the EA quantum QC-LDPC codes $[[25, 8, 4; 1]]_2$ and $[[49, 12, 6; 1]]_2$. For both the codes, we assess the LER against (a) the random depolarizing model and (b) the random depolarizing along with the Markovian noise bursts. We observe the convergence of the LER for both the channels for the two codes when the $\eta \rightarrow 1$ since the code can correct all bursts of length p .

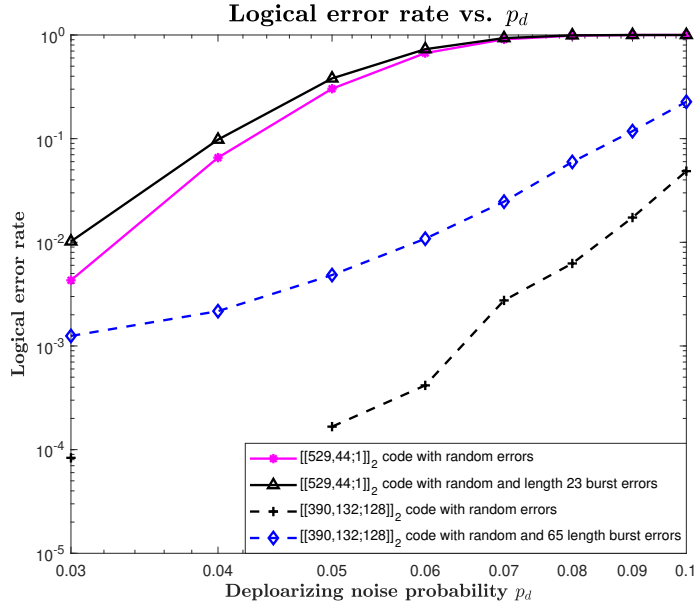


Figure 8: The code performance improvement is seen while using the $[[390, 132; 128]]_2$ EA quantum QC-LDPC code having girth greater than 6 compared to the $[[529, 44; 1]]_2$ having girth greater than 4 while using the quaternary decoder over the random depolarizing and random depolarizing with Markovian burst error channels. Even though the length of EA quantum QC-LDPC code $[[390, 132; 128]]_2$ is less than the length of the EA quantum QC-LDPC code $[[529, 44; 1]]_2$, the code $[[390, 132; 128]]_2$ is performs better than $[[529, 44; 1]]_2$ with good burst error correction capability of 65 as compared to 23 due to the inherent block structure of the permutation matrices of the EA quantum QC-LDPC codes $[[390, 132; 128]]_2$ and $[[529, 44; 1]]_2$.

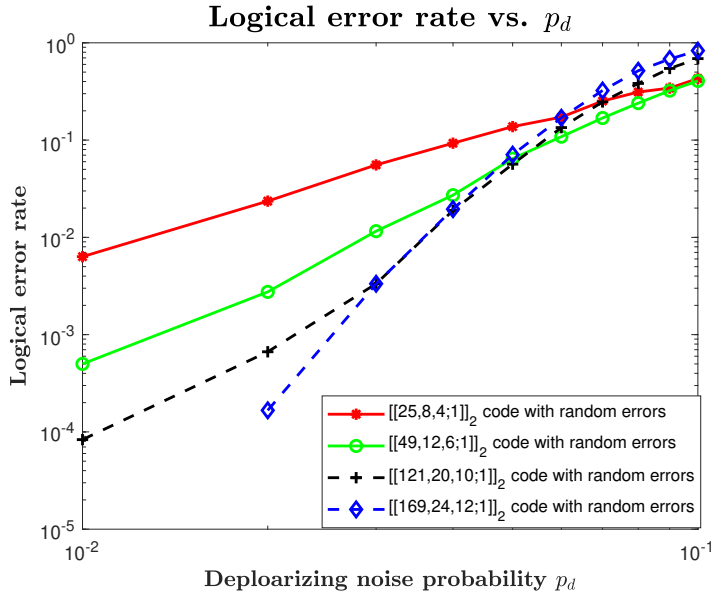


Figure 9: The code performance curves for various EA quantum QC-LDPC codes $[[25, 8, 4; 1]]_2$, $[[49, 12, 6; 1]]_2$, $[[121, 20, 10; 1]]_2$ and $[[169, 24, 12; 1]]_2$ with underlying tiled permutation matrices of orders 5, 7, 11 and 13, respectively, against the random depolarizing noise model are plotted. Plots of the logical error rate of EA quantum QC-LDPC codes $[[121, 20, 10; 1]]_2$ and $[[169, 24, 12; 1]]_2$ intersect at 0.03 after which $[[121, 20, 10; 1]]_2$ code performs better than $[[169, 24, 12; 1]]_2$. Near the depolarizing error rate threshold of 0.075, the LER plots for the all the codes intersect after which an increment in the length of the code does not improve LER performance.

of length p when $\eta \simeq 1$.

Figure 8 shows a comparison between the $[529, 44; 1]$ code, which has a girth greater than 4, and the $[390, 132; 128]$ code, which has a girth greater than 6. Clearly, the $[[390, 132; 128]]_2$ code is performing better in comparison to the $[[529, 44; 1]]_2$ code over a quaternary decoder even though the length⁶ of the code $[[529, 44; 1]]_2$ is greater than that of $[[390, 132; 128]]_2$. Improvement in the girth will significantly improve the error correction performance of the code.

Figure 9 shows the plots of the several EA quantum QC-LDPC codes of with underlying tiled permutation matrices of orders 5, 7, 11, and 13, respectively, with code-parameters $[[25, 8, 4; 1]]_2$, $[[49, 12, 6; 1]]_2$, $[[121, 20, 10; 1]]_2$ and $[[169, 24, 12; 1]]_2$ against the depolarizing noise. The $[[121, 20, 10; 1]]_2$ and $[[169, 24, 12; 1]]_2$ codes have a pre-threshold around 0.03 and then a global threshold exists around 0.075, after which an increment in the order of the quasi-cyclic does not provide any improvement against the depolarizing noise channel since the distance is not scaling proportionally.

7 Conclusions

We introduced several families of entanglement-assisted quantum QC-LDPC codes, namely (a) spatially-coupled and (b) those that are not spatially-coupled. Both these families are derived from rings of prime and composite orders, requiring only a minimum number of ebits. When the construction is based on two distinct classical codes, we ensure that the

⁶Here the length of the code implies the number of physical qubits that are transmitted through the noisy quantum channel not the overall length of the quantum code containing the physical qubits preshared with the receiver.

overall Tanner graph is devoid of short cycles. Further, while constructing entanglement-assisted quantum codes using a single classical code, the underlying classical code is devoid of short cycles as well. We present two additional families of entanglement-assisted quantum QC-LDPC codes, constructed from a single classical QC-LDPC code, where the Tanner graph has a girth greater than 6. We present simulation results for various classes of entanglement-assisted (EA) quantum QC-LDPC codes under both the random depolarizing channel and the random depolarizing channel with Markovian burst errors. The performance of the codes is evaluated using both binary and quaternary decoders on separate as well as the joint Tanner graphs, with quaternary decoders, showing performance improvements. We also demonstrated that the EA quantum QC-LDPC codes can correct a constant number of burst errors. Furthermore, we compare two codes: an EA quantum QC-LDPC code $[[390, 132; 128]]_2$ with girth greater than 6 and an EA quantum QC-LDPC code $[[529, 44; 1]]_2$ with girth greater than 4, highlighting the advantages of larger girth despite the shorter length of the former. Finally, the codes are simulated by varying the order of the permutation matrices, illustrating their impact on code performance, useful to practice.

References

- [1] Robert G Gallager. “Low-density parity-check codes”. *Ph.D. dissertation, Cambridge University* (1963).
- [2] Tarek Sobh, Khaled Elleithy, Ausif Mahmood, and Mohammad A Karim. “Novel algorithms and techniques in telecommunications, automation and industrial electronics”. *Springer Science & Business Media*. (2008).
- [3] DJC MacKay. “Information theory, inference, and learning algorithms”. *Cambridge University Press*. (2003).
- [4] Zongwang Li, Lei Chen, Lingqi Zeng, Shu Lin, and Wai H Fong. “Efficient encoding of quasi-cyclic low-density parity-check codes”. *IEEE Trans. Commun.* **54**, 71–81 (2006).
- [5] Zhongfeng Wang and Zhiqiang Cui. “A memory efficient partially parallel decoder architecture for quasi-cyclic LDPC codes”. *IEEE Trans. Very Large Scale Integr. VLSI Syst.* **15**, 483–488 (2007).
- [6] Arijit Mondal and Shayan Srinivasa Garani. “Efficient parallel decoding architecture for cluster erasure correcting 2-D LDPC codes for 2-D data storage”. *IEEE Trans. Magn.* **57**, 1–16 (2021).
- [7] Oscar Ferraz, Srinivasan Subramaniyan, Ramesh Chinthala, João Andrade, Joseph R Cavallaro, Soumitra K Nandy, Vitor Silva, Xinmiao Zhang, Madhura Purnaprajna, and Gabriel Falcao. “A survey on high-throughput non-binary LDPC decoders: ASIC, FPGA, and GPU architectures”. *IEEE Commun. Surv. Tutor.* **24**, 524–556 (2021).
- [8] Shuang Chen, Kewu Peng, Jian Song, and Yushu Zhang. “Performance analysis of practical QC-LDPC codes: From DVB-S2 to ATSC 3.0”. *IEEE Trans. Broadcast* **65**, 172–178 (2018).
- [9] Yujun Wu, Bin Wu, and Xiaoping Zhou. “High-Performance QC-LDPC Code Co-Processing Approach and VLSI Architecture for Wi-Fi 6”. *Electronics* **12**, 1210 (2023).
- [10] Tom Richardson and Shrinivas Kudekar. “Design of low-density parity check codes for 5G new radio”. *IEEE Commun. Mag.* **56**, 28–34 (2018).

- [11] Marc PC Fossorier. “Quasicyclic low-density parity-check codes from circulant permutation matrices”. *IEEE Trans. Inf. Theory* **50**, 1788–1793 (2004).
- [12] Shayan Srinivasa Garani, Lara Dolecek, John Barry, Frederic Sala, and Bane Vasić. “Signal processing and coding techniques for 2-D magnetic recording: An overview”. *Proceedings of the IEEE* **106**, 286–318 (2018).
- [13] Shayan Srinivasa Garani and Bane Vasić. “Channels Engineering in Magnetic Recording: from Theory to Practice”. *IEEE BITS: The Information Theory Magazine* Pages 1–36 (2023).
- [14] Lei Chen, Jun Xu, Ivana Djurdjevic, and Shu Lin. “Near-Shannon-limit quasi-cyclic low-density parity-check codes”. *IEEE Trans. Commun.* **52**, 1038–1042 (2004).
- [15] Shrinivas Kudekar, Thomas J Richardson, and Rüdiger L Urbanke. “Threshold saturation via spatial coupling: Why convolutional LDPC ensembles perform so well over the BEC”. *IEEE Trans. Inf. Theory* **57**, 803–834 (2011).
- [16] Shrinivas Kudekar, Tom Richardson, and Rüdiger L Urbanke. “Spatially coupled ensembles universally achieve capacity under belief propagation”. *IEEE Trans. Inf. Theory* **59**, 7761–7813 (2013).
- [17] Zhongwei Si, Ragnar Thobaben, Mikael Skoglund, and Tobias J Oechtering. “Bidirectional broadcasting by using multi-edge type LDPC convolutional codes”. In *Int. Symp. Turbo Codes Iterative Inf. Process. ISTC*. Pages 91–95. IEEE (2012).
- [18] Keigo Takeuchi, Toshiyuki Tanaka, and Tsutomu Kawabata. “Improvement of BP-based CDMA multiuser detection by spatial coupling”. In *IEEE Int. Symp. Inf. Theory - Proc.* Pages 1489–1493. (2011).
- [19] Gianluigi Liva, Enrico Paolini, Michael Lentmaier, and Marco Chiani. “Spatially-coupled random access on graphs”. In *IEEE Int. Symp. Inf. Theory - Proc.* Pages 478–482. (2012).
- [20] Vahid Aref, Nicolas Macris, Rüdiger Urbanke, and Marc Vuffray. “Lossy source coding via spatially coupled LDGM ensembles”. In *IEEE Int. Symp. Inf. Theory - Proc.* Pages 373–377. (2012).
- [21] Peter W Shor. “Algorithms for quantum computation: discrete logarithms and factoring”. In *Proc. - Annu. IEEE Symp. Found. Comput. Sci. FOCS*. Pages 124–134. IEEE (1994).
- [22] Lov K Grover. “A fast quantum mechanical algorithm for database search”. In *Proc. Annu. ACM Symp. Theory Comput.* Pages 212–219. (1996).
- [23] David P Nadlinger, Peter Drmota, Bethan C Nichol, Gabriel Araneda, Dougal Main, Raghavendra Srinivas, David M Lucas, Christopher J Ballance, Kirill Ivanov, EY-Z Tan, et al. “Experimental quantum key distribution certified by bell’s theorem”. *Nature* **607**, 682–686 (2022).
- [24] Gautam Kumar, Sahil Yadav, Aniruddha Mukherjee, Vikas Hassija, and Mohsen Guizani. “Recent advances in quantum computing for drug discovery and development”. *IEEE Access* (2024).
- [25] Yingzhao Zhu and Kefeng Yu. “Artificial intelligence (AI) for quantum and quantum for AI”. *Opt. Quantum Electron.* **55**, 697 (2023).
- [26] Peter W Shor. “Scheme for reducing decoherence in quantum computer memory”. *Phys. Rev. A.* **52**, R2493 (1995).

- [27] Daniel Gottesman. “Stabilizer codes and quantum error correction”. *California Institute of Technology*. (1997).
- [28] A Robert Calderbank, Eric M Rains, Peter W Shor, and Neil JA Sloane. “Quantum error correction and orthogonal geometry”. *Phys. Rev. Lett.* **78**, 405 (1997).
- [29] A Robert Calderbank, Eric M Rains, Peter M Shor, and Neil JA Sloane. “Quantum error correction via codes over GF (4)”. *IEEE Trans. Inf. Theory* **44**, 1369–1387 (1998).
- [30] Avanti Ketkar, Andreas Klappenecker, Santosh Kumar, and Pradeep Kiran Sarvepalli. “Nonbinary stabilizer codes over finite fields”. *IEEE Trans. Inf. Theory* **52**, 4892–4914 (2006).
- [31] Barbara M Terhal. “Quantum error correction for quantum memories”. *Rev. Mod. Phys.* **87**, 307–346 (2015).
- [32] John Preskill. “Lecture notes for physics 229: Quantum information and computation”. *California Institute of Technology* **16**, 1–8 (1998).
- [33] A Yu Kitaev. “Quantum computations: algorithms and error correction”. *Russ. Math. Surv.* **52**, 1191 (1997).
- [34] A Yu Kitaev. “Fault-tolerant quantum computation by anyons”. *Ann. Phys.* **303**, 2–30 (2003).
- [35] Michael H Freedman and David A Meyer. “Projective plane and planar quantum codes”. *Found. Comput. Math.* **1**, 325–332 (2001).
- [36] Sergey B Bravyi and A Yu Kitaev. “Quantum codes on a lattice with boundary” (1998).
- [37] Zijun Chen, Kevin J Satzinger, Juan Atalaya, Alexander N Korotkov, Andrew Dunsworth, Daniel Sank, Chris Quintana, Matt McEwen, Rami Barends, Paul V Klimov, et al. “Exponential suppression of bit or phase flip errors with repetitive error correction” (2021).
- [38] A Robert Calderbank and Peter W Shor. “Good quantum error-correcting codes exist”. *Phys. Rev. A.* **54**, 1098 (1996).
- [39] Alexei Ashikhmin, Simon Litsyn, and Michael A Tsfasman. “Asymptotically good quantum codes”. *Phys. Rev. A.* **63**, 032311 (2001).
- [40] Nikolas P Breuckmann and Jens Niklas Eberhardt. “Quantum low-density parity-check codes”. *PRX Quantum* **2**, 040101 (2021).
- [41] Daniel Gottesman. “Fault-tolerant quantum computation with constant overhead” (2013).
- [42] Emanuel Knill, Raymond Laflamme, and Wojciech H Zurek. “Resilient quantum computation: error models and thresholds”. *Proc. R. Soc. A: Math. Phys. Eng. Sci.* **454**, 365–384 (1998).
- [43] Dorit Aharonov and Michael Ben-Or. “Fault-tolerant quantum computation with constant error”. In *Proc. Annu. ACM Symp. Theory Comput.* Pages 176–188. (1997).
- [44] Mark M Wilde. “Quantum information theory”. *Cambridge University Press*. (2013).
- [45] Laszlo Gyongyosi, Sandor Imre, and Hung Viet Nguyen. “A survey on quantum channel capacities”. *IEEE Commun. Surv. Tutorials* **20**, 1149–1205 (2018).
- [46] Nicolas Delfosse and Gilles Zémor. “Upper bounds on the rate of low density stabilizer codes for the quantum erasure channel” (2012).

- [47] Robert Gallager. “Low-density parity-check codes”. *IEEE Trans. Inf. Theory*. **8**, 21–28 (1962).
- [48] Tom Richardson and Ruediger Urbanke. “Modern coding theory”. *Cambridge University Press*. (2008).
- [49] David JC MacKay, Graeme Mitchison, and Paul L McFadden. “Sparse-graph codes for quantum error correction”. *IEEE Trans. Inf. Theory*. **50**, 2315–2330 (2004).
- [50] Pavel Panteleev and Gleb Kalachev. “Quantum LDPC codes with almost linear minimum distance”. *IEEE Trans. Inf. Theory* **68**, 213–229 (2021).
- [51] Todd Brun, Igor Devetak, and Min-Hsiu Hsieh. “Correcting quantum errors with entanglement”. *science* **314**, 436–439 (2006).
- [52] Jianzhang Chen, Yuanyuan Huang, Chunhui Feng, and Riqing Chen. “Entanglement-assisted quantum MDS codes constructed from negacyclic codes”. *Quantum Inf. Process.* **16**, 1–22 (2017).
- [53] Kenza Guenda, Somphong Jitman, and T Aaron Gulliver. “Constructions of good entanglement-assisted quantum error correcting codes”. *Des. Codes Cryptogr.* **86**, 121–136 (2018).
- [54] Yang Liu, Ruihu Li, Liangdong Lv, and Yuena Ma. “Application of constacyclic codes to entanglement-assisted quantum maximum distance separable codes”. *Quantum Inf. Process.* **17**, 210 (2018).
- [55] Jianfa Qian and Lina Zhang. “On MDS linear complementary dual codes and entanglement-assisted quantum codes”. *Des. Codes Cryptogr.* **86**, 1565–1572 (2018).
- [56] Carlos Galindo, Fernando Hernando, Ryutaroh Matsumoto, and Diego Ruano. “Entanglement-assisted quantum error-correcting codes over arbitrary finite fields”. *Quantum Inf. Process.* **18**, 116 (2019).
- [57] Lan Luo, Zhi Ma, Zhengchao Wei, and Riguang Leng. “Non-binary entanglement-assisted quantum stabilizer codes”. *Sci. China Inf. Sci* **60** (2016).
- [58] Priya J Nadkarni and Shayan Srinivasa Garani. “Encoding of nonbinary entanglement-unassisted and assisted stabilizer codes”. *IEEE Trans. Quantum Eng.* **2**, 1–22 (2021).
- [59] Priya J Nadkarni and Shayan Srinivasa Garani. “Entanglement-assisted Reed–Solomon codes over qudits: theory and architecture”. *Quantum Inf. Process.* **20**, 1–68 (2021).
- [60] Min-Hsiu Hsieh, Wen-Tai Yen, and Li-Yi Hsu. “High performance entanglement-assisted quantum LDPC codes need little entanglement”. *IEEE Trans. Inf. Theory* **57**, 1761–1769 (2011).
- [61] Manabu Hagiwara and Hideki Imai. “Quantum quasi-cyclic LDPC codes”. In *IEEE Int. Symp. Inf. Pages 806–810*. IEEE (2007).
- [62] Sisi Miao, Jonathan Mandelbaum, Jäkel Holger, and Laurent Schmalen. “A joint code and belief propagation decoder design for quantum LDPC codes” (2024).
- [63] Manabu Hagiwara, Kenta Kasai, Hideki Imai, and Kohichi Sakaniwa. “Spatially coupled quasi-cyclic quantum LDPC codes”. In *IEEE Int. Symp. Inf. Theory - Proc. Pages 638–642*. (2011).
- [64] Nithin Raveendran, Priya J Nadkarni, Shayan Srinivasa Garani, and Bane Vasić. “Stochastic resonance decoding for quantum LDPC codes”. In *Int. Conf. Commun. (ICC). Pages 1–6*. IEEE (2017).

- [65] Min-Hsiu Hsieh, Todd A Brun, and Igor Devetak. “Entanglement-assisted quantum quasicyclic low-density parity-check codes”. *Phys. Rev. A* **79**, 032340 (2009).
- [66] Guohua Zhang, Rong Sun, and Xinmei Wang. “New quasi-cyclic LDPC codes with girth at least eight based on sidon sequences”. In *Int. Symp. Turbo Codes Iterative Inf. Process. ISTC*. Pages 31–35. IEEE (2012).
- [67] Shu Lin and Juane Li. “Fundamentals of classical and modern error-correcting codes”. Cambridge University Press. (2021).
- [68] Thomas J Richardson, Mohammad Amin Shokrollahi, and Rüdiger L Urbanke. “Design of capacity-approaching irregular low-density parity-check codes”. *IEEE Trans. Inf. Theory*. **47**, 619–637 (2001).
- [69] Michael G Luby, Michael Mitzenmacher, Mohammad Amin Shokrollahi, and Daniel A Spielman. “Improved low-density parity-check codes using irregular graphs”. *IEEE Trans. Inf. Theory*. **47**, 585–598 (2001).
- [70] Su-Chang Chae and Yun-Ok Park. “Low complexity encoding of regular low density parity check codes”. In *IEEE 58th Vehicular Tech. conf. VTC 2003-Fall (IEEE Cat. No. 03CH37484)*. Volume 3, pages 1822–1826. (2003).
- [71] Tong Zhang and Keshab K Parhi. “An FPGA implementation of-regular low-density parity-check code decoder”. *EURASIP J. Adv. Signal Process.* **2003**, 1–13 (2003).
- [72] Olgica Milenkovic, Navin Kashyap, and David Leyba. “Shortened array codes of large girth”. *IEEE Trans. Inf. Theory*. **52**, 3707–3722 (2006).
- [73] Julia Lieb and Simran Tinani. “A number theoretic approach to cycles in LDPC codes”. *IFAC-Pap.* **55**, 67–72 (2022).
- [74] Shrinivas Kudekar, Thomas J Richardson, and Rüdiger L Urbanke. “Threshold saturation via spatial coupling: Why convolutional LDPC ensembles perform so well over the BEC”. *IEEE Trans. Inf. Theory* **57**, 803–834 (2011).
- [75] Santhosh Kumar, Andrew J Young, Nicolas Macris, and Henry D Pfister. “Threshold saturation for spatially coupled LDPC and LDGM codes on BMS channels”. *IEEE Trans. Inf. Theory* **60**, 7389–7415 (2014).
- [76] Michael Lentmaier, Arvind Sridharan, Daniel J Costello, and Kamil Sh Zigangirov. “Iterative decoding threshold analysis for LDPC convolutional codes”. *IEEE Trans. Inf. Theory* **56**, 5274–5289 (2010).
- [77] Charles H Bennett, Peter W Shor, John A Smolin, and Ashish V Thapliyal. “Entanglement-assisted classical capacity of noisy quantum channels”. *Phys. Rev. Lett.* **83**, 3081 (1999).
- [78] Charles H Bennett, Peter W Shor, John A Smolin, and Ashish V Thapliyal. “Entanglement-assisted capacity of a quantum channel and the reverse Shannon theorem”. *IEEE Trans. Inf. Theory* **48**, 2637–2655 (2002).
- [79] Igor Devetak, Aram W Harrow, and Andreas J Winter. “A resource framework for quantum Shannon theory”. *IEEE Trans. Inf. Theory*. **54**, 4587–4618 (2008).
- [80] Todd A Brun, Igor Devetak, and Min-Hsiu Hsieh. “Catalytic quantum error correction”. *IEEE Trans. Inf. Theory* **60**, 3073–3089 (2014).
- [81] Mark M Wilde and Todd A Brun. “Optimal entanglement formulas for entanglement-assisted quantum coding”. *Phys. Rev. A* **77**, 064302 (2008).

- [82] San Ling and Chaoping Xing. “Coding theory: a first course”. Cambridge University Press. (2004).
- [83] Cibele Cristina Trinca, Clarice Dias De Albuquerque, Reginaldo Palazzo Junior, J. Carmelo Interlando, Antonio Aparecido De Andrade, and Ricardo Augusto Watanabe. “New Quantum Burst-Error Correcting Codes from Interleaving Technique”. In GLOBECOM. Pages 5243–5248. (2022).
- [84] Jihao Fan, Min-Hsiu Hsieh, Hanwu Chen, He Chen, and Yonghui Li. “Construction and performance of quantum burst error correction codes for correlated errors”. In IEEE Int. Symp. Inf. Theory (ISIT). Pages 2336–2340. (2018).
- [85] Chaitanya Kumar Matcha, Shounak Roy, Mohsen Bahrami, Bane Vasic, and Shayan Garani Srinivasa. “2-D LDPC Codes and Joint Detection and Decoding for Two-Dimensional Magnetic Recording”. IEEE Trans. Magn. **54**, 1–11 (2018).
- [86] Nithin Raveendran, Narayanan Rengaswamy, Asit Kumar Pradhan, and Bane Vasić. “Soft Syndrome Decoding of Quantum LDPC Codes for Joint Correction of Data and Syndrome Errors”. In IEEE Int. Conf. Quantum Comput. Eng. (QCE). Pages 275–281. (2022).
- [87] Dimiter Ostrev, Davide Orsucci, Francisco Lázaro, and Balazs Matuz. “Classical product code constructions for quantum calderbank-shor-steane codes”. Quantum **8**, 1420 (2024).